UNIVERSITY OF CALIFORNIA SAN DIEGO

Acanthamoeba: Evaluation of Conazoles as Amebicidal Compounds and Development of a Cysticidal Assay

A dissertation submitted in partial satisfaction of the requirements for the degree Doctor of Philosophy

in

Biomedical Sciences

by

Brian Joseph Shing

Committee in Charge:

Professor James H. McKerrow, Chair
Professor Geoffrey Chang
Professor Peter B. Ernst
Professor William Gerwick
Professor Hemal H. Patel

2022

The dissertation of Brian Joseph Shing is approved, and it is acceptable in quality and form for publication on microfilm and electronically.

University of California San Diego

2022

TABLE OF CONTENTS

LIST OF ABBREVIATIONS

Ac: *Acanthamoeba castellanii*

AK: *Acanthamoeba* Keratitis

AcCYP51: *Acanthamoeba castellanii* sterol 14α demethylase

CHLX: chlorhexidine gluconate

CYP51: sterol 14α demethylase

DMSO: dimethyl sulfoxide

EC_{50}: half maximal effective concentration

ER: endoplasmic reticulum

IC_{50}: half maximal inhibitory concentration

Inh.: inhibition

ISA: isavuconazole

MALS: multiangle light scattering

MCC: minimum cysticidal concentration

MD: molecular dynamics

MM: molecular mass

NTA: nitrilotriacetic acid

P420: cytochrome P420

P450: cytochrome P450

PDB: protein data bank

POPC: 1-palmitoyl-2-oleoyl-sn-glycero-3-phosphocholine

POPE: 1-palmitoyl-2-oleoyl-sn-glycero-3- phosphoethanolamine

POSA: posaconazole

PHMB: polyhexamethylene biguanide

SEC-MALS: size-exclusion chromatography–MALS

spp.: several species

TM: transmembrane

w/v: weight per volume

v/v: volume per volume

LIST OF FIGURES

LIST OF TABLES

ACKNOWLEDGMENTS

I would like to thank and acknowledge all the mentors and collaborators that have been instrumental in making this dissertation possible. In particular, Doctors Anjan Debnath and Jim McKerrow have provided invaluable support and guidance for me as my dissertation and academic advisors. Furthermore, I would also like to thank Doctors Jean Bernatchez and Danielle Skinner for intellectual discussions and advice. These discussisons have been stimulating and offered me insight to grasping new concepts. Throughout all these years, the McKerrow lab has provided the perfect environment for me to explore and develop as a scientist.

Chapter 1, in full, is a reprint of the material as it appears in Brian Shing, Mina Balen, James H McKerrow, Anjan Debnath "*Acanthamoeba* Keratitis: an Update on Amebicidal and Cysticidal Drug Screening Methodologies and Potential Treatment with Azole Drugs" Expert Review Anti-Infective Therapy, 2021. The dissertation author was the primary author and a major contributor to this review.

Chapter 2, in full, is a reprint of the material as it appears in Brian Shing, Seema Singh, Larissa M Podust, James H McKerrow, Anjan Debnath "The Antifungal Drug Isavuconazole is both Amebicidal and Cysticidal against *Acanthamoeba castellanii*" Antimicrobial Agents and Chemotherapy, 2020. The dissertation author was the primary investigator and author on this manuscript.

Chapter 3, in full, is republished with permission of American Society For Pharmacology and Experimental Therapeutics, from the material Domain-Swap Dimerization of *Acanthamoeba castellanii* CYP51 and a Unique Mechanism of Inactivation by Isavuconazole, Vandna Sharma, Brian Shing, Lilian Hernandez-Alvarez,

Anjan Debnath, and Larissa M. Podust, 98, and ©2020; permission conveyed through Copyright Clearance Center, Inc. The dissertation author was a second author and an essential contributor on this manuscript.

Chapter 4, in full, is a reprint of the material as it appears in Brian Shing, Mina Balen, Anjan Debnath “Evaluation of Amebicidal and Cysticidal Activities of Antifungal Drug Isavuconazonium Sulfate against *Acanthamoeba* T4 Strains” Pharmaceuticals, 2021. The dissertation author was the primary author and major contributor to this paper.

Chapter 5, is a print of the manuscript in preparation: Brian Shing, Mina Balen, William Fenical, Anjan Debnath “Development of a Machine Learning-based Cysticidal Assay and Identification of an Amebicidal and Cysticidal Marine Microbial Metabolite against *Acanthamoeba*”. The dissertation author was the primary author and major contributor to this paper.

The author would also like to thank and acknowledge the work and input from the following co-authors in publications referenced in this dissertation. Doctors James McKerrow, Anjan Debnath, Larissa Podust, Vandna Sharma, Lilian Hernandez Alvarez, and Seema Singh.

VITA

2013 – 2017 Bachelor of Arts, University of California Berkeley

2017 – 2022 Doctor of Philosophy, University of California San Diego

PUBLICATIONS

Shing B, Balen M, Fenical W, Debnath A. 2022. Development of a Machine Learning-based Cysticidal Assay and Identification of an Amebicidal and Cysticidal Marine Microbial Metabolite against *Acanthamoeba*. In preparation.

Shing B, Balen M, Debnath A. 2021. Evaluation of Amebicidal and Cysticidal Activities of Antifungal Drug Isavuconazonium Sulfate against *Acanthamoeba* T4 Strains. Pharmaceuticals 14:1294.

Shing B, Balen M, McKerrow JH, Debnath A. 2021. *Acanthamoeba* Keratitis: An Update on Amebicidal and Cysticidal Drug Screening Methodologies and Potential Treatment with Azole Drugs. Expert Review of Anti-Infective Therapy 1—15.

Shing B, Singh S, Podust LM, McKerrow JH, Debnath A. 2020. The Antifungal Drug Isavuconazole Is both Amebicidal and Cysticidal against *Acanthamoeba castellanii*. Antimicrobial Agents and Chemotherapy 64.

Sharma V, Shing B, Hernandez-Alvarez L, Debnath A, and Podust LM. 2020. Domain-Swap Dimerization of *Acanthamoeba castellanii* CYP51 and a Unique Mechanism of Inactivation by Isavuconazole. Molecular Pharmacology 98:770—780.

FIELDS OF STUDY

Major Field: Biomedical Sciences

Studies in pharmaceutical sciences and neglected tropical diseases
Professors Jim McKerrow and Anjan Debnath

ABSTRACT OF THE DISSERTATION

Acanthamoeba: Evaluation of Conazoles as Amebicidal Compounds and Development of a Cysticidal Assay

by

Brian Joseph Shing

Doctor of Philosophy in Biomedical Sciences

University of California San Diego, 2022

Professor James McKerrow, Chair

Acanthamoeba is a genus encompassing several species of free-living amoeba. These amoeba are most notably associated with *Acanthamoeba* keratitis, a severe corneal infection that can lead to permanent blindness. While drug therapies exist to treat *Acanthamoeba* keratitis, literature reports of recalcitrance and treatment failure are not uncommon. This dissertation compiles my work in drug screening and evaluating conazoles as novel treatment options for *Acanthamoeba* keratitis.

Chapter 1. *Acanthamoeba* encompasses several species of free-living ameba encountered commonly throughout the environment. Unfortunately, these species of ameba can cause opportunistic infections that result in *Acanthamoeba* keratitis, granulomatous amebic encephalitis, and occasionally systemic infection.

While several biguanide and diamidine antimicrobial agents are available to clinicians to effectively treat *Acanthamoeba* keratitis, no singular treatment can effectively treat every *Acanthamoeba* keratitis case. Efforts to identify new anti-*Acanthamoeba* agents include trophozoite cell viability assays, which are amenable to high-throughput screening. Cysticidal assays remain largely manual and would benefit from further automation development. Additionally, the existing literature on the effectiveness of various azole antifungal agents for treating *Acanthamoeba* keratitis is incomplete or contradictory, suggesting the need for a systematic review of all azoles against different pathogenic *Acanthamoeba* strains.

Chapter 2. Current treatments for *Acanthamoeba* keratitis rely on a combination of chlorhexidine gluconate, propamidine isethionate, and polyhexamethylene biguanide. These disinfectants are nonspecific and inherently toxic, which limits their effectiveness. Furthermore, in 10% of cases, recurrent infection ensues due to the difficulty in killing both trophozoites and double-walled cysts. Therefore, development of efficient, safe, and target-specific drugs which are capable of preventing recurrent *Acanthamoeba* infection is a critical unmet need for averting blindness. Since both trophozoites and cysts contain specific sets of membrane sterols, we hypothesized that antifungal drugs targeting sterol

14-demethylase (CYP51), known as conazoles, would have deleterious effects on *A. castellanii* trophozoites and cysts. To test this hypothesis, we first performed a systematic screen of the FDA-approved conazoles against *A. castellanii* trophozoites using a bioluminescence-based viability assay adapted and optimized for *Acanthamoeba*. The most potent drugs were then evaluated against cysts. Isavuconazole and posaconazole demonstrated low nanomolar potency against trophozoites of three clinical strains of *A. castellanii*. Furthermore, isavuconazole killed trophozoites within 24 h and suppressed excystment of preformed *Acanthamoeba* cysts into trophozoites. The rapid action of isavuconazole was also evident from the morphological changes at nanomolar drug concentrations causing rounding of trophozoites within 24 h of exposure. Given that isavuconazole has an excellent safety profile, is well tolerated in humans, and blocks *A. castellanii* excystation, this opens an opportunity for the cost-effective repurposing of isavuconazole for the treatment of primary and recurring *Acanthamoeba* keratitis.

Chapter 3. Cytochromes P450 (P450, CYP) metabolize a wide variety of endogenous and exogenous lipophilic molecules, including most drugs. Sterol 14α-demethylase (CYP51) is a target for antifungal drugs known as conazoles. Using X-ray crystallography, we have discovered a domain-swap homodimerization mode in CYP51 from a human pathogen, *Acanthamoeba castellanii* CYP51 (AcCYP51). Recombinant AcCYP51 with a truncated transmembrane helix was purified as a heterogeneous mixture corresponding to the dimer and monomer units. Spectral analyses of these two populations have shown that the CO-bound ferrous form of the dimeric protein absorbed at 448 nm (catalytically competent form), whereas the monomeric form absorbed at 420

nm (catalytically incompetent form). AcCYP51 dimerized head-to-head via N-termini swapping, resulting in formation of a nonplanar protein-protein interface exceeding 2000 $Å^2$ with a total solvation energy gain of -35.4 kcal/mol. In the dimer, the protomers faced each other through the F and G α-helices, thus blocking the substrate access channel. In the presence of the drugs clotrimazole and isavuconazole, the AcCYP51 drug complexes crystallized as monomers. Although clotrimazole-bound AcCYP51 adopted a typical CYP monomer structure, isavuconazole-bound AcCYP51 failed to refold 74 N-terminal residues. The failure of AcCYP51 to fully refold upon inhibitor binding *in vivo* would cause an irreversible loss of a structurally aberrant enzyme through proteolytic degradation. This assumption explains the superior potency of isavuconazole against *A. castellanii*. The dimerization mode observed in this work is compatible with membrane association and may be relevant to other members of the CYP family of biologic, medical, and pharmacological importance.

Chapter 4. *Acanthamoeba* species of amebae are often associated with *Acanthamoeba* keratitis, a severe corneal infection. Isavuconazonium sulfate is an FDA-approved drug for the treatment of invasive as-pergillosis and mucormycosis. This prodrug is metabolized into the active isavuconazole moiety. Isavuconazole was previously identified to have amebicidal and cysticidal activity against *Acanthamoeba* T4 strains, but the activity of its prodrug, isavuconazonium sulfate, against trophozoites and cysts remains unknown. Since it is not known if isavuconazonium can be metabolized into isavuconazole in the human eye, we evaluated the activities of isavuconazonium sulfate against trophozoites and cysts of three T4 genotype strains of *Acanthamoeba*.

Isavuconazonium displayed amebicidal activity at nanomolar concentrations as low as 1.4 nM and prevented excystation of cysts at concentrations as low as 136 μM. We also investigated the cysticidial activity of isavuconazonium sulfate in combination with a currently used amebicidal drug polyhexamethylene biguanide (PHMB). Although combination of isavuconazonium with PHMB did not elicit an obvious synergistic cysticidal activity, the combination did not cause an antagonistic effect on the cysts of *Acanthaomoeba* T4 strains. Collectively, these findings suggest isavuconazonium retains potency against *Acanthamoeba* T4 strains and could be adapted for *Acanthamoeba* keratitis treatment.

Chapter 5. Traditional cysticidal assays for *Acanthamoeba* species revolve around treating cysts with compounds and manually observing the culture for evidence of excystation. This method is time-consuming, labor-intensive, and low-throughput. We adapted and trained a YOLOv3 machine learning, object-detection neural network to recognize *A. castellanii* trophozoites and cysts in microscopy images to develop an automated cysticidal assay. This trained neural network was used to count trophozoites in wells treated with marine-derived compounds of interest to determine if a compound treatment was cysticidal. We validated this new assay with known cysticidal and non-cysticidal compounds. In addition, we undertook a large-scale bioluminescence-based screen of 9,286 structurally-unique marine microbial metabolites against the trophozoites of *A. castellanii* and identified 29 trophocidal hits. These hits were then subjected to this machine learning-based automated cysticidal assay. One marine microbial metabolite fraction was identified as both trophocidal and cysticidal.

Chapter 1: *Acanthamoeba* Keratitis: An Update on Amebicidal and Cysticidal Drug Screening Methodologies and Potential Treatment with Azole Drugs

1.1 Introduction

Acanthamoeba are several species of ubiquitous free-living ameba found throughout the world. While *Acanthamoeba* spp. are most commonly found in wet environments, such as lakes and swimming pools, they can be found in less hospitable environments, such as heating, ventilation, and air conditioning vents, and contact lens solutions.

Depending on environmental conditions, *Acanthamoeba* can exist as a trophozoite or cyst (Fig. 1.1A, 1.1B). Trophozoites are the motile, reproductive stage of *Acanthamoeba.* This stage exists in favorable environments with ample nutrients and appropriate temperature. Trophozoites can range in size from 25-40 μm in length (1). Trophozoites move via pseudopodia and ingest bacteria, yeast, and cell debris through phagocytosis or food cup formation (2). Trophozoites utilize pinocytosis to ingest nutrients present in the liquid environment (1).

Cysts are dormant and are composed of a cell within a double cyst wall composed of chitin, protein, and cellulose. Cysts walls are rigid and cysts are spherical in shape with a size ranging from 13-20 μm in diameter. Cysts are resistant to harsh environmental conditions that would be fatal to trophozoites. The outer wall of a cyst contains a high amount of cellulose, which results in a high degree of drug resistance (3). This drug resistance allows cysts to survive otherwise effective medical therapies for killing the parasite (4).

Acanthamoeba trophozoites reproduce through binary fission. Excystation from a

cyst to a trophozoite usually follows after an environment becomes suitable. The trophozoite stage of the parasite is considerably less durable than its cyst counterpart, and is sensitive to antimicrobial agents (5).

While *Acanthamoeba* spp. are typically free-living, they can be opportunistic pathogens and produce disease in humans. Trophozoites and cysts are both able to infect humans and produce *Acanthamoeba* keratitis, granulomatous amebic encephalitis, and disseminated infections (Fig. 1.1C) (6).

Acanthamoeba spp. are often associated with *Acanthamoeba* keratitis, a severe corneal infection. This infection typically occurs in contact-lens wearers, but it can also occur in patients with recent corneal trauma. Most keratitis infections are caused by the T4 genotype. Clinical testing has been performed on strains of this genotype, taken from the affected patients (7). While effective therapies, such as topical combinations of chlorhexidine gluconate and polyhexamethylene biguanide (PHMB), exist to treat *Acanthamoeba* keratitis, the parasite can encyst in the ocular tissue to resist current standard-of-care therapies and lead to recurrent keratitis. As such, discovering and identifying therapeutics that are effective against both stages of the parasite would be critical to reducing *Acanthamoeba* keratitis recurrence and improving existing therapies. This review will discuss current treatments and advances in screening and identifying novel therapeutics for *Acanthamoeba* keratitis treatment.

1.2 Clinical Symptoms

Acanthamoeba keratitis can trigger a number of symptoms in patients. Common early symptoms or signs of infection include ocular pain and irritation, excessive tear

production, light sensitivity, blurry vision, pseudodendritiformic epitheliopathy, corneal opacity, conjunctival hyperemia, multifocal stromal infiltrates, and ring and perineural infiltrates (1, 8, 9). While the parasites are largely confined to the cornea and active infections typically do not penetrate past the Descemet's membrane of the cornea, the presence of *Acanthamoeba* parasites in the cornea may trigger further inflammation through molecular mimicry or stimulating delayed type hypersensitivity (10–12). In advanced cases of *Acanthamoeba* keratitis, patients can suffer from iris atrophy, secondary glaucoma, cataracts, uveitis, scleritis, and chorioretinitis (1, 9, 13, 14).

1.3 Diagnosis

Early on, 75 - 90% of *Acanthamoeba* keratitis are misdiagnosed and inappropriately treated as bacterial, mycotic, or viral keratitis (9). Since delays in proper treatment can allow the infection to progress and negatively affect patient outcomes, proper diagnosis is crucial. To this end, clinicians employ a number of diagnostic techniques, including microbial culture, histopathology, confocal microscopy, and PCR analysis to identify *Acanthamoeba* keratitis in patients (1, 9).

Microbial culture is still one of the primary diagnostic techniques for identifying *Acanthamoeba* keratitis. In microbial culture, samples collected from corneal scrapings, biopsies, or contact lens swabs are cultured on *E. coli* plated non-nutrient agar plates (15). The cultures are observed under microscopy to morphologically identify if *Acanthamoeba* trophozoites or cysts are present (9, 15). While *Acanthamoeba* trophozoites can become apparent on the culture medium within several days, this diagnostic technique can take up to several weeks to return a definitive diagnosis

depending on the initial parasite load (9, 15).

Histopathological techniques rely upon staining corneal samples with various dyes and observing for evidence of *Acanthamoeba* trophozoites and cysts. Periodic acid Schiff, Masson, Gram, Giemsa, Grocott-methenamine-silver, hematoxylin and eosin, or calcofluor white stains can all be used to enhance contrast of trophozoites and cysts for detection (9, 15–17). Since this diagnostic technique is subjective and dependent on the skill of the examiner, diagnostic accuracy can vary significantly.

In vivo confocal microscopy is another diagnostic technique that allows for rapid diagnosis of *Acanthamoeba* keratitis (18, 19). Care providers will examine the patient's eye using a confocal microscope to try identifying cysts, which appear as hyper-reflective circular structures; trophozoites can be more difficult to identify using *in vivo* confocal microscopy as they can resemble leukocytes and keratocytes (9, 15, 19). *In vivo* confocal microscopy can have detection sensitivities as high as 90 - 100%, but diagnostic outcomes are highly dependent upon the training and experience of the examiner (9, 19–21).

In PCR analysis, *Acanthamoeba*-specific 18s rRNA primers, such as Nelson, ACARNA, JDP1/JDP2, and Acant, can be used to detect *Acanthamoeba* parasites to inform a diagnosis (22–26). PCR has added advantages of rapid results and the sensitivity to detect low numbers of parasites that may be missed by other techniques (27). PCR diagnostic results can vary depending on the primers used and assay conditions, but diagnostic sensitivities have been reported to be >70% and can be further improved by using multiple primers to validate diagnostic assay results (22, 28). While PCR can be a useful diagnostic, it is limited by its inability to distinguish between genetic

material from viable and nonviable parasites and clinicians should consider this during determining a diagnosis (9, 29).

1.4 Current treatments

Acanthamoeba keratitis is a severe corneal infection that, if left untreated, can result in permanent visual impairment or blindness. *Acanthamoeba* spp. parasites adhere to the surface of the corneal epithelium through a mannose-binding protein (30, 31). Once adhered, the parasites secrete proteases that kill corneal epithelial cells and allow further invasion into the corneal stroma (31).

Since untreated *Acanthamoeba* keratitis can lead to severe and life-altering consequences, clinicians have focused on removing infected tissue and killing the parasites. A number of chemotherapeutic and surgical interventions have been utilized.

There are a whole suite of chemotherapeutic agents available to treat *Acanthamoeba* keratitis, including biguanide, diamidine, antiseptic, antiparasitic, photodynamic, antibiotic, and antifungal agents (Table 1.1) (1, 16, 32, 33). The most commonly used biguanides are chlorhexidine gluconate and polyhexamethylene biguanide (PHMB) while diamidines include propamidine isethionate and hexamidine isethionate (16). *In vitro* data suggest antiseptic povidone-iodine can have anti-*Acanthamoeba* activity, but these results have not been clinically validated (16, 34, 35). Antiparasitic drug miltefosine has also been utilized clinically in managing *Acanthamoeba* keratitis and given orphan drug status by the FDA (16, 36–41). Photodynamic therapy utilizes photosensitive agents to kill parasites (42). Antibiotics, such as neomycin and polymyxin B, and antifungal agents, including amphotericin B, natamycin, and azoles,

have also been clinically utilized to manage and treat *Acanthamoeba* keratitis (1, 9, 16, 43).

While exact treatment regimens can vary among clinical practitioners, *Acanthamoeba* keratitis therapies frequently employ chlorhexidine or PHMB as monotherapy or in combination with propamidine isethionate and hexamidine (44, 45). Commonly reported combinations include, but are not limited to, PHMB with propamidine, chlorhexidine with propamidine, chlorhexidine with PHMB, and PHMB with propamidine and neomycin (46). Typically, these therapies are initially administered topically hourly for several days. Afterwards, the frequency of dosing is adjusted per patient needs and can last up to 6 to 12 months for successful keratitis resolution (32, 44, 47).

Surgical interventions focus on physically removing corneal tissue to remove the nidus of infection or physical methods of killing *Acanthamoeba* parasites. Debridement involves scraping or irritating the cornea using a blade in an effort to surgically remove infected tissue (48). Penetrating keratoplasty involves removing infected tissue and replacing it with a clean donor cornea (45, 49, 50). It has been shown to resolve cases that other methods were unable to (51). Other surgical treatments, such as cryotherapy, seek to physically treat the infection by freezing portions of the cornea to directly eradicate the parasites (52–54). In advanced cases where surgery and chemotherapies are unsuccessful at resolving the infection, clinicians may resort to enucleation of the infected eye (1, 49).

Biguanides. Most cases of *Acanthamoeba* keratitis are treated with a combination of biguanides, which is a class of cationic antimicrobial compounds. This class of

antimicrobials disrupts negatively charged cell membranes to kill microbes. The two most effective and widely used biguanides are polyhexamethylene biguanide (PHMB) and chlorhexidine gluconate (45). Initial dosing for *Acanthamoeba* keratitis treatment typically begins at 0.02% for both chlorhexidine and PHMB. In refractory cases, clinicians can increase the dosage of PHMB up to 0.06% (47).

Chlorhexidine gluconate is a broad-spectrum antiseptic effective against bacteria and fungi (55). It is commonly found in hygiene products, such as hand-cleaning products and oral antiseptics (56). Chlorhexidine is effective against both trophozoites and cysts (15). While the mechanism of action for chlorhexidine is to disrupt the cell membrane and cause cell lysis, cyst walls can help physically block uptake of chlorhexidine and act as a resistance mechanism (55, 56).

In vitro studies have reported chlorhexidine to be highly potent against both trophozoites and cysts. Chlorhexidine has been found to be trophocidal at concentrations as low as 8 µg/mL (8×10^{-4} %) (57). Alizadeh *et al* (2009) identified chlorhexidine to be trophocidal at a concentration of 10 µg/mL (1×10^{-3} %) (58). Chlorhexidine has been found to be cysticidal at concentrations as low as 1.56 µg/mL (1.56×10^{-4} %) (59). Lee *et al* (2007) reported chlorhexidine to have a minimum cysticidal concentration of 7.02 µg/mL (7.02×10^{-4} %) (60).

There has been a limited number of clinical trials evaluating chlorhexidine's effectiveness in treating *Acanthamoeba* keratitis. Kosrirukvongs *et al* (1999) treated six eyes with 0.006% chlorhexidine and reported curing infection in five of the eyes (61). Lim *et al* (2008) reported chlorhexidine monotherapy administered as 0.02% eye drops resolved 85.7% of keratitis cases (62). Additionally, chlorhexidine treatment resulted in

greater visual acuity improvement and less corneal scarring than PHMB monotherapy, which suggests chlorhexidine may be more tolerable for patients (62).

PHMB is a wide-spectrum antiseptic utilized in a wide variety of applications, such as wound care, cosmetic preservatives, contact lens cleaners, and pool cleaners (63–65). In *Acanthamoeba*, PHMB is taken up into the parasite, where it disrupts the cell membrane and causes cell death (66).

PHMB is commonly used in conjunction with other biguanides and diamidines in the treatment of *Acanthamoeba* keratitis (45). *In vitro*, PHMB has demonstrated excellent potency against trophozoites and cysts with reported minimum trophozoite amebicidal concentrations as low as 2.5 µg/mL (2.5 x 10^{-4} %) (57). Heaselgrave *et al* (2019) reported PHMB to be amebicidal against trophozoites at 3.9 µg/mL (35). In terms of cysticidal activity, PHMB was found to have a minimum cysticidal concentration of 2.37 µg/mL (2.37 x 10^{-4} %) while Narasimhan *et al* (2002) demonstrated a minimum cysticidal concentration of 25 µg/mL (2.5 x 10^{-3} %) (59, 60).

Clinically, PHMB has been evaluated as a monotherapy agent for treating *Acanthamoeba* keratitis. Lim *et al* (2008) reported PHMB monotherapy in 0.02% eye drops resolved 78% of keratitis cases and was comparable in efficacy to chlorhexidine-based monotherapy, but they also cautioned that PHMB appeared to cause more corneal scarring, which may limit its utility (62).

Chlorhexidine and PHMB have been clinically evaluated and reported to be efficacious in resolving *Acanthamoeba* keratitis (61, 62). *In vitro*, the reported minimum trophozoite amebicidal or cysticidal concentrations vary between reports, but the independently reported values demonstrate chlorhexidine and PHMB are extremely

potent against *Acanthamoeba* and suggest even the starting clinical dose of 0.02% is sufficient to kill *Acanthamoeba* trophozoites and cysts. Despite this, reports of refractory *Acanthamoeba* keratitis cases following prolonged biguanide treatment and reports detailing clinical isolates with high resistance reveal biguanides are not a guaranteed panacea (67–69). Furthermore, these antiseptic agents are nonspecific and have cytotoxicity against corneal epithelial cells and keratocytes at clinically relevant doses. This may limit the maximum tolerable dose (60, 70).

Diamidines. Diamidines are a class of cationic compounds with broad-spectrum antimicrobial activity against bacteria, fungi, ameba, and other protozoa (71). Diamidines are believed to exert their antimicrobial activity by disrupting cell membranes, denaturing cytosolic proteins, and inhibiting DNA synthesis (47, 72). In the treatment of *Acanthamoeba* keratitis, commonly used diamidines include 0.1% propamidine isethionate and hexamidine at 0.1% (47).

Propamidine isethionate is a DNA synthesis inhibitor, and it was one of the first agents shown to be effective for treating *Acanthamoeba* keratitis (32, 72, 73). In a retrospective study of 111 cases of *Acanthamoeba* keratitis, it was used in conjunction with PHMB to significantly improve visual acuity of the majority (>79%) of *Acanthamoeba* keratitis cases (74). Propamidine has also been combined with a number of other general purpose antimicrobials, such as neomycin, PHMB, chlorhexidine, polymyxin B, and gramicidin for *Acanthamoeba* keratitis treatment (75–77).

Reports of propamidine's minimum trophozoite amebicidal concentration range from values as low as 15.6 µg/mL (1.56×10^{-3} %) to estimates as high as 1,000 µg/mL (1

x 10^{-1} %) (35, 78). Its minimum cysticidal concentration has also been reported to be as low as 250 µg/mL (2.5 x 10^{-2} %) and as high as 421 µg/mL (4.21 x 10^{-2} %) (35, 67). Clinically, propamidine and neomycin as a combination therapy has been evaluated and reported to have high efficacy. Hargrave *et al* (1999) treated *Acanthamoeba* keratitis patients with 0.1% propamidine solution and neomycin and reported 50 of 60 eyes (83%) resolved successfully (76). These clinical and *in vitro* reports suggest propamidine is broadly efficacious against both *Acanthamoeba* trophozoites and cysts and can be utilized to alleviate *Acanthamoeba* keratitis.

Hexamidine was originally developed as a trypanocidal agent (79). More recently, it is now formulated into a number of over-the-counter medications as an antiseptic and antimicrobial agent (80). For *Acanthamoeba* keratitis treatment, it was first reported by Brasseur *et al* (1994) that topical 0.1% hexamidine successfully cleared a case of *Acanthamoeba* keratitis recalcitrant to propamidine treatment (81). Since then, hexamidine has been utilized in conjunction with a number of other antimicrobials, such as chlorhexidine, PHMB, and propamidine to successfully treat patients (77).

In vitro, hexamidine isethionate has been reported to be effective against *Acanthamoeba* cysts and trophozoites (35, 72). Hexamidine's minimum trophozoite amebicidal concentration has been reported to range from 7.5 µg/mL (7.5 x 10^{-4} %) to 31.3 µg/mL (3.13 x 10^{-3} %) (35, 78). It has also been reported to be cysticidal at significantly higher concentrations, with reports of cysticidal activity at concentrations of 222 µg/mL (2.22 x 10^{-2} %) and 250 µg/mL (2.5 x 10^{-2} %) (35, 67).

Despite various promising reports that chlorhexidine, PHMB, propamidine, and hexamidine are effective against *A. castellanii* trophozoites and cysts, clinical reports of

5-10% of cases being refractory even to extended courses of these combination therapies suggest the need for compounds with better efficacy and less clinical resistance (32, 67).

Antiseptic Agents. Povidone-iodine is an iodophor that penetrates microorganisms and oxidizes cytosolic cell components to cause death (82). It is generally well tolerated and is used as a broad-spectrum antiseptic agent for wound care (83). Furthermore, povidone-iodine has also been adapted for ophthalmic use in contact lens cleaning and care (84–86).

In terms of *in vitro* characterization, povidone-iodine has been found to be cysticidal and trophocidal (34, 84–87). Roongruangchai *et al* (2009) reported povidone-iodine had a minimum cysticidal concentration of 0.04% and identified structural damage to treated cysts, such as the breakdown of cyst walls and the parasite cell membranes (88). Sunada *et al* (2014) demonstrated povidone-iodine was cysticidal against 56 different *Acanthamoeba spp.* clinical isolates even at concentrations as low as 0.1% (89). Shi *et al* (2020) reported 0.25% povidone-iodine completely trophocidal and had significant cysticidal effects (~80% inhibition) (90).

However, several *in vitro* reports suggest povidone-iodine to be ineffective. Pelletier *et al* (2011) reported 0.4% povidone-iodine and 0.1% dexamethasone were not cysticidal (91). Lim *et al* (2000) reported povidone-iodine had poor activity against trophozoites with a minimum inhibitory concentration exceeding 100 µg/mL (0.01%) and no detectable cysticidal activity against clinical isolates collected in Australia (92). These conflicting reports may be due to differences in strain susceptibility and testing conditions. While povidone-iodine may be useful for *Acanthamoeba* keratitis management, its

efficacy has yet to be clinically validated and strain susceptibility tests should be considered before widespread usage (16).

Antiparasitic Agents. Miltefosine is an alkylphosphocholine antiparasitic agent commonly used for treating leishmaniasis and other parasitic infections (93). Miltefosine is believed to induce apoptosis in *Acanthamoeba* through inhibiting proteinase kinase B (32). As an anti-*Acanthamoeba* agent, it is administered orally at 50 mg three times daily, and clinical case reports have reported miltefosine treatment successfully resolved *Acanthamoeba* keratitis cases (36–41).

In vitro, miltefosine has been verified to have trophocidal and cysticidal properties (94, 95). Chao *et al* (2020) reported miltefosine to be cysticidal at 2.42 mM (94). Mrva *et al* (2011) previously reported miltefosine to be weakly active against *Acanthamoeba sp.* and *Acanthamoeba lugdunensis* clinical isolates with minimum trophocidal concentrations of 250 µM and 500 µM, respectively (96). Miltefosine's dual activity against trophozoites and cysts makes it potentially useful for treating recalcitrant *Acanthamoeba* keratitis cases.

Photodynamic Agents. Photodynamic therapy (PDT) is a form of chemotherapy in which photosensitive compounds are stimulated by light to kill cells of interest, and this therapy can be used to treat a number of diseases (97). A number of *in vitro*, animal, and clinical case studies highlight the potential for applying photosensitive agents, including tetracationic phthalocyanine RLP068, hypocrellin B, tin porphyrin, methylene blue,

riboflavin, titanium dioxide, chorin derivative TONS504, and rose bengal against *Acanthamoeba* (98–111).

Most photodynamic therapy studies have been limited to *in vitro* testing on *Acanthamoeba* isolates. Kassab *et al* (2003) reported RLP068-PDT caused nuclear damage and cell death in *A. palestinensis* trophozoites (98). Chen *et al* (2008) found hypocrellin B-PDT had a dose-dependent inhibition of trophozoites and cysts, but also noted corneal cytotoxicity (99). Siddiqui and Khan (2012) reported tin porphyrin-PDT as amoebastatic (100). Mito *et al* (2012) found methylene blue-PDT to be trophocidal and synergized with PHMB and amphotericin B (101). Del Buey *et al* (2012) evaluated riboflavin-PDT on *Acanthamoeba* isolates and reported a single dose did not completely eradicate all parasites (102). Lamy *et al* (2016) used riboflavin-PDT in doses up to ten times higher than recommended for treatment and found it did not enhance the efficacy of PHMB or chlorhexidine (103). Gomart *et al* (2018) evaluated titanium dioxide-PDT and found it yielded dual activity against *Acanthamoeba* trophozoites and cysts (104). Pertiwi *et al* (2019) evaluated chorin-derivative TONS504 and found it to cause necrosis in trophozoites and apoptosis in cysts (106). Collectively, these *in vitro* studies highlight the trophocidal and cysticidal potential of photodynamic agents.

While several agents have been evaluated *in vitro*, only a few agents have been evaluated in rabbit animal models. Pertiwi *et al* (2020) evaluated TONS504-PDT in rabbit models and reported the treatment resolved 58% of infections (105). Atalay *et al* (2020) evaluated rose bengal-PDT and reported the therapy decreased parasite loads in the rabbit corneas (107).

In regards to human clinical data, both riboflavin and rose bengal have been reported as effective. Despite equivocal *in vitro* data, several reports have noted *Acanthamoeba* keratitis resolution following riboflavin-PDT (108–110). Moren *et al* (2010), Khan *et al* (2011), and Price *et al* (2012) all reported successfully treating *Acanthamoeba* keratitis patients with riboflavin-PDT (108–110). Naranjo *et al* (2019) used rose bengal-PDT to treat a number of keratitis cases caused by various bacterial, fungal, and protozoal agents and reported a 72% case resolution rate (111). Considering several reports on riboflavin-PDT have reported successful treatment suggests this agent warrants further investigation and attention as a potential *Acanthamoeba* keratitis therapeutic.

Photodynamic therapy could potentially expand *Acanthamoeba* keratitis management options, but currently existing literature is mostly restricted to *in vitro* work. As such, photodynamic therapy warrants further investigation. Additionally, a significant effort should be made to expand the number of randomized clinical trials evaluating photodynamic agents.

Antibiotics. Several antibiotics, particularly neomycin and polymyxin-B, have been commonly used in *Acanthamoeba* keratitis management. Neomycin is a broad-spectrum aminoglycoside antibiotic that binds the ribosomal subunit to inhibit translation and protein synthesis (16). Polymyxin-B binds and disrupts microbial cell membranes (32). Neomycin, polymyxin-B, and bacitracin are also combined to form the triple antibiotic (Neosporin), which is in common ophthalmic use (43, 112).

Clinically, several case reports have detailed usage of neomycin and polymyxin-B with propamidine isethionate to resolve *Acanthamoeba* keratitis (112–116). Most notably, Hargrave *et al* (1999) performed a clinical trial evaluating neomycin-polymyxin B-gramicidin in conjunction with 0.1% propamidine isethionate and reported favorable *Acanthamoeba* keratitis outcomes (76). As such, while there is only one notable clinical trial documenting the usage of neomycin and polymyxin-B, case studies do support antibiotics being helpful in *Acanthamoeba* keratitis management. Furthermore, the use of antibiotics in treatment of *Acanthamoeba* keratitis can be prudent, as infected corneas often have co-infection with bacterial organisms as well.

Antifungal Agents. Natamycin is an antifungal agent that binds sterols in fungal cell membranes, leading to cell permeabilization and death (117). *In vitro*, natamycin has demonstrated cysticidal effects against *Acanthamoeba* (89). Clinically, natamycin can be used in conjunction with other antimicrobial agents. Kitagawa *et al* (2003) reported applying 1% natamycin ointment six times daily in combination with 0.02% chlorhexidine steadily improved cases of *Acanthamoeba* keratitis over the course of a week (118). The report also suggested the combination therapy of chlorhexidine, natamycin, and debridement as a useful keratitis management strategy (118).

Amphotericin B is a polyene antifungal agent that binds ergosterol and causes membrane instability and cell death of the pathogen (119). *In vitro*, Taravaud *et al* (2017) evaluated amphotericin B against *A. castellanii* and reported *A. castellanii* gradually displayed higher resilience to amphotericin B over time (120). Apart from *in vitro* data, clinical data and case reports on amphotericin B's use for treating *Acanthamoeba* keratitis

is limited. However, amphotericin B is commonly used to resolve keratitis cases caused by other microorganisms. Biser *et al* (2004) reported 0.5% topical amphotericin B rapidly resolved a case of *Arthrographis* keratitis that mimicked *Acanthamoeba* keratitis (121). 0.3 - 0.5% amphotericin B has been considered for fungal keratitis intervention, but its utility is limited due to its toxicity (122). Behrens-Baumann *et al* (1990) evaluated amphotericin B in a rabbit *Candida* keratitis model and recommended a combination of amphotericin B and fluconazole for *Candida* keratitis (123). As such, amphotericin B is a commonly used keratitis drug that can be considered as a potential antimicrobial agent for *Acanthamoeba* keratitis management.

1.5 Azoles as Anti-*Acanthamoeba* Agents

Azoles are a class of antifungal agents originally developed to target sterol 14a demethylase (CYP51) and inhibit ergosterol biosynthesis (124). Since *Acanthamoeba* spp. encode for CYP51 with 31-35% sequence identity to fungal CYP51, antifungal azoles have been considered and evaluated for treating *Acanthamoeba* keratitis (125). Clinically, several azoles have been evaluated in very limited clinical cases for treating *Acanthamoeba* keratitis. These include imidazole (clotrimazole, miconazole, and ketoconazole) and triazole (itraconazole, fluconazole, and voriconazole) class antifungal azoles (Table 1.2). Several azoles have been identified and suggested to have potent amebicidal and cysticidal properties against *Acanthamoeba* spp., suggesting new treatments for *Acanthamoeba* keratitis (126). Azoles are attractive for *Acanthamoeba* keratitis treatment as they are generally well tolerated (125). However, considerations into the method of administration, ophthalmic formulation, and adjunctive surgical

preparations have to be made as topically applied imidazoles poorly penetrate the corneal epithelium (127–131).

Clotrimazole. Clotrimazole is an antifungal therapy that has proven to be cysticidal *in vitro* against various *Acanthamoeba* strains (132). As such, clotrimazole is commonly used as a primary therapy against *Acanthamoeba* keratitis in combination with propamidine (133).

Four *Acanthamoeba* keratitis patients were treated with a combination therapy of 1% clotrimazole with topical neomycin sulfate-polymyxin B sulfate-gramicidin and propamidine isethionate. This therapy was coupled with 0.25% fluorometholone, four times a day, and systematic 200 mg of ketoconazole therapy twice daily (132). 1% clotrimazole was suspended in artificial tears and found to be well tolerated by patients (132).

In terms of *in vitro* data, Duma and Finley (1976) reported clotrimazole inhibited trophozoite motility at concentrations as low as 50-100 µg/mL at 24 hours and ≥100 µg/mL at 48 hours (134). Elder *et al* (1994) reported low cysticidal activity of clotrimazole with a minimum cysticidal concentration >500 µg/mL (4). Despite seemingly contradictory *in vitro* data with clotrimazole alone, a combination therapy with clotrimazole has demonstrated clinical efficacy in clearing *Acanthamoeba* keratitis cases.

There is no reported data on the corneal penetration of clotrimazole following systemic application. However, topical clotrimazole has been demonstrated to readily penetrate the cornea in rabbit models (123). Furthermore, when paired with penetrating keratoplasty, 1% clotrimazole suspended in artificial tears successfully controlled

recurrent *Acanthamoeba* keratitis, suggesting adjunctive surgical interventions can enhance clotrimazole's ocular bioavailability (132).

Miconazole. Miconazole is a relatively new antifungal agent, with limited testing outside of research settings. Several patients affected with AK were treated with 0.1% miconazole and 150 mg of oral itraconazole hourly (135). Ishibashi *et al* (1990) reported the patients showed improvement with the resolution of the *Acanthamoeba* keratitis following treatment with miconazole and itraconazole (135). In this clinical study, the patients tolerated the treatment with no adverse effects.

Miconazole's effectiveness was tested in comparison to topical neomycin-polymyxin B-bacitracin (Neosporin). Neosporin, given as four drops hourly was compared to Neosporin with 10 mg/mL miconazole, and Sharma *et al* (1990) reported miconazole did not significantly affect patient recovery (43). Ultimately, this study confirmed that miconazole did not show promise as a new antifungal therapy in the clinical setting.

Nagington *et al* (1976) reported miconazole had a minimum inhibitory concentration towards trophozoite ranging from 10-100 µg/mL and a minimum cysticidal concentration of 1000 µg/mL *in vitro* (136). In contrast, Saunders *et al* (1992) reported that 1% miconazole was not cysticidal against *Acanthamoeba* cysts (137). The mixed clinical and *in vitro* efficacy data on miconazole may be due to varying susceptibility of different *Acanthamoeba* strains.

Miconazole is not commonly administered orally, so there is little data about its circulation following oral administration. In rabbit models, de-epithelializing corneas prior to topical miconazole administration significantly improved miconazole's bioavailability in

the aqueous humor (138). Additionally, topical miconazole paired with oral itraconazole and debridement has been utilized successfully to resolve *Acanthamoeba* keratitis (135). These reports suggest adjunctive surgical preparations can enhance the bioavailability of topically applied miconazole.

Ketoconazole. Ketoconazole has been commonly prescribed as a combination therapy for the treatment of *Acanthamoeba* keratitis. Demirci *et al* (2006) reported ketoconazole administration to a patient affected with *Acanthamoeba* keratitis (139). 0.02% chlorhexidine was given hourly along with 50 mg ketoconazole administered orally daily (139). This study demonstrated the effectiveness of ketoconazole in eliminating the corneal inflammation (139). Wynter-Allison *et al* (2005) reported that the treatment with 200 mg oral ketoconazole daily, topical 0.02% chlorhexidine hourly, ciprofloxacin every four hours, and 1% atropine twice daily resulted in rapid clearance of the keratitis within a week (140). However, recurrent *Acanthamoeba* keratitis occurred, which suggests ketoconazole to be ineffective (140).

Ketoconazole's bioavailability has been evaluated in rabbit models. Hemady *et al* (1992) reported detecting high concentrations of ketoconazole in the cornea following topical or oral administration and confirmed this could be further enhanced by debriding the eyes prior to topical treatment (141). Clinically, systemic administration of ketoconazole in combination with topical miconazole has also been used successfully to prevent recurrent *Acanthamoeba* keratitis following penetrating keratoplasty (142).

Ketoconazole's contrasting results suggest further characterization of it as monotherapy and combination therapy is required to identify if ketoconazole is effective

in treating *Acanthamoeba* keratitis. Furthermore, additional characterization of ketoconazole's ocular bioavailability would help inform clinicians of its treatment potential.

Itraconazole. Itraconazole is a relatively new azole that has demonstrated extensive, broad-spectrum antimicrobial activity (143). However, Hernández-Martínez *et al* (2019) reported that *A. castellani* was minimally sensitive to itraconazole *in vitro* at a concentration of $20.14 \pm 4.93\ \mu M$ (144). After comparing itraconazole to voriconazole, they concluded that voriconazole should be used in place of itraconazole since voriconazole had more potent cysticidal effects (144).

Clinically, itraconazole has been used to treat several *Acanthamoeba* keratitis patients. Three patients were administered 150 mg oral itraconazole along with 0.1% topical miconazole following debridement, and the patients showed improvement and no sign of recurrent infection (135).

Oral itraconazole was used in combination with topical miconazole and debridement and successfully resolved *Acanthamoeba* keratitis (135). Even though oral itraconazole is commonly used for ocular infections, it appears to have poor corneal availability. 1% topical itraconazole had poor corneal penetration, suggesting that a suitable vehicle to prepare itraconazole may improve corneal penetration (145).

Fluconazole. Fluconazole is a commonly prescribed, readily available oral antifungal with broad-spectrum antimicrobial activity (146). Amoils *et al* (1999) reported administering 300 mg of fluconazole orally daily for 8 weeks following cryosurgery and

found the *Acanthamoeba* keratitis resolved in that time (52).

In vitro, Lamb *et al* (2015) reported fluconazole as a weak inhibitor (IC_{50}: 30 μM) that did not inhibit cell proliferation since its minimum inhibitory concentration toward trophozoites exceeded 64 μg/mL(125). Anwar *et al* (2018) reported that conjugating fluconazole to silver nanoparticles did not improve its anti-*Acanthamoeba* activity (147). Interestingly, Anwar *et al* (2019) reported that conjugating fluconazole to gold nanoparticles improved the drug's inhibition of *Acanthamoeba* by 11% at 5 μM (148). In summary, *in vitro* data suggests fluconazole has minimal activity against *Acanthamoeba*, but chemical modifications may improve its overall activity.

In terms of corneal bioavailability, O'day *et al* (1990) found 20 mg/kg oral fluconazole easily reached all ocular tissues in rabbit models (149). Abbasoglu *et al* also reported topical 0.2% fluconazole easily penetrated into the aqueous humor (150). Additionally, in case reports, fluconazole was effective when paired with cryosurgery, which broke the walls of the cornea, and the infection resolved in eight weeks following (52). Collectively, these reports suggest fluconazole can reach sufficiently high concentrations in the cornea.

Isavuconazole. Isavuconazole is a relatively new second-generation broad spectrum triazole (151). Isavuconazole is a promising antifungal therapy that has demonstrated cysticidal activity against *A. castellanii*, and has proven fast-acting against mycotic keratitis in clinic (152, 153). Furthermore, isavuconazole has a favorable safety profile and is well tolerated in patients (151, 154).

Isavuconazole is well tolerated and has shown success clinically. Mada *et al*

(2018) reported a patient with mycotic keratitis was administered 372 mg of isavuconazole daily for six weeks (153). After three months, the patient's eyes were reported to be free of microorganisms (153).

In vitro, Shing *et al* (2020) reported isavuconazole as amebicidal and cysticidal with an IC_{50} of 4.65 nM and a minimum cysticidal concentration of 70 μM (152). Shing *et al* (2020) also reported isavuconazole prevented excystation, suggesting isavuconazole could potentially be used to resolve recurrent *Acanthamoeba* keratitis (152). Isavuconazole's amebicidal activity was also confirmed by Rice *et al* (2020), who reported the prodrug isavuconazonium had an IC_{50} of 0.09 ± 0.02 μM (155). Interestingly, Brunet *et al* (2020) reported isavuconazole to only be mildly amoebostatic with no cysticidal activity (156). While isavuconazole has been utilized to treat fungal keratitis and *in vitro* data exists to suggest isavuconazole's effectiveness against *Acanthamoeba*, there does not appear to be clinical or *in vitro* data evaluating its corneal penetration or clinical efficacy following topical or systemic administration, suggesting the need for further evaluation.

Voriconazole. Voriconazole is an antifungal used for treating fungal infections that do not respond to other antifungal therapies (157). It has been utilized in a limited number of cases of *Acanthamoeba* keratitis.

Hou *et al* (2017) showed that while a topical treatment of 0.02% chlorhexidine and 1% voriconazole was unsuccessful, an oral administration of 200 mg of voriconazole twice daily was successful in resolving a case of *Acanthamoeba* keratitis (158). Tu *et al* (2010) also demonstrated successful treatment of three *Acanthamoeba* keratitis patients

with oral voriconazole (159). Masselam *et al* (2008) reported that five patients treated with 1% voriconazole and 0.02% PHMB showed improvement in *Acanthamoeba* keratitis (160).

Voriconazole has been reported to have a minimum inhibitory concentration versus trophozoites of 1-2 μg/mL (125). Voriconazole's cysticidal activity has been debated in conflicting reports. Iovenio *et al* (2014) reported voriconazole's minimum cysticidal concentrations to be 33.13 ± 22.83 μg/mL for clinical isolates and 46.25 ± 23.26 μg/mL for cell culture strains (161). However, Talbott *et al* (2019) reported voriconazole was not cysticidal and even antagonized chlorhexidine and propamidine activity (162). Gueudry *et al* (2018) could not recapitulate voriconazole's cysticidal activity even at concentrations of 200 μg/mL (163). Since studies of voriconazole convey equivocal findings, further characterization is necessary to evaluate voriconazole's potential clinical efficacy for *Acanthamoeba* keratitis.

Voriconazole has demonstrated corneal penetration in rabbit models and patients. 10 μg/mL topical voriconazole penetrated the cornea in rabbit models, which suggests locally applied voriconazole may penetrate the human eye as well (164). This has been validated by Lau *et al* (2008) who found 1% voriconazole eye drops readily penetrated the corneal epithelium in humans (165).

Posaconazole. Posaconazole is another broad-spectrum antifungal agent commonly used for treating recalcitrant fungal infections (166). Posaconazole has shown promise as a potential *Acanthamoeba* keratitis treatment due to its significant *Acanthamoeba* cysticidal activity (161). After identifying two cases of keratitis resistant to

other antifungal treatments, Altun *et al* (2014) prioritized treating these patients with posaconazole (167). 4 mg/mL of topical posaconazole was applied hourly and the patients demonstrated significant improvement within 5 days (167).

In vitro, reports of posaconazole's IC_{50} against trophozoites range from estimates as low as 3 nM to as high as 7.50 ± 0.39 μM depending upon strain (152, 168). Iovenio *et al* (2014) reported posaconazole as cysticidal with a minimum cysticidal concentration of 43.75 ± 25.04 μg/mL for clinical and 52.5 ± 23.75 μg/mL for cell culture strains (161). Sifaoui *et al* (2019) showed posaconazole's cysticidal effects against three strains at lower concentrations (168). Interestingly, Shing *et al* (2020) reported not being able to recapitulate posaconazole's cysticidal activity even at 200 μM (152). It is possible that the activity of posaconazole against cysts may depend on the use of different *Acanthamoeba* strains.

Posaconazole has excellent tissue penetration and was successful in resolving three cases of keratitis infections (169). Oral posaconazole is preferred for keratitis treatment as it has demonstrated excellent ocular availability as compared to relatively insoluble topical formulations (170). While *in vitro* data suggest posaconazole to be highly potent against trophozoites and potentially even cysts, there are still no clinical case studies into posaconazole's effectiveness or corneal bioavailability in treating *Acanthamoeba* keratitis.

1.6 Drug Screening Methodologies

While existing treatments and therapies effectively treat most cases of *Acanthamoeba* keratitis, a small fraction of patients suffer recurrence. Furthermore,

current treatments are nonspecific and can result in cytotoxicity to the cornea. Identifying new more-targeted agents against *Acanthamoeba* spp. would yield better treatments.

Amebicidal Screening. *Acanthamoeba* trophozoites are proliferative and metabolically active, which are useful properties to utilize for high-throughput screening. Several cell viability assays have commonly been utilized to screen compound libraries and identify amebicidal compounds (Fig. 1.2). In particular, trypan blue exclusion staining, Alamar Blue, and CellTiter-Glo cell viability assays have been utilized to assay trophozoite viability and identify amebicidal compounds.

In trypan blue exclusion staining, trophozoites treated with compounds of interest are stained with trypan blue. Live trophozoites will exclude the dye while dead trophozoites will take up the dye. Investigators can then manually determine the cell viability percentage as a function of drug concentration and identify if a compound is amebicidal. This technique has been utilized by several groups to evaluate the amebicidal effects of antimicrobials. For instance, Alizadeh *et al* (2009) assessed the efficacy of Alexidine on trophozoites by counting the number of viable trophozoites after 24 hours of Alexidine exposure (58). Padzik *et al* (2018) treated patient-isolated *Acanthamoeba* parasites with povidone iodine, chlorhexidine, and toyocamycin and counted the viable trophozoites over the course of six days (87).

While manual counting of cells in trypan blue exclusion staining is relatively inexpensive and can be easily performed with minimal equipment, it is a labor-intensive technique that is not amenable for high-throughput screening. As such, this technique is

best reserved for secondary screening on lead compounds that have already been identified through other higher-throughput screening techniques.

In addition to trypan blue exclusion staining, several cell viability assays, such as Alamar Blue and CellTiter-Glo cell viability assays have also been utilized to screen amebicidal compounds against *Acanthamoeba* spp. These assays have the benefit of being amenable to high-throughput screening.

The Alamar Blue cell viability assay is a colorimetric and fluorescent method that relies upon the reduction of resazurin (171). In this assay, metabolically active *Acanthamoeba* trophozoites reduce resazurin, which is blue and weakly fluorescent, to resorufin, which is pink and strongly fluorescent (171). This reduction can be read using an automated colorimetric or fluorescence plate reader by measuring absorbance (λ_{Abs} 570 nm and 600 nm or 540 nm and 630 nm) or fluorescence (λ_{ex} 530 - 560 nm; λ_{Em} 590 nm) (171).

McBride *et al* (2005) developed a high-throughput assay by adapting the Alamar Blue cell viability assay (172). Since its development, the Alamar Blue assay has been utilized routinely to assess the viability of *Acanthamoeba* trophozoites in primary and secondary screens to evaluate potential amebicidal compounds (144, 173–177). While the Alamar Blue cell viability assay provides higher-throughput screening than manual counting techniques, the time required for cells to reduce resazurin and provide a measurable signal can span from several hours to a day (178). This lengthy incubation period can decrease the overall throughput of a screen performed using Alamar Blue.

As an alternative to the Alamar Blue assay, the CellTiter-Glo assay is a luminescence-based cell viability assay (179). In this assay, the ATP from lysed live cells

is utilized by luciferase to catalyze the conversion of luciferin to oxyluciferin and provide a luminescent signal that can be measured by a luminescence plate reader (179).

Since *Acanthamoeba* trophozoites are highly metabolically active, measuring ATP levels can determine the relative inhibition of proliferation as a function of drug concentration. Rice *et al* (2020) screened the MMV pandemic response box with the CellTiter-Glo cell viability assay (Promega) and identified several amebicidal compounds against *A. castellanii* (155). CellTiter-Glo has also been utilized to screen azole and statin activity against *A. castellanii* (152, 180). Since CellTiter-Glo has a significantly shorter incubation time than Alamar Blue, utilizing this viability assay in primary screening of a compound library can help increase throughput (178, 179).

Cysticidal Screening. Considering that 5 to 10% of *Acanthamoeba* keratitis patients suffer recurrence due to cyst resistance and persistence through therapy, identifying drugs that are both highly amebicidal and cysticidal is of the utmost importance for improving *Acanthamoeba* keratitis outcomes (32, 67).

Currently, two techniques are commonly used to determine if a drug is cysticidal. The first technique revolves around trypan blue exclusion staining of drug-treated cysts (94, 174, 181). The second technique involves an excystation assay, where treated cysts are manually observed over a time course for evidence of excystation or release of trophozoites from cysts and multiplication of metabolically active trophozoites (Fig. 1.3) (7, 58, 161).

Trypan blue exclusion staining is a cell viability assay where intact, live cells exclude the trypan blue dye. In this assay, drug-treated cysts are stained and manually

assessed for viability by counting to determine the percentage of viable cysts. This technique has been utilized to assay the cysticidal activity of a number of compounds. For instance, Mafra *et al* (2013) utilized trypan blue exclusion staining with an automated cell counter to determine the viability of cysts following chlorhexidine and PHMB treatment (70). Jha *et al* (2014) utilized this technique to assay *Acanthamoeba* cyst viability following chloroquine treatment (182).

In an excystation assay, *Acanthamoeba* trophozoites are cultured on non-nutrient agar plates containing heat-killed *Escherichia coli* to generate cysts (59). The cysts are collected, treated with compounds of interest for 48 hours, plated onto new non-nutrient agar plates, and observed daily under a microscope for a week (59). Compounds are considered cysticidal if there is no evidence of excystation, such as proliferating trophozoites, even after 7 days on the new agar plates (59). This technique has been utilized to evaluate numerous potentially cysticidal antimicrobials. Alizadeh *et al* (2009) evaluated Alexidine's cysticidal activity (58). Iovieno *et al* (2014) assayed several azole and antifungal agents to identify two potentially cysticidal compounds using this technique (161).

Evaluating the cysticidal effects of antimicrobial compounds can be inherently challenging, as manual counting and observation of cysts under a regular microscope is labor-intensive, subject to human error, and low-throughput. These limitations prevent trypan blue viability and excystation assays from being effectively utilized to screening large compound libraries. As such, development of a high-throughput cysticidal assay amenable to automation would significantly increase the rate at which anti-*Acanthamoeba*

cysticidal compounds can be identified.

1.7 Conclusions

Acanthamoeba keratitis is a relatively rare infection and while biguanide and diamidine-based treatments are quite effective at resolving most cases, there are some clinical reports of recalcitrance and resistance (32, 67). As such, discovery of new chemotherapeutic agents could significantly expand *Acanthamoeba* keratitis treatment options.

Current efforts to identify new anti-*Acanthamoeba* compounds rely primarily upon trophocidal assays that utilize commercially available cell viability assays while cysticidal assays require manual observation of drug-treated cysts for evidence of excystation or counting viable cysts through trypan blue cell viability staining (59, 94, 152, 155, 172, 174). Since no *Acanthamoeba* keratitis panacea currently exists and cysts likely contribute to treatment failure, assays that can identify cysticidal compounds will be crucial. Excystation-based assays that measure if cysts can excyst following drug treatment provide direct evidence of a drug's cysticidal potential. As such, any drug leads that are identified to be trophocidal should also be screened through cysticidal assays, such as excystation assays or trypan blue viability assays, to identify drugs with dual activity against trophozoites and cysts.

Clinical studies and *in vitro* drug screens on the efficacy of azole antifungal agents against *Acanthamoeba* spp. have yielded varying results with reports suggesting a number of azoles are effective against *Acanthamoeba* spp. Compounds, such as posaconazole, isavuconazole, clotrimazole, voriconazole, itraconazole, and miconazole

have been reported to be effective against trophozoites (125, 134, 136, 144, 152, 168). Posaconazole and isavuconazole have been reported to be cysticidal as well (152, 161). Fluconazole and ketoconazole have conflicting reports regarding their activities against trophozoites and cysts (125, 140, 148).

Considering the availability and general tolerability of azole antifungal agents, they could be worthwhile additions to the clinical armamentarium against *Acanthamoeba* keratitis if evaluated further. While antifungal azoles are generally believed to not penetrate the corneal epithelium well when topically applied, alterations in the method of administration, formulation changes, and adjunctive surgical preparations could enhance corneal penetration and improve the efficacy of azole antifungal agents.

1.8 Expert Opinion

Within the next five to ten years, research into screening and identifying new compounds effective against *Acanthamoeba* will likely continue to be driven by academic institutions rather than the pharmaceutical or contact lens industries. Since trophozoites are less labor-intensive to work with and typically more susceptible to drugs than cysts are, the rate of discovery for trophocidal compounds will likely far exceed that of cysticidal compounds. Despite this, identifying cysticidal compounds will still be paramount as cysts are a likely contributor to recalcitrance and treatment failure in *Acanthamoeba* keratitis.

Considering the difficulty and laborious nature of cysticidal assays, this could be a key area for research and development. Current cysticidal assays either rely upon trypan blue viability staining or manual observation of cysts for evidence of trophozoite excystation. Since both of these approaches are manual and low-throughput, any

developments in automation and miniaturization could significantly increase the throughput of cysticidal drug screens to yield new cysticidal compounds. Developing a commercially available biochemical viability assay that is unaffected by the cysts' metabolic dormancy and resilient cyst walls and highly amenable to high-throughput screening would also further speed up cysticidal drug discovery.

Since combination therapies have proven more successful than single-drug monotherapies, researchers should strongly consider employing drug combination experiments in both trophocidal and cysticidal assays. While combination experiments in *in vitro* trophocidal assays are straightforward and the dose-effect relationships between two drugs can be assessed by classical isobolograms, development of a combination experiment in the cysticidal assay *in vitro* may prove challenging due to trypan blue staining being low-throughput and excystation-based cysticidal assays revolving on a "cysticidal-or-not" basis rather than percentage inhibition. Additionally, testing the efficacy of combination therapies *in vivo* introduces an additional layer of complexity. Despite these challenges, it is worthwhile to test compounds *in vitro* in monotherapy and combination therapy during the early stages of drug discovery and development as this will provide researchers direction on the selection of compounds that may bring a greater chance of success in *in vivo* efficacy experiments.

Several hurdles remain in discovering and implementing new anti-*Acanthamoeba* agents clinically. *Acanthamoeba* keratitis is relatively rare with estimates as low as one to two per million contact lens wearers annually developing *Acanthamoeba* keratitis (183). Since there are relatively few *Acanthamoeba* keratitis patients, there is minimal need and financial incentive for the pharmaceutical and contact lens industries to invest in the

discovery of new antimicrobial agents. However, considering the rarity of the disease, identification of a lead that is efficacious in the animal model of *Acanthamoeba* keratitis also brings an advantage of receiving orphan drug status from the FDA, which may encourage more research efforts into identifying anti-*Acanthamoeba* therapeutics.

Medical precedence also poses an additional hurdle to implementing any newly discovered antimicrobial agents as biguanide and diamidine therapies work well for the majority of *Acanthamoeba* keratitis patients. In spite of these challenges, it is possible that the infection is underdiagnosed as a retrospective study from a single center in Iowa showed that the average number of new *Acanthamoeba* keratitis cases per year among Iowa residents doubled during 2010-2017 (183). The rapid increase in *Acanthamoeba* keratitis case numbers has led the National Institutes of Health to label *Acanthamoeba* keratitis as an Emerging Infectious Disease.

Since *Acanthamoeba* keratitis is an Emerging Infectious Disease, this re-emphasizes the importance for the discovery of better therapies for its treatment. Identifying novel antimicrobial agents with dual activity against *Acanthamoeba* trophozoites and cysts would yield more potential therapy options for clinicians to treat *Acanthamoeba* keratitis and reduce the prevalence of patient relapse and recalcitrant infections to improve patient outcomes.

Acknowledgments

Chapter 1, in full, is a reprint of the material as it appears in Brian Shing, Mina Balen, James H McKerrow, Anjan Debnath "*Acanthamoeba* Keratitis: an Update on Amebicidal and Cysticidal Drug Screening Methodologies and Potential Treatment with

Azole Drugs” Expert Review Anti-Infective Therapy, 2021. The dissertation author was the primary author and a major contributor to this review.

1.9 Figures and Tables

TABLE 1.1 Common Drugs and Concentrations used for Treating *Acanthamoeba* Keratitis. *Treatment dosing not well standardized.

Drug (treatment concentration)	**Reference**
Chlorhexidine (0.02 - 0.1% topical eye drops)	(50)
PHMB (0.02 - 0.06% topical eye drops)	(50)
Hexamidine (0.1% topical eye drops)	(50, 81)
Propamidine (0.1% topical eye drops)	(50)
Natamycin*	(118)
Amphotericin B*	(32)
Neomycin*	(73, 75, 76)
Polymyxin B*	(32)
Povidone-iodine*	(16)
Miltefosine (50 mg oral)	(36, 39, 40)

TABLE 1.2 *Acanthamoeba* Keratitis Experimental Therapies.

Experimental azole-based drug combinations	
0.02% PHMB + 0.1% propamidine	(74)
0.02% chlorhexidine + 0.1% propamidine	(77)
200 mg ketoconazole + 0.2% chlorhexidine + ciprofloxacin + 1% atropine	(140)
Oral itraconazole + 0.1% topical miconazole + surgical debridement	(135)
0.1% miconazole + 150 mg oral itraconazole	(135)
0.02% chlorhexidine + 50 mg ketoconazole	(139)
1% voriconazole + 0.02% PHMB	(160)
Cryosurgery + 300 mg oral fluconazole	(52)
4 mg/mL topical posaconazole	(167)

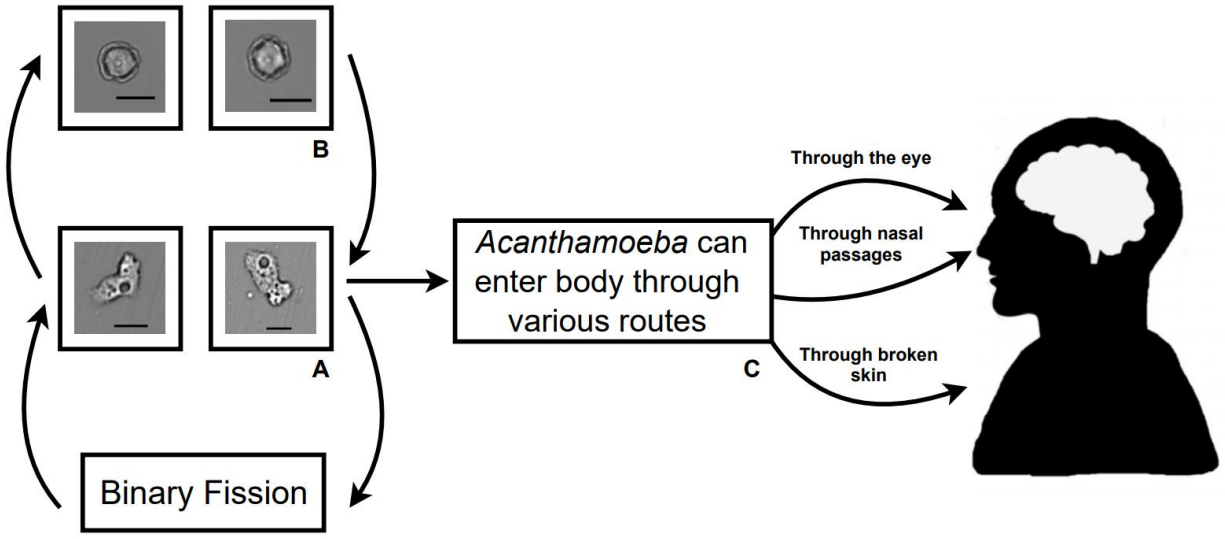

Figure 1.1 Life Cycle and Pathogenesis of *A. castellanii*. (A) *Acanthamoeba* spp. proliferates via binary fission as motile trophozoites. (B) Under sub-optimal growth conditions, *Acanthamoeba* spp. can encyst to form dormant, double-walled cysts. (C) *Acanthamoeba* spp. trophozoites or cysts can be opportunistic pathogens and infect humans through the eyes, nose, or broken skin. Magnification: 200x; Scale bar: 30 µm.

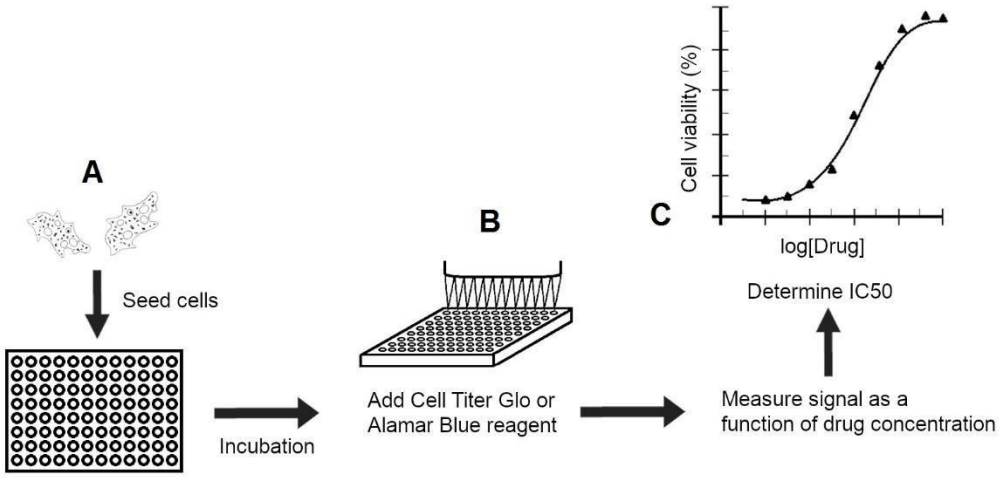

Figure 1.2 Current Amebicidal Screening Techniques. (A) Current high-throughput amebicidal drug screening techniques incubate trophozoites in multiwell screening plates with compounds of interest. (B) The screening plates are then assayed through Alamar Blue or CellTiter-Glo cell viability assays to determine cell viability as a function of drug concentration. (C) Compounds with potent activity at low drug concentrations are considered hits and assessed further to determine the IC_{50} through secondary screens.

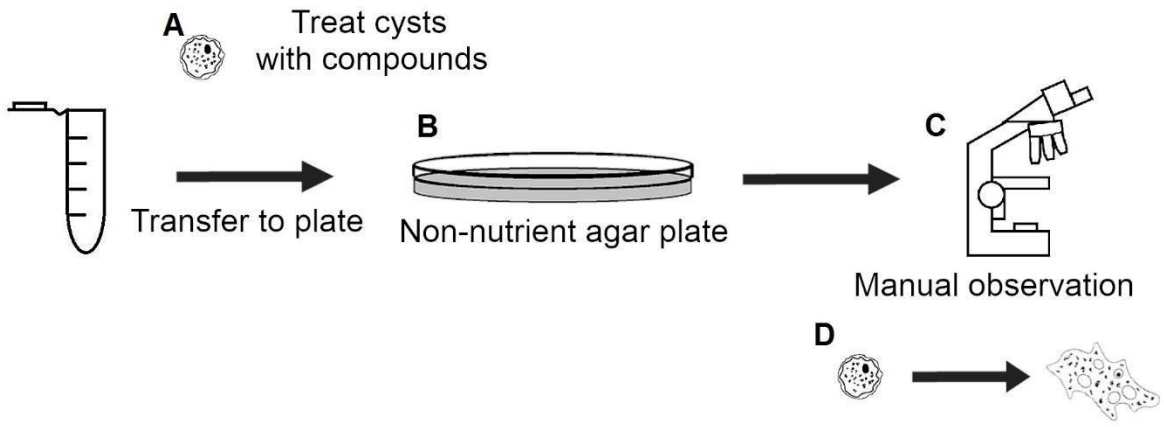

Figure 1.3 Traditional Cysticidal Screening Workflow. (A) Cysts are treated and incubated with compounds of interest. (B) Treated cysts are transferred to non-nutrient agar plates with *E. coli*. (C) Plates are manually imaged and observed daily for evidence of excystation. (D) Observe excystation and proliferation of trophozoites or trails left behind in agar media to manually determine if compound of interest was cysticidal.

Chapter 2: The Antifungal Drug Isavuconazole is both Amebicidal and Cysticidal against *Acanthamoeba castellanii*

2.1 Introduction

Acanthamoeba castellanii is a free-living ameba. It has been encountered in and isolated from various environmental sources, such as soil, dust, atmosphere, and water (184, 185). Its life cycle consists of a motile, feeding, and replicative ameboid stage (trophozoite) and a dormant cyst stage that is resistant to suboptimal environmental conditions (186).

A. castellanii may cause skin and brain infections, but is typically associated with *Acanthamoeba* keratitis, a painful, severe infection of the cornea that can result in blindness or visual impairment (187). While *Acanthamoeba* keratitis is rare, it is an emerging disease that has steadily increased in incidence over the past several decades (188, 189).

The most common routes of *Acanthamoeba* infection are through improperly cleaned contact lenses or corneal trauma (15). Once the trophozoites enter the eye, they invade the corneal epithelium and surrounding stroma (1, 15). The infection causes the rapid depletion of corneal keratocytes (1, 190). The infection may then trigger severe inflammation of the conjunctiva, cornea, episclera, and sclera (1, 190). In response, neutrophils and macrophages will infiltrate the cornea (15, 190). Infiltration of neutrophils leads to further necrosis in the cornea (1).

If the infection is not cleared through medical intervention, the trophozoites can spread to the retina and cause chorioretinitis (191–193). The most aggressive and severe

cases of *Acanthamoeba* keratitis require corneal grafts or surgical removal of the eye (194). *Acanthamoeba* keratitis can occur in immunocompetent patients, and clearance of the infection does not provide sterilizing immunity (1).

In the United States, the majority (>80%) of *Acanthamoeba* keratitis cases involve contact lens wearers (195, 196). As of 2017, the contact lens industry generates $11.5 billion annually and serves approximately 45 million contact lens wearers in the United States. Nevertheless, there has been minimal interest in identifying and developing new drugs to effectively treat or prevent *Acanthamoeba* keratitis (32, 197, 198).

Current *Acanthamoeba* keratitis treatments rely on diamidines, biguanides, and antifungal azole derivatives (conazoles) to kill the trophozoites (15). Treatment typically consists of a combination of chlorhexidine gluconate, propamidine isethionate, and polyhexamethylene biguanide (PHMB) (189). While PHMB and chlorhexidine are effective at killing *Acanthamoeba* trophozoites, these drugs are aggressive and cannot be tolerated at high doses, which limits their effectiveness (60). Antifungal azole derivatives, such as clotrimazole, miconazole, ketoconazole, and itraconazole, have also been used clinically with limited efficacy to treat *Acanthamoeba* keratitis (1). Overall, in approximately 10% of all *Acanthamoeba* keratitis cases, recurrent infection ensues due to the difficulty of killing both *Acanthamoeba* trophozoites and cysts (32).

While A. *castellanii* has proven to be a difficult pathogen to treat effectively, previous work, including clinical studies, has suggested sterol biosynthesis could be targeted to inhibit *Acanthamoeba* trophozoites (125, 199). In *Acanthamoeba* trophozoites, ergosterol is indispensable and the major biosynthetic pathway for producing ergosterol is through the conversion of cycloartenol (200, 201). Sterol 14-

demethylase (CYP51) is an essential enzyme in ergosterol biosynthesis both in fungi and protozoa. A. *castellanii* encodes a CYP51 with sequence identity of 31 to 35% to fungal CYP51 (125). Previous studies demonstrated that inhibition of CYP51 led to reduced growth of A. *castellanii* trophozoites and induced encystment that produced nonviable cysts (125, 200, 202).

Antifungal azole derivatives known as conazoles are FDA-approved CYP51 inhibitors that include itraconazole, voriconazole, posaconazole, fluconazole, ketoconazole, clotrimazole, isavuconazole, and miconazole (124, 203). These drugs inhibit fungal CYP51 to prevent the conversion of lanosterol to ergosterol, which causes the rapid depletion of ergosterol and the accumulation of ergosterol precursors and nonphysiological end products (204, 205). Since ergosterol is a major component of fungal membranes, depleting this sterol causes leakage of cell membranes, leading to cell death (205). While azole derivatives have primarily been approved for treating fungal infections, some of these drugs have also been evaluated for treating *Acanthamoeba* keratitis, but with limited success.

Current methods used for identifying amebicidal compounds against *Acanthamoeba* are labor-intensive and rely upon microscopy and traditional cell-counting methods using hemocytometers and staining agents (59, 206–208). Until recently, most efforts to identify new anti-*Acanthamoeba* compounds via whole parasite screening have focused on the development of screening methodology and its validation by reference drugs, such as chlorhexidine (208). In this study, we optimized a commercially available bioluminescence-based viability assay for high-throughput screening of compounds against *Acanthamoeba* trophozoites. Using this assay, we systematically assessed the

FDA-approved conazoles and identified isavuconazole as the most potent target- specific anti-*Acanthamoeba* agent. As an added benefit, isavuconazole was effective against both A. *castellanii* trophozoites and cysts.

2.2 Results

Viability assay for A. *castellanii* trophozoites. Assays commonly used to assess amebicidal activity of compounds against *Acanthamoeba* are labor-intensive and not easily amenable to high-throughput compound screening (59, 206–208). To accelerate anti- *Acanthamoeba* drug discovery, we adopted the CellTiter-Glo luciferase-based assay (Promega) that is based on the correlation between the number of live microorganisms and the ATP level. In *Acanthamoeba*, the relationship between the number of trophozoites seeded into 96-well plates and luminescence from the CellTiter-Glo assay showed a strong linear correlation (R^2 0.88) (Fig. 2.1A). A total of 5 x 10^3 trophozoites per well were used in subsequent experiments. When various amounts of dimethyl sulfoxide (DMSO) were added to a culture of 5 x 10^3 trophozoites in the 96-well microtiter plate format, trophozoites readily tolerated up to 0.5% (vol/vol) DMSO with no statistically significant degradation of growth rate (Fig. 2.1B). At 1% DMSO (vol/vol) treatment, trophozoites showed significant growth inhibition (Fig. 2.1B).

In vitro activity of CYP51 inhibitors against *A. castellanii* trophozoites. Given that activity of some azole antifungal drugs against *A. castellanii* has been demonstrated by different laboratories (125, 200, 209), we took advantage of the newly developed microtiter plate ATP bioluminescence-based assay to systematically evaluate eight FDA-

approved conazoles, including the latest addition to the armamentarium of the antifungal drugs, isavuconazole. For the drug screen, we selected the *A. castellanii* Ma strain, representing the T4 genotype, because nearly all reported *Acanthamoeba* keratitis infections are associated with the T4 genotype (210). The drugs demonstrated activity against *A. castellanii* in a range of 3% growth inhibition at 50 μM for fluconazole to a 50% effective concentration (EC_{50}) of 5 nM for isavuconazole (Table 1.1). Notably, the in vitro potency of isavuconazole, voriconazole, clotrimazole, posaconazole, and ketoconazole exceeded that of the current drugs chlorhexidine and PHMB. Isavuconazole, posaconazole, clotrimazole, and voriconazole were an order of magnitude more potent than chlorhexidine, while ketoconazole was equipotent to chlorhexidine. Since isavuconazole and posaconazole demonstrated a low nanomolar potency against the *A. castellanii* Ma strain, their potencies against other *A. castellanii* clinical strains of T4 genotype were also evaluated. In the *A. castellanii* CDC:V240 and *A. castellanii* MEEI 0184 strains, the 48-h EC_{50} values of isavuconazole were determined to be 0.9 nM and 25.7 nM, respectively (Fig. 2.2B and 2.2C), which are comparable in magnitude to the A. *castellanii* Ma strain's 48-h EC_{50} of 4.6 nM (Fig. 2.2A). Posaconazole was also assayed against A. *castellanii* CDC:V240 and A. *castellanii* MEEI 0184 and the 48-h EC_{50} values were determined to be 65.3 nM and 3.0 nM, respectively (Fig. 2.2E and 2.2F), which are comparable to the A. *castellanii* Ma strain's 48-h EC_{50} of 44.5 nM (Fig. 2.2D). These growth inhibition curves suggest that the two most potent drugs, isavuconazole and posaconazole, are broadly efficacious against A. *castellanii* trophozoites (Table 2.1).

Growth inhibition as a function of time. To assess how quickly isavuconazole and posaconazole kill trophozoites, growth inhibition of A. *castellanii* Ma strain trophozoites was measured at 16, 24, 36, and 48 h of drug exposure. Trophozoites were exposed to isavuconazole or posaconazole serially diluted from 50 μM to 5.96 pM in DMSO. The resulting growth inhibition curves (Fig. 2.3) show that isavuconazole and posaconazole have similar inhibitory effects. Both drugs reached 50% inhibition at 24 h of exposure and 90% at 36 h of exposure. The effect of both drugs maximized at 48 h, when the isavuconazole potency (EC_{50} of 0.005 M) exceeded the posaconazole potency (EC_{50} of 0.04 M) by 10-fold (Fig. 2.3). Although chlorhexidine (EC_{50} of 1.7 M) and PHMB (EC_{50} of 7.3 M) were faster-acting drugs than conazoles, with measurable inhibition as early as 16 h of exposure (Fig. 2.3), target-specific posaconazole and isavuconazole demonstrated potency 40-fold and 300-fold, respectively, higher than the current standard- of-care chlorhexidine.

Effect of isavuconazole on trophozoite morphology and viability. Since isavuconazole was the most potent anti-*Acanthamoeba* azole identified in this study, we assessed the effect of isavuconazole on trophozoite viability and morphology. A. *castellanii* Ma strain trophozoites were treated with 45 nM (~10x EC50 concentration) of isavuconazole and the effect elicited by this concentration of isavuconazole was compared with the effect elicited by 16.6 μM chlorhexidine (~10x EC50 concentration). Trophozoites treated with 0.5% DMSO displayed normal morphology and growth. The trophozoites displayed membrane integrity at 24, 36, and 48 h. Each trophozoite displayed clearly visible food vacuoles and a large nucleus containing the nucleolus.

There was no evidence of DMSO growth inhibition at 24, 36, or 48 h (Fig. 2.4A). Treatment with 16.6 μM chlorhexidine led to cell death as early as 24 h postexposure (Fig. 2.4B). No cell proliferation was observed from 24 to 48 h. Instead, significant amounts of cell debris and membrane components were observed in the medium of chlorhexidine- treated trophozoites, which is consistent with cell lysis. Chlorhexidine-treated trophozoites displayed abnormal morphology characterized by a significant increase in cellular granularity and the disappearance of food vacuoles and nucleolus structure. Treatment with isavuconazole at 45 nM likewise resulted in significant growth inhibition and cell death (Fig. 2.4C). At 24 h, isavuconazole-treated trophozoites began showing signs of cellular rounding compared to the DMSO-treated trophozoites. At 36 and 48 h, the trophozoites completely rounded and detached from the bottom of the culture plate. There was also an appreciable increase in cellular granularity and no significant cellular proliferation between 36 and 48 h (Fig. 2.4C). Furthermore, the medium of isavuconazole-treated trophozoites displayed more cellular debris and membrane components than that of 16.6 μM chlorhexidine.

Evaluation of cysticidal activity. The cysticidal activity of isavuconazole and posaconazole was evaluated using cysts of the A. *castellanii* Ma strain. Preformed cysts were treated with various concentrations (200, 150, 100, 90, 80, 70, 60, 50, 40, and 30 μM) of isavuconazole or posaconazole. Chlorhexidine (0.02% [wt/vol], equivalent to 395.7 μM) and PHMB (equivalent to 1079.5 μM) were used as positive controls, while 0.5% DMSO was used as a negative control. Isavuconazole was cysticidal at 70 μM (Fig. 2.5A). At isavuconazole concentrations below 70 μM (Fig. S2.1A and S2.1B), various levels of

delayed excystation were observed. Excystation was only apparent at day four. Following treatment with 30 μM isavuconazole, cultures became confluent with trophozoites by day six (Fig. S2.1B).

Remarkably, treatment with posaconazole did not prevent excystation. The highest concentrations of posaconazole tested (200 and 150 M) still showed signs of excystation and became confluent with healthy trophozoites by day six (Fig. 2.5B, Fig. S2.1C).

Treatment with chlorhexidine or PHMB (0.02% [wt/vol]) prevented excystation (Fig. 2.5C and 2.5D), suggesting that chlorhexidine and PHMB killed the cysts. By day four, the DMSO-treated cysts displayed normal excystation (Fig. 2.5E) with no evidence of any remaining cysts and became confluent with healthy trophozoites.

2.3 Discussion

In this study, a luciferase-based viability assay was adopted and optimized for *Acanthamoeba* to accelerate screening for amebicidal compounds. This assay was previously used with a number of other pathogens, including trypanosomes, *Entamoeba*, *Giardia*, and *Naegleria* (211–217). It represents a clear improvement over current *Acanthamoeba* methods that require a tedious liquid and cell transfer and prolonged read-outs. It also reduces the cost of reagents and hours of labor required to screen large compound libraries. The utility of the newly developed luciferase-based method was validated for A. *castellanii* trophozoites by systematically assessing a set of drugs, known as conazoles or antifungal azoles, which target the 14-demethylation step in sterol biosynthesis catalyzed by CYP51.

Conazoles were developed as antifungal agents, but their therapeutic potential has also been demonstrated in kinetoplastids (199) and Naegleria (201). Select azole antifungals tested in previous studies against A. *castellanii* exhibited potencies comparable to that of chlorhexidine (125, 144, 200), which encouraged us to systematically assess this class of drugs for A. *castellanii* growth inhibition. We identified two azoles, posaconazole and isavuconazole, to be about 40-fold and 300-fold more potent against A. *castellanii* Ma strain than the current standard-of-care chlorhexidine. While posaconazole was about 17- to 300-fold more potent than chlorhexidine against CDC:V240 and MEEI 0184 strains, isavuconazole exhibited about 40- to 1,000-fold more activity than chlorhexidine against MEEI 0184 and CDC:V240 strains. Posaconazole was previously reported as amebicidal (177). However, isavuconazole, a newer broad-spectrum antifungal drug, is demonstrated here to be the most potent amebicidal agent among conazoles tested so far. Isavuconazole was approximately 10-fold and 65-fold more potent than posaconazole against Ma and CDC:V240 strains, respectively, and exhibited low nanomolar potency against three clinical strains of A. *castellanii*. Both isavuconazole and posaconazole were relatively fast-acting against *A. castellanii* trophozoites, with 50% growth inhibition achieved as early as 24 h postexposure. The rapid activity of isavuconazole was also evident from morphological studies, where nanomolar concentrations of isavuconazole promoted rounding of cells within 24 h of treatment and had effects comparable to low micromolar concentrations of chlorhexidine.

The inhibitory activity of isavuconazole and posaconazole against trophozoites led us to test their effectiveness against A. *castellanii* cysts. A sterol metabolome study of A. *castellanii* revealed that marked changes in sterol composition are associated with ameba

differentiation (202). Stage-specific sterol profiling during the growth and encystment phases identified metabolic markers for viable and nonviable cysts. This previous metabolome study showed that only viable cysts can excyst into trophozoites (202). To determine if posaconazole and isavuconazole could suppress excystment of preformed *Acanthamoeba* cysts into trophozoites, we established an *Acanthamoeba* encystation assay in a 96-well format and treated mature cysts with different concentrations of drugs. Our microscopy-based assay found that treating mature cysts of the *A. castellanii* Ma strain for 48 h with 70 M (30.6 g/ml) of isavuconazole prevented excystation. Treatment of cysts of the same strain with 200 M posaconazole did not prevent excystation. This is in contrast to a reported study where the minimal cysticidal concentration of posaconazole was found to be 57 μM or 114 μM against two different strains of A. *castellanii* (161). It is not clear if the differences in the cysticidal activity of posaconazole are due to the differences in the strains used in the excystation studies or due to the differences in the methods used to demonstrate the cysticidal activity of posaconazole.

Isavuconazonium sulfate, a water-soluble isavuconazole prodrug, is the most recently developed antifungal triazole drug, approved in 2015 by the FDA for treating adults with invasive aspergillosis or invasive mucormycosis. Isavuconazole is given either in an intravenous (IV) or oral formulation at 200 mg once daily, following a loading dose of 200 mg every 8 h for the first 48 h (218). The drug is readily absorbed when administered orally, with a bioavailability of 98% (219). It has a half-life of 130 h (218) and a large volume of distribution (400 to 500 liters) (220). A phase 3 clinical trial that assessed the efficacy and safety of isavuconazole and voriconazole in patients with invasive aspergillosis found that isavuconazole was well tolerated with significantly fewer

drug-related adverse events of the skin, eye, and hepatobiliary systems than voriconazole (221).

Although isavuconazole is only currently available in IV and oral formulations and *Acanthamoeba* keratitis treatment conventionally requires topical administration, CYP51 inhibitors can meet the demand for development of topical anti-*Acanthamoeba* keratitis agents. Ophthalmic formulation has been developed to topically administer another antifungal azole drug, econazole, which has poor aqueous solubility (222).

An economic model to determine the costs and cost-effectiveness of isavuconazole versus voriconazole in hospitalized patients with invasive aspergillosis suggested that isavuconazole was a cost-effective option (223). Based on the wholesale acquisition costs from ReadyPrice (Thomson), the price of 372 mg of isavuconazonium sulfate (equivalent to 200 mg of isavuconazole) was $238.50 and $70.00 for the IV and oral formulations, respectively (223). Considering the shorter treatment schedule for *Acanthamoeba* keratitis, treatment with isavuconazole may be cost-effective.

Future studies will involve the development of an ophthalmic formulation and testing the efficacy of isavuconazole in an animal model of *Acanthamoeba* keratitis. Based on its excellent safety profile, isavuconazole presents an opportunity to cost-effectively repurpose this drug for the treatment of primary and recurring *Acanthamoeba* keratitis.

2.4 Materials and Methods

A. castellanii strains and cultures. The *A. castellanii* reference strain Ma was acquired from the American Type Culture Collection (number 50370). The A. *castellanii*

CDC:V240 strain of the T4 genotype was acquired from the Centers for Disease Control and Prevention (CDC) and the A. *castellanii* MEEI 0184 strain of the T4 genotype (224) was obtained from Tufts University. *A. castellanii* trophozoites were cultured and maintained at 28°C and 5% CO2 in peptone yeast glucose (PYG) medium supplemented with 1% penicillin-streptomycin (225, 226).

Cyst generation. *A. castellanii* (Ma strain) encystment was induced by culturing trophozoites in a modified Page's ameba saline encystation medium (95 mM NaCl; 5 mM KCl; 8 mM MgSO4; 0.4 mM CaCl2;1 mM NaHCO3; 20 mM Tris-HCl, pH 9.0) (227). A. *castellanii* trophozoites were collected by centrifugation at 200 g for 5 min. The trophozoites were then washed in phosphate-buffered saline (PBS) twice before being resuspended in encystation medium. The cells were cultured in the encystation medium for at least 48 h to generate cysts prior to any experiments requiring A. *castellanii* cysts.

Viability assay for A. *castellanii* trophozoites. The assay was developed in sterile 96-well microtiter plates with exponentially grown, 48 h-old A. *castellanii* Ma strain trophozoites. ATP is an essential cofactor for biogenesis in A. *castellanii*, so a luciferase-based assay was used to validate the correlation between the number of viable trophozoites and their ATP levels. Trophozoites were counted and 2.5 x 10^3, 5 x 10^3, 10 x 10^3, or 20 x 10^3 trophozoites in 100 µl of PYG medium were seeded into the wells of 96-well microtiter plates under sterile conditions. Assay plates were incubated for 48 h at 28°C and 5% CO_2. At the end of the incubation, the plates were equilibrated to room temperature for 30 min. An aliquot of 25 µl of CellTiter-Glo luminescent cell viability assay

solution (Promega) was added to each well. The microplates were shaken on a microplate orbital shaker (VWR) at 360 rpm for 10 min to facilitate cell lysis, and the plates were then incubated for an additional 10 min to stabilize the luminescent signal. The resulting ATP-bioluminescence of the trophozoites was measured by an EnVision 2104 Multilabel Reader (Perkin Elmer) at room temperature.

Once the number of viable trophozoites that would be used in the subsequent experiments was determined, trophozoites were then treated with various amounts of DMSO (ranging from 0% to 1%) to optimize the percentage of DMSO that *Acanthamoeba* could tolerate. Trophozoites were incubated at 28°C and 5% CO_2 for 48 h, and the ATP-bioluminescence was assayed at the end of the incubation.

In vitro activity of CYP51 inhibitors against *A. castellanii* trophozoites. Azole stocks were prepared in DMSO at a concentration of 20 mM, while PHMB and chlorhexidine control drugs were dissolved in DMSO at a concentration of 10 mM. The conazoles and control drugs were serially diluted one to two parts 24 times in DMSO to generate solutions from 10 mM to 1.2 nM. The compounds were then added to 96-well Greiner Bio-One Cellstar white, flat bottom microplates. Aliquots of 0.5 µl of drugs were added to each well. *A. castellanii* trophozoites were counted, and 5×10^3 trophozoites in 99.5 µl of PYG media were added to each well.

After incubation for 48 h at 28°C and 5% CO_2, cell viability measurements were taken using the CellTiter-Glo luminescent cell viability assay on the EnVision 2104 Multilabel Reader. The data were analyzed on GraphPad Prism 6 to determine EC50 values and 95% confidence intervals.

Growth inhibition as a function of time. To determine the rate of killing, growth inhibition of the *A. castellanii* Ma strain trophozoites was measured for isavuconazole, posaconazole, chlorhexidine, and PHMB at 16 h, 24 h, 36 h, and 48 h of exposure to serially diluted drug concentrations ranging from 50 μM to 5.96 pM. The growth inhibition assay was done in triplicate in three independent experiments and the EC_{50} values of isavuconazole and posaconazole were determined at different time points by CellTiter-Glo luminescent cell viability assay.

Effect of isavuconazole on trophozoite morphology and viability. 5 x 10^3 trophozoites in 99.5 μl of PYG medium were plated onto clear 96-well flat bottom microplates and the trophozoites were treated with 0.5% DMSO, 16.6 μM of chlorhexidine, and/or 45 nM isavuconazole for 48 h. The effect of isavuconazole on cellular morphology was determined by imaging the trophozoites at 24, 36, and 48 h and compared to the effect of chlorhexidine. Images were acquired using the Molecular Devices ImageXpress Micro XLS and adjusted for brightness and contrast in ImageJ.

Evaluation of cysticidal activity. A. *castellanii* trophozoites were collected by centrifugation at 200 g for 5 min. The trophozoites were then washed in PBS three times before resuspension in encystation medium. Aliquots of 5 x 10^3 trophozoites were added to each well of a 96-well plate and wells were filled to 100 μl with encystation medium. The cells were then incubated for 48 h prior to addition of compounds.

After 48 h, the encystation medium in each well was exchanged for encystation medium with 200,150, 100, 90, 80, 70, 60, 50, 40, or 30 μM azole (isavuconazole or posaconazole). DMSO at 0.5% served as a negative control, while 0.02% (wt/vol) chlorhexidine and 0.02% (wt/vol) PHMB served as positive controls. The mature cysts were then incubated with compounds for an additional 48 h. At the end of 96 h, the encystation medium was washed three times with PBS before addition of 100 μl of PYG medium. A. *castellanii* cysts were then incubated in PYG media and imaged daily on a Zeiss Axio Vert.A1 microscope and Molecular Devices ImageXpress Micro XLS. After every additional 48 h, the medium was exchanged for 100 μl of fresh PYG medium. Images were adjusted for brightness and contrast in ImageJ.

Acknowledgments

We are grateful to Noorjahan Panjwani of Tufts University and Ibne K. Ali of the CDC for providing A. *castellanii* MEEI 0184 and CDC:V240 strains, respectively. This work was partially supported by a UC San Diego Chancellor's Research Excellence Scholarship (to A.D.). A. D. was supported by grant 1KL2TR001444 from the NIH and grants R21AI133394 and R21AI141210 from the NIAID. L.M.P. was supported in part by a UCSD Academic Senate Research grant.

Chapter 2, in full, is a reprint of the material as it appears in Brian Shing, Seema Singh, Larissa M Podust, James H McKerrow, Anjan Debnath "The Antifungal Drug Isavuconazole is both Amebicidal and Cysticidal against *Acanthamoeba castellanii*" Antimicrobial Agents and Chemotherapy, 2020. The dissertation author was the primary investigator and author on this manuscript.

2.5 Figures and Tables

TABLE 2.1 EC_{50} Screening Values. EC_{50} values of different azoles, chlorhexidine, and PHMB against A. *castellanii* trophozoites. [a]For two azoles, fluconazole and itraconazole, the value given is the percentage of growth inhibition at the highest tested concentration, as the mean EC50 value was not identified. [b]CL, confidence limit.

Compound	Strain	EC_{50} (μM)		
		Mean	95% lower CL[b]	95% upper CL[b]
Azoles				
Fluconazole	Ma	3% at 50 μM[a]		
Itraconazole	Ma	54% at 50 μM[a]		
Miconazole	Ma	6.9	5.8	8.3
Ketoconazole	Ma	1.8	1.4	2.0
Voriconazole	Ma	0.6	0.4	0.8
Clotrimazole	Ma	0.2	0.1	0.2
Posaconazole	Ma	0.045	0.039	0.051
	MEEI 0184	0.003	0.002	0.004
	CDC:V240	0.065	0.054	0.079
Isavuconazole	Ma	0.005	0.004	0.006
	MEEI 0184	0.026	0.023	0.028
	CDC:V240	<0.001	<0.001	0.001
Standards of care				
Chlorhexidine	Ma	1.7	1.4	1.9
	MEEI 0184	1.0	0.9	1.1
	CDC:V240	1.1	1.0	1.2
PHMB	Ma	7.2	6.6	8.0
	MEEI 0184	4.6	3.0	7.1
	CDC:V240	11.8	10.5	13.4

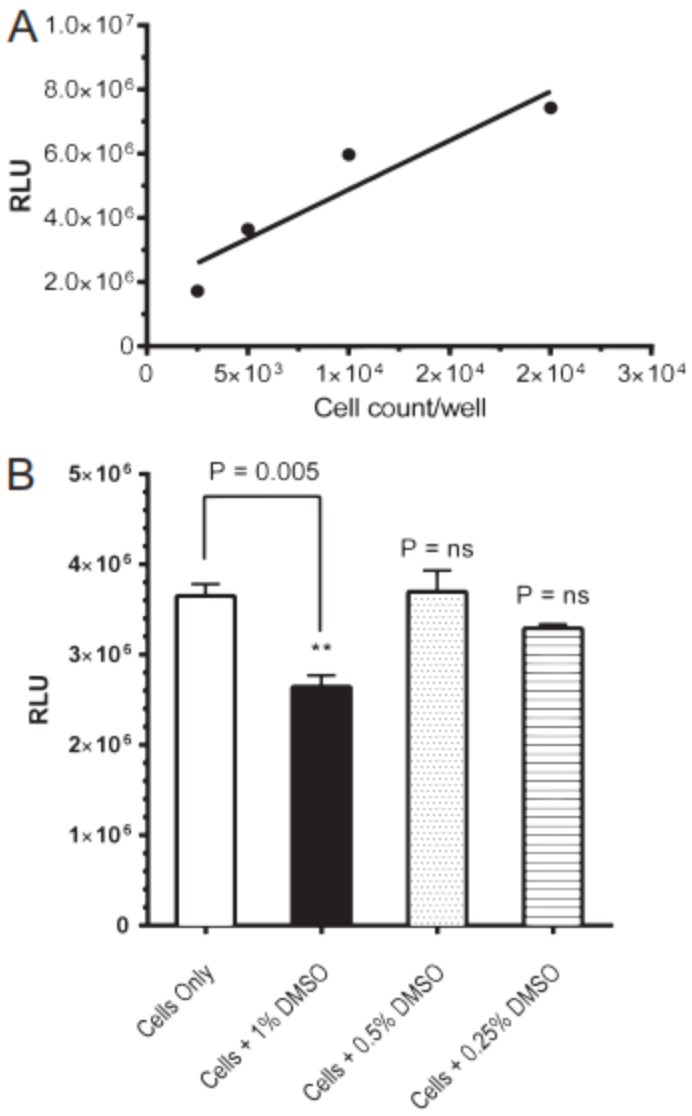

Figure 2.1 Viability Assays for *A. castellanii* Trophozoites. (A) Correlation between the number of viable A. *castellanii* trophozoites and ATP-bioluminescence in a 96-well microtiter plate. Values plotted are the means and standard deviations of triplicate wells. The line represents a regression curve for plotted data. RLU, relative light unit. (B) Tolerability of DMSO by A. *castellanii* trophozoites. Trophozoites (5 x 10^3) were either treated with different concentrations of DMSO (%) or left untreated in a 96-well plate format. ATP-bioluminescence was measured after 48 h. Values plotted are the means and standard deviations of triplicate wells. ns, not significant, with P > 0.05 by Student's t-test compared to untreated A. *castellanii* trophozoites.

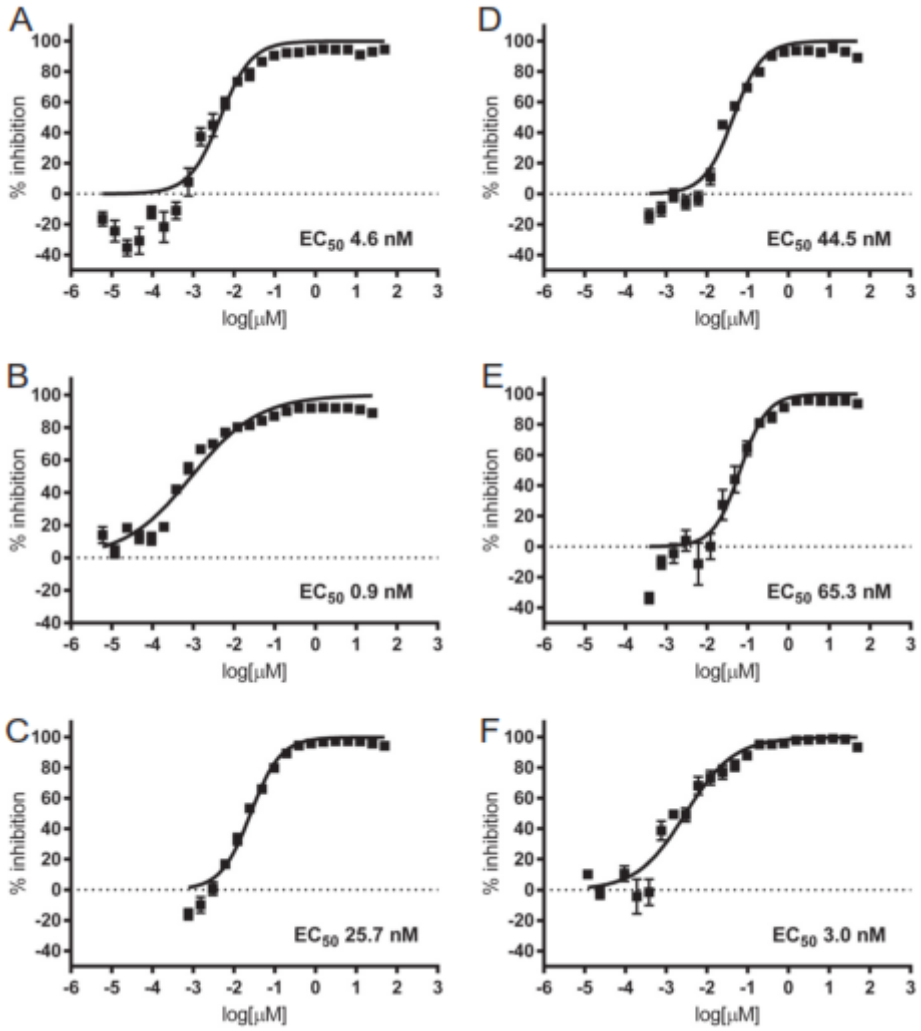

Figure 2.2 Concentration-Dependent Inhibition of Growth of Three Strains of A. *castellanii* Trophozoites by Isavuconazole and Posaconazole. Growth inhibition curve comparisons between A. *castellanii* Ma, A. *castellanii* CDC:V240, and A. *castellanii* MEEI 0184 strains at 48 h. (A) A. *castellanii* Ma treated with isavuconazole; (B) A. *castellanii* CDC:V240 treated with isavuconazole; (C) *A. castellanii* MEEI 0184 treated with isavuconazole; (D) *A. castellanii* Ma treated with posaconazole; (E) A. *castellanii* CDC:V240 treated with posaconazole; and (F) A. *castellanii* MEEI 0184 treated with posaconazole. Data points represent mean percentage growth inhibition and standard error of mean (SEM) of different concentrations of isavuconazole and posaconazole. EC50 curves were generated from mean values of percentage growth inhibition SEM of isavuconazole and posaconazole against A. *castellanii*.

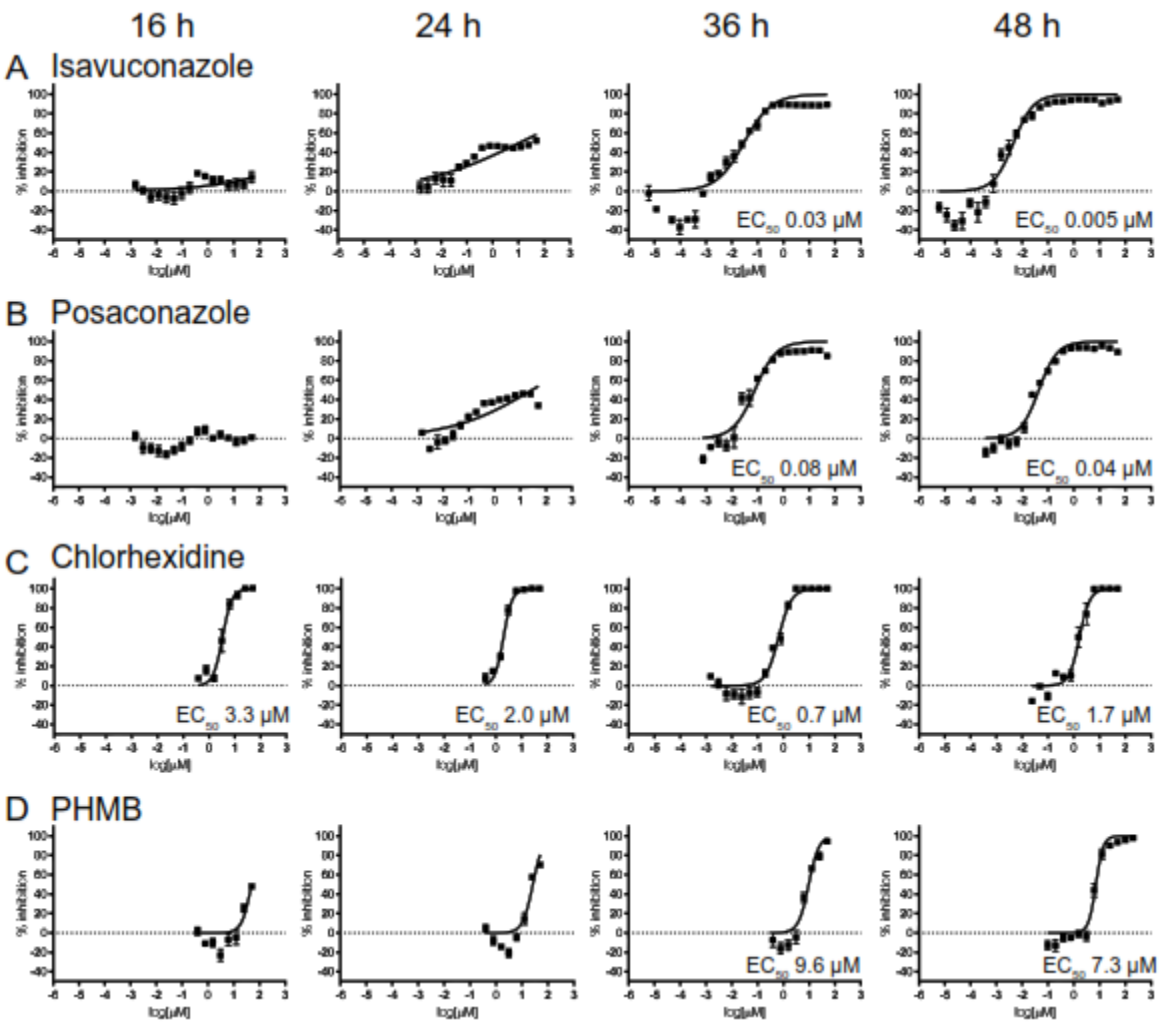

Figure 2.3 Growth Inhibition Curves of A. *castellanii* Ma Strain at Different Time Points. Growth inhibition curves of trophozoites treated with isavuconazole (A), posaconazole (B), chlorhexidine (C), and PHMB (D) at 16, 24, 36, and 48 h. Data points represent mean percentage growth inhibition and standard error of the mean (SEM) of different concentrations of compounds.

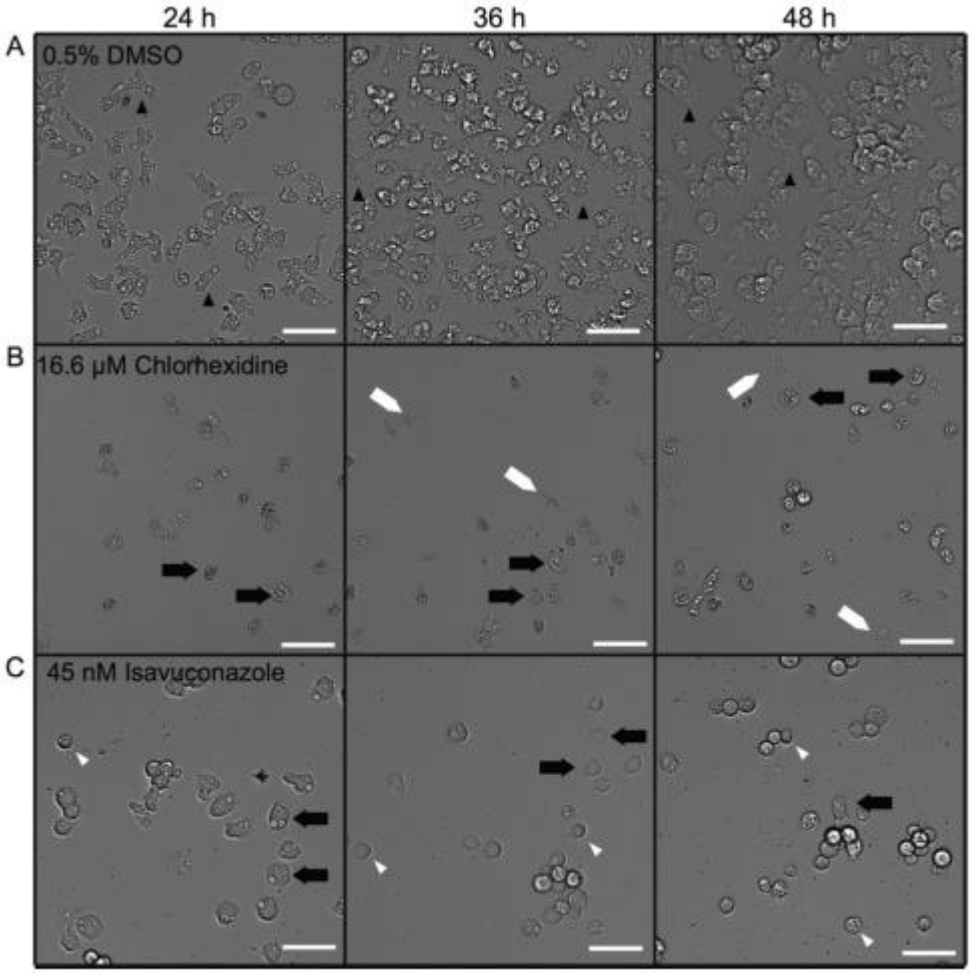

Figure 2.4 Effect of Isavuconazole and Chlorhexidine on the Morphology and Viability of A. *castellanii* Ma Trophozoites. Trophozoites were treated with 0.5% DMSO (A), 16.6 µM chlorhexidine (~10x EC50 value) (B), and 45 nM isavuconazole (~10x EC_{50} value) (C). Trophozoites were imaged at 24, 36, and 48 h. Black arrowheads indicate healthy and proliferating trophozoites. White arrowheads indicate stressed and rounded trophozoites. Black arrows indicate shrunken trophozoites. White arrows indicate lysed cells. Magnification, 200x; bars, 50 µm.

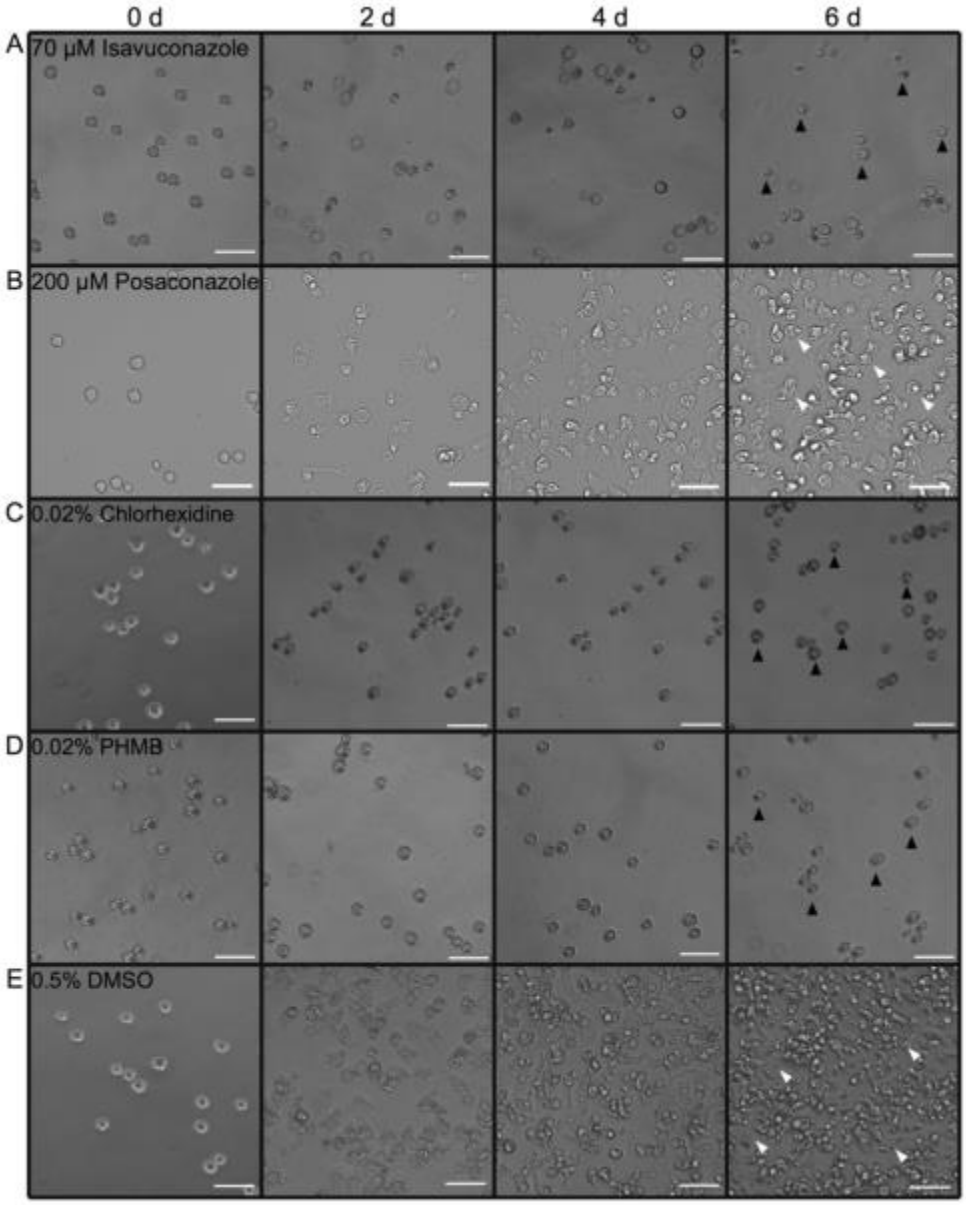

Figure 2.5 Effect of Isavuconazole on the Morphology of *A. castellanii* Ma Cysts. Cysts were treated with (A) 70 µM isavuconazole (A), 200 µM posaconazole (B), 0.02% (wt/vol) chlorhexidine (C), 0.02% (wt/vol) PHMB (D), and 0.5% (vol/vol) DMSO (E) for 48 h and switched to PYG medium 48 h posttreatment. Cyst morphology and excystation were monitored over the course of a week after exchanging the old medium with fresh PYG medium. Black arrowheads indicate unviable cysts, white arrowheads indicate trophozoites that excysted. Magnification, 200x; bars, 50 µm.

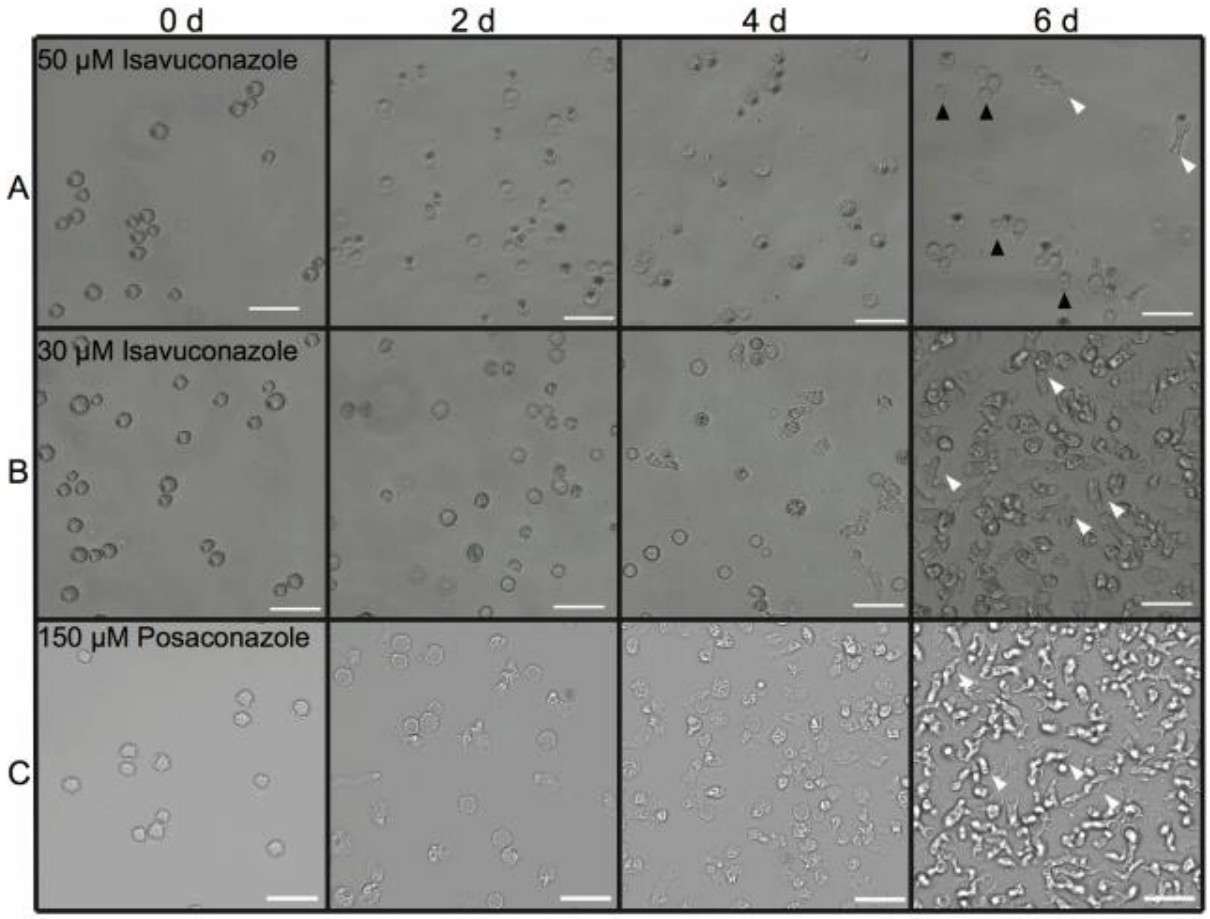

Figure S2.1 Effect of Isavuconazole on *A. castellanii* Ma Cysts. Cysts were treated with (A) 50 μM isavuconazole, (B) 30 μM isavuconazole, and (C) 150 μM posaconazole for 48 hours and switched to PYG medium 48 hours post-treatment. Cyst morphology and excystation were monitored over the course of a week after exchanging the old medium with fresh PYG medium. Black arrowheads indicated unviable cysts; white arrowheads indicate trophozoites that excysted. Magnification: 200x; Bars: 50 μm.

Chapter 3: Domain-Swap Dimerization of *Acanthamoeba castellanii* CYP51 and a Unique Mechanism of Inactivation by Isavuconazole

3.1 Introduction

Acanthamoeba is a water- and soil-dwelling amoeba and an opportunistic pathogen of clinical interest. It is responsible for several diseases in humans, involving infections of the eye, brain, and skin (1). *Acanthamoeba* has two distinct stages: trophozoite and cyst (189). Sterol 14a-demethylase (CYP51) in *Acanthamoeba castellanii* is an essential enzyme in the biosynthesis of ergosterol, a functional analog of cholesterol in mammalian cells (125, 200). CYP51 is a validated drug target in fungi and emerging drug target in the eukaryotic human pathogens, including *Trypanosoma cruzi*, *Naegleria fowleri*, and *Acanthamoeba* (152, 199–201, 228–234). Repurposing of the antifungal azole drugs targeting CYP51 (known as conazoles) is a promising strategy to combat *Acanthamoeba* infections (152, 200, 234).

The majority of antifungal conazoles have submicromolar or low micromolar potency against Acanthamoeba in cell-based assays (125, 200, 209). However, the activity of isavuconazole against proliferating trophozoites is superior to both standard anti-*Acanthamoeba* therapy and other conazole drugs (152). Depending on the *A. castellanii* strain, isavuconazole potency varies in different strains from 26 nM (MEEI 0184) to 4.6 nM (Ma) to 1 nM (CDC:V240) (152). Against the *A. castellanii* Ma strain, isavuconazole potency (EC_{50} of 4.6 nM) was one order of magnitude higher than that of posaconazole (EC_{50} of 44.5 nM) or clotrimazole (EC_{50} of 200 nM) (152). Furthermore, isavuconazole at 70 mM completely prevented excystation of viable *Acanthamoeba* cysts

(152). Potency against both trophozoite and cyst makes isavuconazole a promising drug candidate to block the propagation of trophozoite–cyst cycling of *Acanthamoeba* in *Acanthamoeba* keratitis.

In the context of our drug discovery and drug repurposing efforts, we pursued elucidation of the drug-target interactions for inhibitors targeting *Acanthamoeba castellanii* CYP51 (AcCYP51). In the course of these studies, we have observed an unusual property of AcCYP51 to form a stable dimer that sustained size-exclusion chromatography during purification. As we discovered subsequently, the dimerization occurred via a domain-swap mechanism through the exchange of the N-terminal regions between two protomers. Domain swapping has not been reported in CYP protein family P450 previously. In this article, we use abbreviation CYP to denote a P450 protein family, while P450 term is reserved for the ferrous CO-bound form with iron Soret band at ~450 nm in order to distinguish it from the P420 form. The recombinant CYP enzymes of bacterial origin are monomeric, whereas CYP enzymes of higher eukaryotes, when expressed heterologously, tend to form random aggregates in solution, and their multimolecular assemblies have been detected in crystal structures (235).

At physiologic conditions, endoplasmic reticulum (ER)-bound CYP enzymes presumably exist as homo- or even hetero- oligomers. The fluorescence resonance energy transfer and bimolecular fluorescence complementation in living cells suggest that CYP2C2 forms homo-oligomers and that the homo-oligomerization is dependent on the signal membrane anchor sequence (236, 237). Homodimerization in intact cellular membranes was suggested for the steroidogenic CYP17 and CYP19 by fluorescence resonance energy transfer coupled with quartz crystal microbalance and atomic force

microscopy (238). Homodimerization for the drug-metabolizing CYP2C8 was demonstrated by cysteine-scanning mutagenesis and crosslinking of sulfhydryl groups (239). Finally, homo- and hetero-oligomerization in microsomal membranes was demonstrated for CYP3A4, CYP3A5, and CYP2E1 by luminescence resonance energy transfer (240). Despite these biophysical and biochemical observations, the CYP oligomerization mode is unknown. The random intermolecular protein-protein interfaces observed crystallographically are heterogeneous and planar and have a relatively small interaction area ranging from 290 to 550 $Å^2$ (241–244).

In this work, we have structurally characterized CYP51 from the lower eukaryote *A. castellanii* strain Neff (AcCYP51), which is expressed with a truncated transmembrane helix. We found that only dimeric AcCYP51 had spectral characteristics typical of the functionally competent CYP enzymes. By X-ray crystallography, we demonstrated that AcCYP51 alone is dimerized via N-termini swapping, resulting in formation of a 2000 $Å^2$ nonplanar protein-protein interface. When bound to the azole inhibitors clotrimazole and isavuconazole, AcCYP51 crystallized in the monomeric form with the 74 N-terminal residues disordered in the AcCYP51-isavuconazole complex. The AcCYP51 X-ray structures confirmed a novel dimerization mechanism and elucidated differences in the clotrimazole- and isavuconazole-binding modes that plausibly explain the superior potency of isavuconazole against *A. castellanii* (152).

3.2 Results

Oligomerization of AcCYP51 in Solution. An expression construct of AcCYP51 lacking the transmembrane helix and containing an exogenous 10–amino acid lead

sequence at the N terminus and a hexahistidine tag at the C terminus was synthesized (Data S3.1). Four chromatographic steps were used to purify AcCYP51: affinity chromatography on Ni-NTA resin, ion-exchange chromatography on Q Sepharose, hydroxyapatite chromatography, and, finally, size-exclusion chromatography on Superdex 200 XK 26 coupled to multi- angle light scattering (SEC-MALS).

On the size-exclusion column, AcCYP51 migrated in two peaks corresponding to molecular masses (MMs) of 100.0 ± 0.1 kDa (major peak, P1) and 57.40 ± 0.06 kDa (minor peak, P2) according to a calibration curve (R^2 = 0.9999) built using commercial MM markers (catalog 1511901; Bio-Rad Laboratories, Hercules, CA) (Fig. 3.1A and 3.1B). The absolute MM of the P1 fraction determined by MALS constituted 100.0 ± 9.5 kDa (Fig. 3.1C). On SDS-PAGE, P1 migrated consistent with the MM calculated for one polypeptide chain (52.4 kDa) (Fig. 3.1D). These data demonstrated that 1) AcCYP51 forms a dimer in solution and 2) the dimer is stable enough to undergo size-exclusion chromatography. We have not observed any higher oligomers, suggesting that the highest oligomeric state of AcCYP51 in solution was a dimer.

UV-Visible Spectroscopic Properties of Recombinant AcCYP51. The dimeric and monomeric protein fractions separated by size-exclusion chromatography were individually analyzed by UV-visible spectroscopy (Fig. 3.2). The ferric AcCYP51 dimer, P1 fraction, had a typical CYP spectrum with the absorbance maxima at 418 nm and the ratio of absorbance at λ_{max} of the Soret band, 418 nm, to that at 280 nm of 1.8 to 1.9 (Fig. 3.2A, solid line). The ferrous-CO complex of the dimeric AcCYP51 had a high content of the P450 form (Fig. 3.2A and 3.2B, dashed line). The monomeric AcCYP51, P2 fraction,

was largely P420 (Fig. 3.2C and 3.2D). A trace of P450 absorbance was likely due to residual contamination with the P1 fraction. To confirm that the AcCYP51 dimer in the crystals remained in the P450 form, we harvested the crystals, dissolved them in assay buffer, and recorded the UV-visible difference spectra. Upon sodium dithionite reduction and carbon monoxide binding, peak at 448 nm was observed (Fig. 3.2E and 3.2F).

Overall X-Ray Structure of the AcCYP51 Dimer. The dimeric AcCYP51 readily crystallized in the absence of added ligands. The crystal structure at 1.8 Å revealed a symmetrical head-to-head homodimer with swapped N termini (Fig. 3.3A). The first seven amino acids of the lead sequence were disordered and not visible in electron density. The next three exogenous residues from the lead sequence (K40-G41-K42, yellow in Fig. 3.3B) followed by authentic AcCYP51 sequence participated in the N-terminal swapping. As shown in Fig. 3.3B, only the main chain of the K40-G41-K42 fragment participates in intermolecular protein-protein interactions, whereas the lysine side chains face the bulk solvent.

The overall protein scaffold was similar to that of monomeric CYP enzymes with the qualification that the region of K40-P52 containing the first strand of the β-sheet-1 (β1-1) was swapped between the two protomers and was parallel to the β1-2 of the interacting protomer instead of folding with the own polypeptide chain (Fig. 3.3A). Because of the swap, the A' helix (F53-G63) established close intramolecular contacts with the F' helix, blocking access to the active site. This block of access to the active site was reinforced by the intermolecular contacts in the dimer interface where the protomers faced each other through the A', F', F, and G α-helices (Fig. 3.3A). A dimer protein-protein

interface of 2000 $Å^2$ was calculated using the Protein Interfaces, Surfaces, and Assemblies software (245). Altogether, 16 H-bonds and two salt bridges stabilized the protein-protein interface formed by 40 hydrophobic residues provided by each protomer. The buried surface constituted 10% of the accessible surface of AcCYP51 and provided total solvation energy gain of -35.4 kcal/mol. F84 had the most prominent single residue input of -2.1 kcal/mol (Fig. 3.3C). This protein-protein interface was strong enough to sustain size-exclusion chromatography and crystallization in up to 1 M urea. Crystals obtained in 0.55 M urea diffracted to 1.85 Å and had intact dimeric structure similar to that seen in native conditions.

Heme Binding. An unusual feature of the AcCYP51 dimer was heme "wobbling." Despite the multiple H-bonding interactions with Y114, Y127, and Q110 and a salt bridge with R368 formed by the heme propionate moieties, two alternative conformations were required to approximate the heme position in the ligand-free AcCYP51 (Fig. 3.3D). In heme conformers, the Fe-S bond length was refined between 2.33 and 2.41 Å. The 2.41-Å bond length goes beyond the range reported for other crystallographically resolved P450 enzymes (246). Consistent with the ferric resting state, the water molecule was modeled in both protomers as a sixth, axial iron ligand at the distances of ≤2.64 Å of the heme iron (Fig. 3.3D).

Overall X-Ray Structures of the Inhibitor-Bound AcCYP51. AcCYP51 cocrystallized with clotrimazole or isavuconazole as a monomer; crystals diffracted to a resolution of 2.9 Å. In both structures, the asymmetric unit contained six inhibitor-bound

AcCYP51 molecules. In each molecule, electron density for the bound inhibitor was unambiguously defined as evidenced by the omit maps in Fig. 3.4A and 3.4B. In clotrimazole-bound AcCYP51, the β1-1 region folded back to its own polypeptide chain, restoring a typical P450 scaffold. Two consecutive glycine residues in the A-A' loop, G^{62}-G^{63}, served as a hinge facilitating swinging of the upstream part (Fig. 3.4C and 3.4D). In a remarkable contrast to clotrimazole, 74 N-terminal residues were disordered and missing from the electron density of the AcCYP51-isavuconazole complex (Fig. 3.4E). From the comparison of three structures (Fig. 3.4C–E), the β1-1 strand and the A', B', and F' helices progressively loose the canonical H-bonding patterns from ligand-free dimer to clotrimazole complex to isavuconazole complex. In the AcCYP51-isavuconazole structure, the β1-1, A', and A atomic coordinates are not included.

AcCYP51-Clotrimazole Complex in the Crystal. The structure determined in this work is the first of the CYP51-clotrimazole complex. Similar to other P450-clotrimazole structures [CYP46A1 (PDB ID: 3MDV), P450 BM3 (6H1T), EryK (2XFH), and OleP (4XE3)], clotrimazole bound in the active site of AcCYP51 via a coordination bond provided to the heme iron by the aromatic nitrogen of the imidazole moiety and via the hydrophobic interactions mediated by the phenyl moieties of the drug. The orientation of the chlorophenyl moiety in clotrimazole varies between different CYP enzymes. In AcCYP51, the short side chain of S117 defines orientation of the chlorophenyl moiety by providing space to accommodate a bulky Cl substituent that is within 5.1 Å of the serine carboxyl group (Fig. 3.4A). Other contacts within 5 Å of clotrimazole involve Y114, F116, S117, F121, V126, T127, L216, A290, F293, A294, H297, L363, and V366. Compared

with the inhibitor-free AcCYP51, the first-tier residues in the substrate- binding site are shifted away from clotrimazole to accommodate the inhibitor. To compensate for the inhibitor-introduced distortions, this trend was propagated to the second and third tier residues. From the perspective of drug design, the tight fit in the active site leaves room for derivatization of only one phenyl moiety in clotrimazole.

AcCYP51-Isavuconazole Complex in the Crystal. The structure determined in this work is the first of the P450- isavuconazole complex. Similar to clotrimazole, isavuconazole bound in the heme pocket via coordination to the heme iron and protein-drug interactions (Fig. 3.4B). In the heme pocket, the set of interacting residues is similar to that of clotrimazole excluding L216 and H297. More-elongated isavuconazole molecule also makes interactions with F365, M367, and M471 with the thiazolyl benzonitrile moiety of the drug. The nitrile group points toward the opening created by disordering of the A' and F' helices.

Stability of the AcCYP51-Ligand Complexes in Solution. The binding of the inhibitors and substrates was assessed by the shift of the Fe Soret band in the UV-visible spectra of dimeric AcCYP51 (Fig. 3.5). Type II binding spectra were obtained upon clotrimazole and isavuconazole binding (Fig. 3.5A). Type I spectra were obtained upon binding sterols lanosterol and 31-norlanosterol, with qualification that 31-norlanosterol generated a larger spectral response than lanosterol (Fig. 3.5B). Binding kinetics of AcCYP51 at saturating ligand concentrations showed that both isavuconazole and clotrimazole reached saturation for <10 minutes, whereas more than 30 minutes were

required for 31-norlanosterol to reach the saturation (Fig. 3.5C and 3.5D). Magnitude of the spectral changes suggested that only 10%–20% of AcCYP51 resulted in the formation of enzyme-ligand complexes (Table 3.2). When AcCYP51 was titrated with clotrimazole, a typical binding curve was obtained, and K_D of 152.3 ± 10.0 nM was calculated by fitting binding data using the Morrison “quadratic” equation (Fig. 3.5E) (247). For isavuconazole, the binding plateau could not be reached (Fig. 3.5E). In the context of our structural data, isavuconazole may have affected integrity of AcCYP51 and the magnitude of the Soret spectral shift by partial protein unfolding.

Modeling AcCYP51 Dimer Interactions with the ER Membrane. To assess compatibility of the domain-swap dimerization with membrane binding, we built a molecular model of AcCYP51-membrane interactions. The wild-type N-terminal residues omitted from the recombinant AcCYP51 were added computationally. The fully reconstructed AcCYP51 dimer was embedded into a lipid membrane constituted of phospholipids, POPC/POPE, and cholesterol found in the membranes of higher eukaryotes. Cholesterol was used in MD simulations to optimize conformation of the TM helix (residues 10–30) and its flanking regions because the Amber force field does not have the parameter for ergosterol found in the membranes of lower eukaryotes.

The model demonstrated that the dimerization mode observed in the crystal structure is compatible with the membrane association (Fig. 3.6A). The TM helices are separated in space and run virtually orthogonal to the lipid bilayer, which is consistent with the relatively short TM helix in AcCYP51. The region connecting the TM helix with the globular CYP domain is predicted to be a flexible loop up to the downstream segment

44–51, which adopts a β-strand structure (β1-1) running parallel to β1-2 of the interacting protomer.

In addition to the TM helix, protein-lipid interactions occur through the regions corresponding to residues 31–43 (Fig. 3.6B). This fragment has several charged amino acids (i.e., K31, R33, E34, R36 and K37), which interact with the zwitterionic heads of POPC and POPE phospholipids. On the other hand, the presence of hydrophobic residues, such as V32 and L43, enables the nonpolar interactions between the linker regions and lipid tails (Fig. 3.6B). Finally, W35, Y38, and Y41 act as anchoring residues, which are usually located between the polar group and the hydrophobic core of the lipid bilayer in the glycerol region of the membrane (248).

The β5-β6 segment (residues 372–380) also faces the membrane in our model and is partially immersed in its hydrophobic environment. Finally, in one of the monomers, residues R273, G274, and E275 tend to associate with lipid heads (Fig. 3.6B). The electrostatic potential density at the surface of AcCYP51 dimer shows that the membrane-associated protein surface comprises charged patches, thus supporting the reliability of our membrane-insertion model (Fig. 3.6C).

3.3 Discussion

CYP enzymes are a superfamily of *b*-type heme-containing monooxygenases descended from a single common ancestor (249). They share structural features, such as a common protein scaffold, the similarity in positioning of the heme group, and the access/egress pathways for substrates and products (250). The heme group is bound via a thiolate sulfur bond donated by the universally conserved “proximal” cysteine residue

at the fifth, axial coordination of the heme iron. The heme iron binds molecular oxygen, O_2, as a sixth ligand in the “distal” pocket, which also serves as a site for substrate binding. CO resembles O_2 in size and heme- binding properties. By replacing O_2, CO blocks the enzymatic turnover of the CYP enzymes. CO is used as a sensitive probe of local conformation and dynamics in the active site of heme-thiolate proteins. Absorption spectra of the CO-bound ferrous CYP enzymes (Fe^{2+}–CO) often display two Soret bands in the blue region of the visible range, which are denoted P420 and P450. The 420- and 450-nm bands are arguably assigned to CYP species having, respectively, a protonated (thiol) and deprotonated (thiolate) cysteine side chain as axial iron ligands (251–254). Alternatively, recruitment of a histidine residue to replace the native cysteine thiolate ligand has been suggested (255, 256). Finally, theoretical calculations indicate that stretching the Fe-S bond by only 0.2 Å could induce the spectral transition of ferrous CO P450 to P420 (257). A variety of extreme conditions, such as heating, hydrostatic pressure, organic solvents, and denaturants, were used to convert P450 to P420 (255, 258–260). On a few occasions, P420 could be converted back to P450 (252, 261).

The mechanistic knowledge accumulated in the field supports the assumption that a CYP monomer is sufficient for catalytic function, and CYP dimerization is not required for the act of catalysis. At the same time, there are reports of CYP-CYP interactions both in microsomal membranes and in recombinant CYP proteins (235–240, 262–271). CYP-CYP interactions are suggested to play regulatory rather than catalytic role (244). Despite biophysical and biochemical evidence, details of CYP-CYP interaction mode(s) remain obscure. The protein-protein interfaces reported in the crystal structures of the multimolecular complexes of eukaryotic CYP enzymes are random and have small

interaction areas (244). These considerations encouraged us to determine the first X-ray structure of a sustainable CYP51 dimer. This in turn led to discovery of the domain-swap dimerization mode.

The P450 character of the AcCYP51 dimer contrasts with the P420 character of the AcCYP51 monomer. The propensity of AcCYP51 to convert into a P420 form even in mild purification conditions was consistent with the flexibility of the heme pocket manifested by heme wobbling and lengthening of the Fe-S bond as observed in the crystal structure. We speculate that dimerization in AcCYP51 plays a stabilizing role to maintain the functional status of the heme.

The modifications introduced at the N terminus of AcCYP51 to enable expression in the bacterial host may potentially affect the behavior of the recombinant protein. However, truncation of the TM helix and insertion of an exogenous lead sequence is a commonly used practice to express microsomal CYP enzymes, but CYP dimerization via N-termini swap has not been reported. Furthermore, exogenous residues in the lead sequence are not involved in the dimer interface, making N-termini swapping an interesting paradigm of CYP dimerization. The interactions between CYP enzymes and cell membranes are crucial for establishing protein orientation in the membrane, which is described as a dynamic process (272). The membrane positioning is recognized as an essential factor facilitating substrate/product channeling to the active site and interactions with the redox partners (272). Our modeling studies demonstrated that N-termini swap dimerization is compatible with membrane topology both spatially and electronically. It also does not contradict experimental data obtained elsewhere by different biophysical and biochemical methods. A model of the *Saccharomyces cerevisiae* CYP51 monomer

embedded in phospholipid bilayer serves as a current paradigm of CYP-membrane interactions (273). The F-G loop region involved in protein-protein interactions in AcCYP51 dimer is predicted to be embedded in the lipid bilayer in *S. cerevisiae* CYP51 (273). Hypothetically, transition between the two membrane-association modes would depend on the flexibility of the hinge region (two consecutive glycine residues, G^{62}-G^{63}, in the A-A' loop of AcCYP51). A flexible hinge would facilitate dissociation of globular domain from the lipid bilayer and association into a homodimer.

We inspected the glycine-rich and highly variable A-A' loop in human CYP enzymes. Two consecutive glycine residues are especially prominent in human CYP46A. This is an important central nervous system enzyme that converts cholesterol to 24S-hydroxycholesterol, thereby initiating the major pathway of cholesterol removal from the brain (274). Multiple X-ray structures of CYP46A1 in complex with a variety of drugs (antidepressants, anticonvulsants, and antifungals) are available in the PDB. Remarkably, in all these entries, CYP46A1 is missing 50 N-terminal residues and is therefore truncated shortly upstream of the G-G motif. This observation supports our hypothesis that the CYP globular domain may be loosely associated with the N terminus and has freedom to dimerize on the membrane surface.

Based on the structural insights obtained from AcCYP51 alone and the AcCYP51-inhibitor complexes, the superior potency of isavuconazole against *A. castellanii* may be explained by partial denaturing of the AcCYP51 target. Given that access to the AcCYP51 active site is blocked by dimerization, to bind an inhibitor or substrate the dimer has to dissociate. This assumption is consistent with the slow rate of ligand binding (10 minutes for clotrimazole and isavuconazole and 30 minutes for 31-norlanosterol), low drug-target

complex fraction (10%–20%), and the monomeric form of the AcCYP51- clotrimazole and AcCYP51-isavuconazole complexes observed in the crystals. Partial denaturing of AcCYP51 in response to inhibitor binding (74 disordered N-terminal residues in the AcCYP51-isavuconazole complex) suggests a mechanism of action fundamentally different from conventional enzyme inhibition by blocking the active site. In living cells, structurally aberrant AcCYP51 may undergo further denaturation and be permanently deactivated by proteolytic degradation. In the context of the superior activity of isavuconazole, this phenomenon can be exploited for designing other AcCYP51 inhibitors that target the dimerization interface.

3.4 Materials and Methods

AcCYP51 Expression and Purification. AcCYP51, which is codon-optimized for bacterial expression, had a coding sequence with 42 N-terminal membrane-anchoring residues replaced with the MAKKTSSKGK. A hexahistidine tag was added at the C terminus to increase protein yield and recovery during purification (see Data S3.1). This construct was generated synthetically (GenScript, Piscataway, NJ) and cloned into the pCW-LIC expression vector obtained from the nonprofit plasmid repository (Addgene, Cambridge, MA).

To improve the P450/P420 ratio, the original protocol used to isolate recombinant *N. fowleri* CYP51 was modified (see Data S3.2) (201). Briefly, the modifications included a switch to the HMS174 *Escherichia coli* strain, coexpression of chaperones, omitting detergent 3-[(3-cholamidopropyl)dimethylammonio]-1-propanesulfonate (CHAPS) used initially to facilitate protein release from the membrane, and replacement of imidazole with

histidine during elution from the Ni-NTA column. Exposure to imidazole led to quick loss of the 450-nm band in the absorbance spectra of the CO-bound ferrous AcCYP51. Finally, additional purification step of size-exclusion chromatography (SEC) on a Superdex 200 XK 26 column coupled to MALS (SEC-MALS) was used to separate P450 form, which was eluted as a dimer, from P420 form, which was eluted as a monomer. Collectively, after four chromatographic steps, including Ni-NTA affinity chromatography, Q-Sepharose ion-exchange chromatography, hydroxy- apatite chromatography, and size-exclusion chromatography, fractions containing AcCYP51 with ~80% P450 content were pooled, concentrated to ~1 mM, aliquoted, and frozen at -80°C.

SEC-MALS. SEC-MALS experiments were performed using in-line multiangle light scattering (MALS) detector (miniDAWN; Wyatt Technology, Santa Barbara, CA) at 7°C. Two-milliliter protein sample was injected onto pre-equilibrated Superdex 200 XK26 column using 2-mL sample loop at a flow rate of 0.5 mL/min. The composition of the equilibration and sample buffer used was 50 mM potassium phosphate, pH 8.0, and 5% glycerol. Data of SEC-MALS thus obtained were analyzed by ASTRA 6.1 software provided by the instrument manufacturer.

UV-Visible Analysis of AcCYP51. The spectra were recorded using a Thermo Scientific Multiscan Go UV-visible spectrophotometer. Protein samples were diluted in assay buffer (50 mM potassium phosphate, pH 8.0, and 10% glycerol) and allowed to equilibrate to room temperature for 10 minutes prior to readings. Spectra were recorded from 250 to 700 nm for the ferric and dithionite-reduced ferrous AcCYP51 in assay

cuvette. Baseline was established using buffer alone and was subtracted from the sample signal prior to analysis using SkanIt software provided by the manufacturer. The CO difference spectrum was recorded by placing dithionite-reduced ferrous AcCYP51 into the sample cuvettes and recording the baseline. Then CO was bubbled into the same cuvette, and the difference spectrum was recorded. The concentration of AcCYP51 was approximated from the absorption peak at 450 nm using the extinction coefficient ε_{450} = 91 $mM^{-1}cm^{-1}$ (275).

To assess the spectral properties of the crystallized AcCYP51 dimer, crystals were harvested individually; each crystal was washed thoroughly in a well solution and then dissolved in 50 mL of assay buffer. The number of crystals required for a single analysis varied from 10 to 20 depending on the crystal size. The UV-visible spectra of the dissolved crystals were recorded at ambient temperature in 50-mL cuvette (952010077; Eppendorf). To generate ferrous-CO spectra, a few crystals of sodium dithionite were added to the CO-bubbled ferric protein sample.

Inhibitor Binding by UV-Visible Spectroscopy.

Type I and Type II Binding. To determine binding modes of different ligands used in the study, 20-mM ligand stock solutions were prepared in corresponding solvents. Isavuconazole and clotrimazole were prepared in DMSO, and 31-norlenosterol was dissolved in isopropanol. Prior to analysis, 5 µM AcCYP51 in assay buffer was mixed with 20 µM ligand. After 30 minutes of incubation at room temperature, absorbance spectra were recorded from 300 to 500 nm. To determine difference spectra, blank readings were

taken for protein alone in assay buffer with respective ligand vehicle under given experimental conditions.

Binding Kinetics. To determine binding kinetics of the ligands, 5 μM AcCYP51 in assay buffer was mixed with 20 μM ligand. After mixing, spectra from 300 to 500 nm were recorded every 5 minutes of incubation. Blank readings were determined from incubation of protein alone with respective ligand vehicle under given experimental conditions. AcCYP51 stock concentration was determined by absorbance of the CO-bound ferrous form at 450 nm (ε_{450} = 91 $mM^{-1}cm^{-1}$) (275). Concentration of the AcCYP51-norlanosterol complex was determined using the peak-to-trough extinction coefficient, $\varepsilon_{390\text{-}420} \approx 100$ $mM^{-1}cm^{-1}$) (276). Concentration of the AcCYP51-inhibitor complex was estimated using the peak-to- trough extinction coefficient, $\varepsilon_{430\text{-}411} \approx 110$ $mM^{-1}cm^{-1}$) (277). The experiment was conducted with two replicates.

Binding Isotherms. The DMSO stock solutions for clotrimazole and isavuconazole were freshly prepared at concentrations of 0.2 and 0.4 mM. The AcCYP51 stock was diluted to 1 μM in assay buffer. Two milliliters of the AcCYP51 solution was split evenly into a reference and a sample cuvette [1-cm polymethyl methacrylate cuvette (cat. no. 759150; BrandTech Scientific, Essex, CT)]. The AcCYP51 solution was allowed to equilibrate for 30 minutes to room temperature prior to absorption readings. The absorption readings were performed at 20°C on a Cary 1E Dual Beam UV-visible spectrophotometer (Varian). The experiment was conducted with two replicates.

In the course of titration, 1 µl of DMSO was added to the reference cuvette, whereas 1 µl of inhibitor dissolved in DMSO was added to the sample cuvette in 200- (data points 1–4) and 400-nM (data points 5–10) increments. The cuvette content was mixed with a transfer pipette prior to each reading. Absorbance readings were taken from 350 to 500 nm, and the binding isotherm was generated by plotting the differences between the absorbance minimum at 410 nm and absorbance maximum at 430 nm as a function of added drug concentration. The data were analyzed in GraphPad Prism 6.07 with the rearrangement of the Morrison binding equation to determine the dissociation constants:

$$\Delta A = (\frac{\Delta A_{max}}{2[E]})((K_D + [L] + [E]) - ((K_D + [E] + [L])^2 - 4[E][L])^{0.5})$$

in which ΔA is the difference between absorbance maximum and minimum, ΔA_{max} is the extrapolated maximum absorbance difference, [L] is the ligand concentration, and [E] is the enzyme concentration (247).

Crystallization and Structure Determination. Prior to crystallization, AcCYP51 stored at -80°C in 50 mM potassium phosphate, pH 8.0, and 5% glycerol was diluted 2-fold to 0.5 mM with water or buffer containing a ligand at 1.2 molar access. Screening of crystallization conditions was performed using commercial high-throughput screening kits available in deep-well format from Hampton Research (Aliso Viejo, CA) or Qiagen (Germantown, MD), a nanoliter drop-setting Mosquito robot (TTP LabTech, Melbourn, UK) operating with 96-well plates, and a hanging drop crystallization protocol. For diffraction quality, crystals were further optimized in 96-well plates configured using the Dragonfly robot (TTP LabTech) and the Designer software (TTP LabTech). All crystals

were obtained at 23°C. Clotrimazole and isavuconazole stock solutions were prepared fresh in DMSO. The 1:1.2 molar ratio protein-inhibitor mix was incubated for 30 minutes on ice prior to mixing with the well solutions. Optimized crystallization conditions are provided in Table 3.1.

Diffraction data were collected remotely at beamline 8.3.1, Advanced Light Source, Lawrence Berkeley National Laboratory. Data indexing, integration, and scaling were conducted using XDS (278). *T. cruzi* CYP51 structure [sequence identity 38%, Protein Data Bank (PDB): 4C27] was used as a molecular replacement model. The initial AcCYP51 model was built and refined using the BUCCANEER and REFMAC5 modules of the CCP4 software suite (Collaborative Computational Project, Number 4, 1994) and COOT software (279). Data collection and refinement statistics are shown in Table 3.1.

Molecular Modeling and Simulation. A full-length AcCYP51 homodimer was constructed computationally by modeling the transmembrane (TM) helix and its flanking regions into the AcCYP51 structure using the Rosetta MP package v3.0 (280). The TM helix (residues 10–30) was modeled ab initio using the helix_from_sequence program (280). The TM helices of each monomer were positioned diagonally opposite one another in agreement with the position of the N termini in the crystal structure. The flexible linker region (residues 31–52) and the N terminus were built for each protomer using the mp_domain_assembly program (281). Five hundred models were generated, and the structure with the lowest value of the Rosetta energy function was selected for further analysis. The energy minimization of the full-length dimer was performed to optimize interatomic distances and angles. Then, the 50-nanosecond molecular dynamics (MD)

simulations were conducted to refine the structure of the linker regions and to obtain the proper arrangement of them in respect to the rest of the dimer. In the course of the simulation, the flexible linkers and the N termini were allowed to move freely, whereas harmonic restraints were applied to the backbone atoms of the rest of the protein.

The fully assembled AcCYP51 dimer was embedded into a 1-palmitoyl-2-oleoyl-*sn*-glycero-3-phosphocholine (POPC)/1-palmitoyl-2-oleoyl-*sn*-glycero-3-phosphoethanolamine (POPE)/cholesterol lipid bilayer composed of 75% POPC, 18% POPE, and 6% cholesterol, corresponding to the abundance of these lipids in the ER (272). Cholesterol is the closest analog of ergosterol and ergosterol-like lipids in *A. castellanii* membranes available in Amber data base and widely used in Amber force-field simulations. The protein-membrane model was constructed using CHARMM-GUI (282). The simulation was conducted in a box containing protein, lipid membrane, water molecules, and ions. The AMBER14SB and LIPID17 force fields were used for protein and lipids, respectively, whereas the heme group parameters were taken from Rydberg et al. (2007) (283–285). Protonation states of the amino acid residues were determined at physiologic pH (pH = 7.14) using the PDB2PQR server (286). Systems setup was performed with tleap program of Amber18 (284). The system was solvated with explicit transferable intermolecular potential with 3 points (TIP3P) water molecules (Jorgensen and Jenson, 1998) in a cubic box extending at least 10 Å from the solute surface treated with periodic boundary conditions. Net charges were neutralized by replacing water molecules with Na^+ and Cl^- ions.

All MD simulations were conducted using NAMD v.2.13 program (287). The 50,000 steps of energy minimization were performed to eliminate the atomic clashes. The lipid

bilayer equilibration procedure was performed at constant pressure (1 atm) and constant temperature (298 K), for 150 nanoseconds with 1 kcal×mol^{-1}×Å^{-2} harmonic position restraints applied to the protein backbone and heme. Further equilibration of the systems was performed at 1 atm and 298 K for 15 nanoseconds with all atoms unrestrained. Conventional MD simulation was performed for 250 nanoseconds at 1 atm and 298 K with a constant ratio constraint applied to the lipid bilayer in the X-Y plane.

Acknowledgments

We thank Michael K. Gilson and Jeffry Setiadi, Skaggs School of Pharmacy and Pharmaceutical Sciences University of California San Diego (SSPPS-UCSD), for providing access to the computational resources; James McKerrow for valuable discussions and support of this project; and the Advanced Light Source (ALS) beamline 8.3.1 personnel James Holton, George Meigs, and Jane Tanamachi for assistance with the data collection.

Chapter 3, in full, is republished with permission of American Society For Pharmacology and Experimental Therapeutics, from the material Domain-Swap Dimerization of *Acanthamoeba castellanii* CYP51 and a Unique Mechanism of Inactivation by Isavuconazole, Vandna Sharma, Brian Shing, Lilian Hernandez-Alvarez, Anjan Debnath, and Larissa M. Podust, 98, and ©2020; permission conveyed through Copyright Clearance Center, Inc. The dissertation author was a second author and an essential contributor on this manuscript.

3.5 Figures and Tables

TABLE 3.1 AcCYP51 Structures Data Collection and Refinement Statistics

[a]Asymmetric unit; [b]Data for the highest resolution shell are shown in parentheses; [c]Polyethylene glycol; [d]Temperature factor; [e]Not applicable; [f]Root-mean-square

Inhibitor (ID) Oligomerization PDB identification	None Dimer 6Q2C	Clotrimazole (CL6) Monomer 6UW2	Isavuconazole (QKM) Monomer 6UX0
Data collection			
Space group	$P2_12_12_1$	$P2_12_12_1$	P1
Cell dimensions			
a, b, c (Å)	100.4, 101.6, 123.7	117.9, 117.2, 181.5	99.5, 99.1, 108.7
α, β, γ (^{0})	90.0, 90.0, 90.0	90.0, 90.0, 90.0	92.6, 96.2, 120.1
Molecules in AU[a]	2	6	6
Wavelength	1.11587	1.11587	1.11587
Resolution range (Å)	1.80—78.50	2.92—127.13	2.93—107.35
Highest shell (Å)	1.80—1.85	2.92—3.00	2.93—3.01
Unique reflections	115,584 (7204)[b]	83.269 (6049)	74,605 (5556)
R_{sym} or R_{merge} (%)	5.9 (286.0)	40.0 (469.4)	19.3 (342.7)
I/σI	17.7 (0.5)	7.1 (0.6)	5.3 (0.3)
Completeness (%)	98.2 (83.9)	100.0 (99.9)	97.9 (97.9)
Redundancy	11.4 (5.4)	13.5 (13.6)	3.4 (3.5)
Crystallization conditions	15% PEG[c] 3350, 200 mM sodium-malate, pH 6.8—7.2	0.1 M Na-cacodylate, 2% Jeffamine M-600, pH 7.0; 0.12 M guanidinium chloride	0.1 M sodium citrate, pH 5.6; 12% PEG 3350
Refinement statistics			
No. refelctions	109,450	79,148	67,944
R_{work}/R_{free} (%)	18.5/22.7 (45.9/45.8)	20.9/29/1 (38.9/38.8)	21.4/30.8 (42.2/49.0)
No. atoms			
Protein	7184	21,135	19,552
Heme	172	258	258
Inhibitor	None	150	186
Solvent	510	46	1
Wilson plot B[d]	44.6	70.6	83.1
Mean B value	49.7	79.0	98.9
B factors			
Protein	50.2	81.0	101.9
Heme	35.5	60.6	67.1
Inhibitor	N/A[e]	70.2	79.5
Solvent	54.0	45.6	41.4
R.m.s[f] deviations			
Bond lengths (Å)	0.019	0.01	0.012
Bond angles (^{0})	1.974	1.577	1.643
Ramachandran statistics			
Preferred (%)	97.14	88.25	83.76
Allowed (%)	2.29	7.48	10.25
Outliers (%)	0.57	4.26	5.99

TABLE 3.2 UV-Visible Quantification of the AcCYP51 Ligand-Bound Fraction[a,b]
[a]Experiments were performed in duplicates. Values for the replicates n1 and n2 are shown separately. [b]Concentrations are in μM

Ligand	[Ligand]	[AcCYP51]	[AcCYP51 ligand]		Ligand-bound AcCYP51 %	
			n1	n2	n1	n2
Clotrimazole	20.0	5.0	0.81	0.66	16.2	13.0
Isavuconazole	20.0	5.0	0.47	0.38	9.4	7.6
31-Norlanosterol	20.0	5.0	0.90	1.00	18.0	20.0

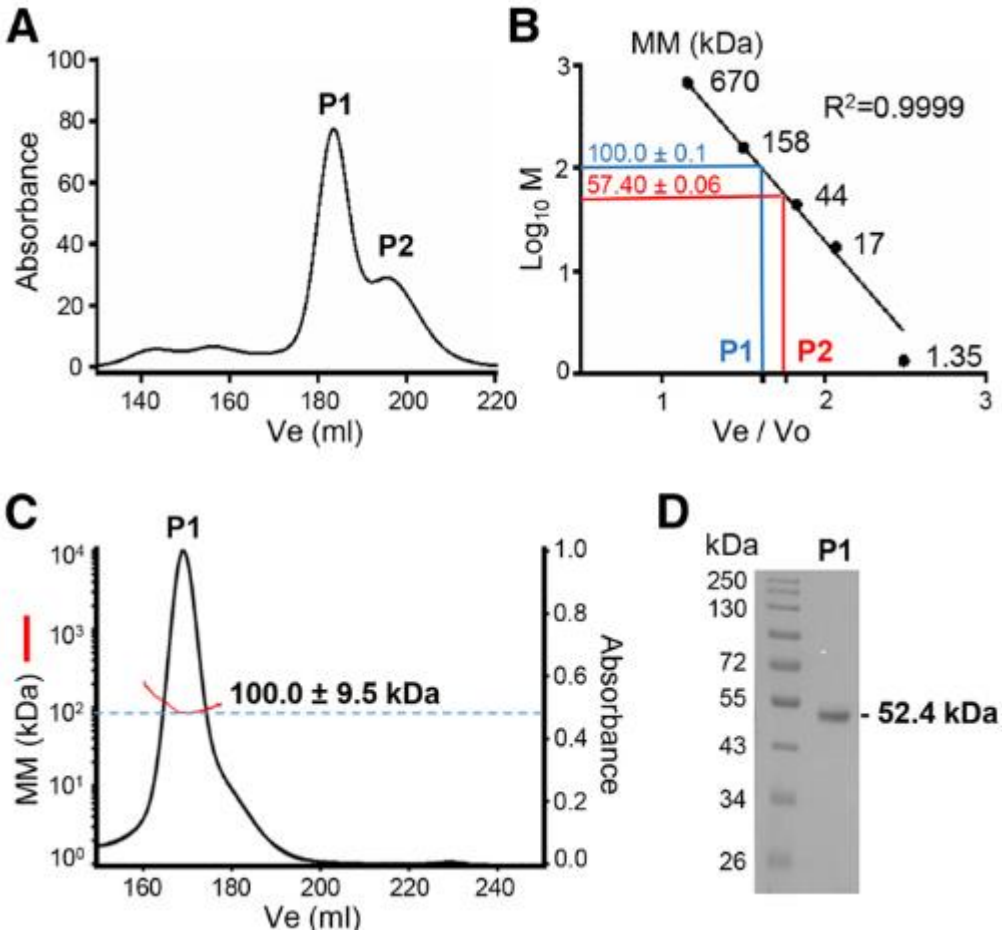

Figure 3.1 Size-Exclusion Chromatography and SDS-PAGE of Recombinant AcCYP51. (A) Size-exclusion chromatography profile of the heterogenous mixture of recombinant AcCYP51 on the Superdex 200 XK 26 column. (B) Molecular mass (MM) estimation of the P1 and P2 fractions. *y*-Axis represents log of MM in kilodaltons; *x*-axis represents ratio of elution volume (V_e) and void volume (V_o). Black dots (•) represent MM of the gel-filtration standards from the commercial calibration kit. Blue and red lines orthogonal to the axes correspond to different AcCYP51 populations: P1 with MM of 100.0 kDa and P2 with MM of 57.4 kDa. (C) SEC-MALS analysis of P1 peak showing experimental MM of the P1 fraction of 100.0 kDa (red line). (D) SDS-PAGE analysis of the purified P1 fraction.

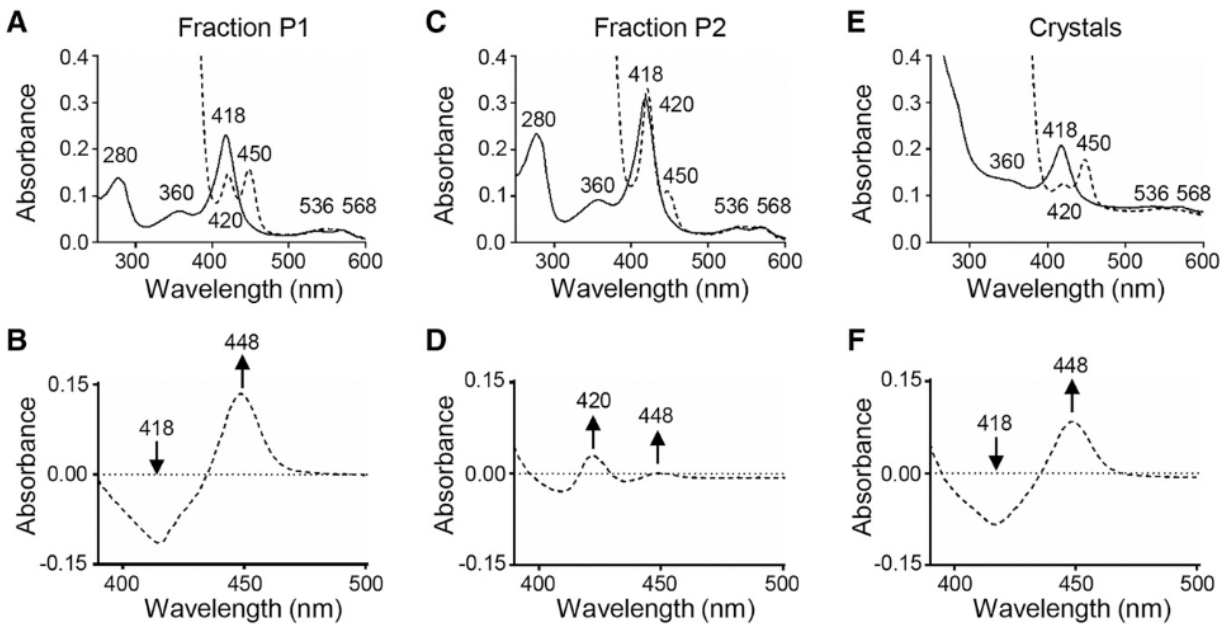

Figure 3.2 UV-Visible Spectroscopy Analysis of AcCYP51. (A) Absolute UV-visible spectra of the purified P1 fraction of AcCYP51 showing characteristic peaks at 280, 360, 418, 536, and 568 nm; ferric Fe^{3+}, solid line. Sodium dithionite–reduced CO-bound ferrous-Fe^{2+} form shows peaks at 420 and 450 nm, dashed line. (B) CO-bound difference spectra of the sodium dithionite–reduced dimeric fraction, P1. (C) Absolute spectra of the monomeric fraction, P2; ferric Fe^{3+}, solid line; CO-bubbled sodium dithionite–reduced ferrous Fe^{2+}, dashed line. (D) CO-bound difference spectra of the sodium dithionite–reduced monomeric fraction, P2. (E) Absolute spectra of the AcCYP51 recovered from the dimer crystals; ferric Fe^{3+}, solid line; CO-bubbled sodium dithionite–reduced ferrous Fe^{2+}, dashed line. High absorbance <300 nm is an artifact of measurements in plastic cuvette. (F) CO-bound difference spectra of the sodium dithionite–reduced AcCYP51 recovered from the dimer crystals.

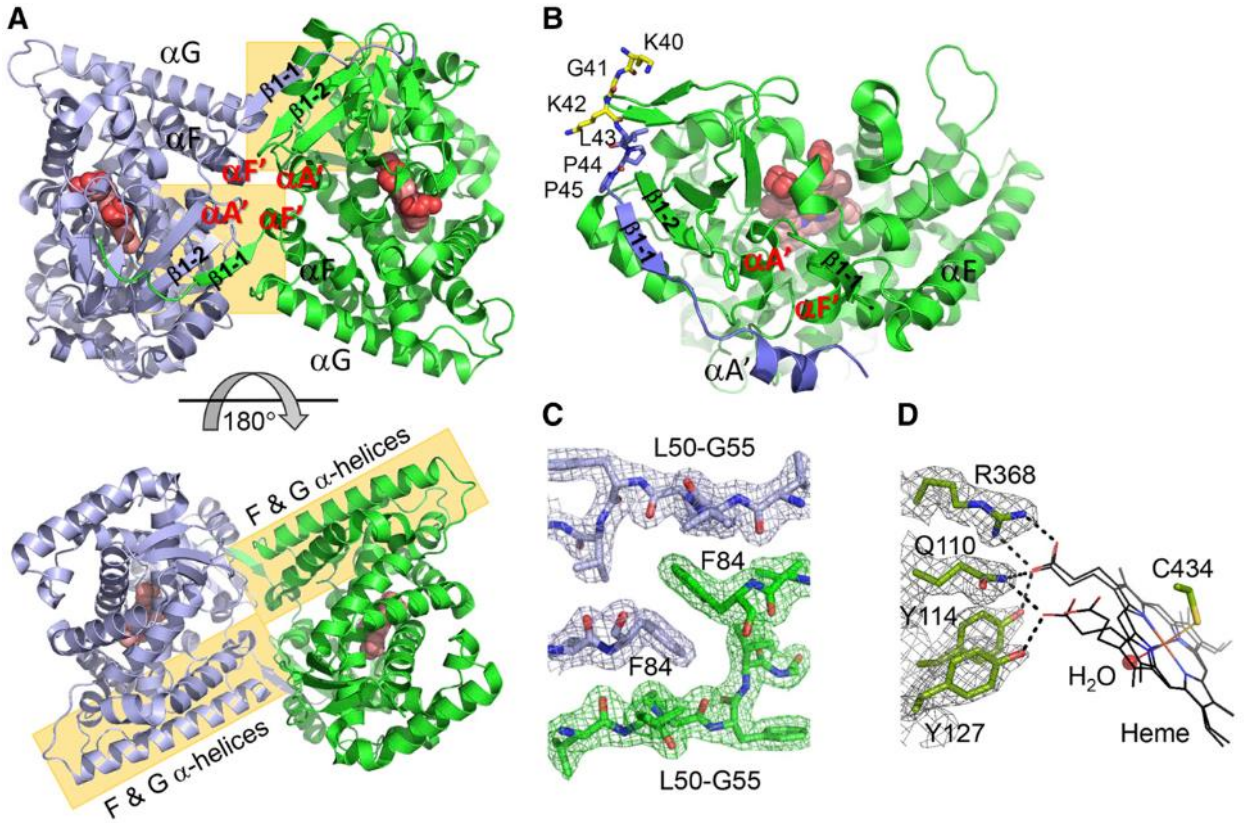

Figure 3.3 X-Ray Structure of the AcCYP51 Dimer. (A) Head-to-head dimer is shown in ribbon representation. The protomers are in blue and green. The heme prosthetic group is in pink Van der Waals spheres; oxygen atoms of the heme propionate moieties are in red. Interfacing secondary structure elements are shaded in yellow. (B) Interactions of the swapped fragment (blue) with adjacent protomer (green). A fragment of the exogenous leading sequence is shown in yellow. Authentic AcCYP51 sequence is in blue. (C) A fragment of the $2F_o$-F_c electron density map contoured at 1.2 σ (blue and green mesh) shows interactions of F84, a residue at the dimer interface with the most prominent solvation energy gain. (D) Heme in two alternative conformations is shown in black lines. Heme propionate groups interactions with the amino acid residues within 3.2 Å are indicated by the dashed lines. Coordination bonds to the heme axial ligands C434 and water molecule (red sphere) are shown.

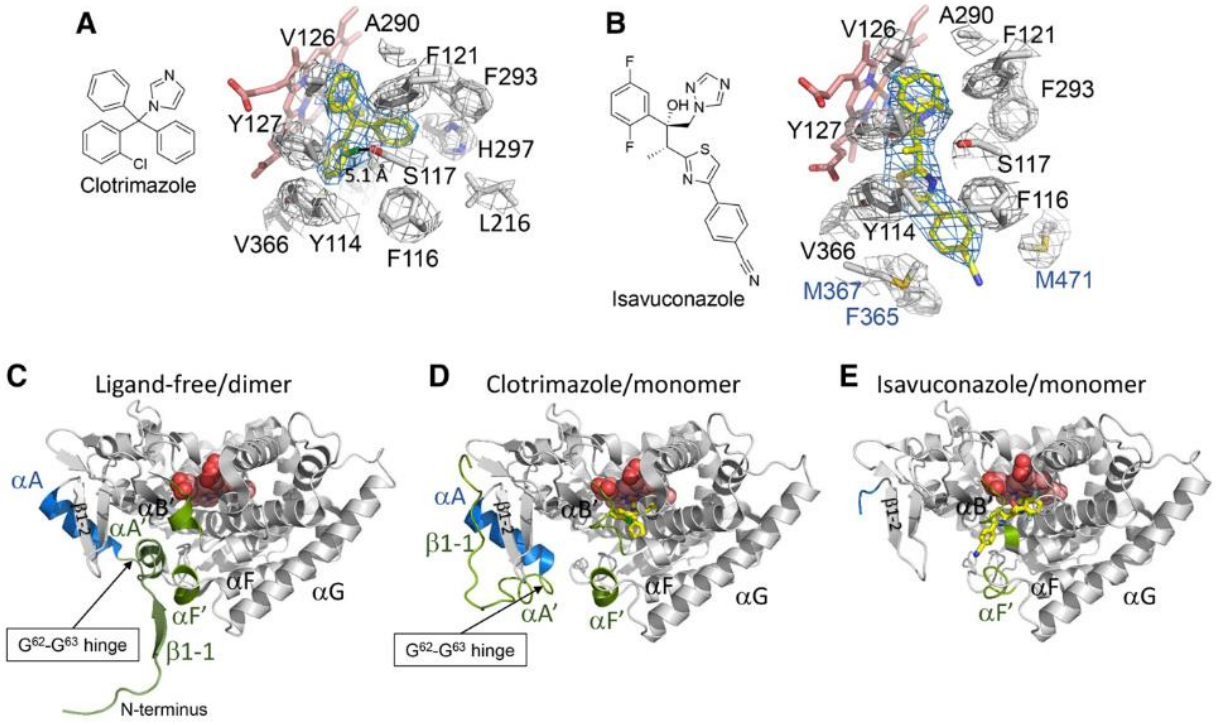

Figure 3.4 AcCYP51-Inhibitor Complexes. (A) Clotrimazole bound in the active site. (B) Isavuconazole bound in the active site. In (A and B), inhibitors are shown in yellow, heme is shown in pink, and amino acid side chains within 5 Å are shown in gray. The fragments of the $2F_o$-F_c electron density omit map (blue and gray mesh) are countered at 1.0 σ. Chemical structures of the inhibitors are shown as two-dimensional diagrams. (C–E) Ribbon representations of the superimposed AcCYP51 from the inhibitor-free (dimeric) and inhibitor-bound (monomeric) structures. The equivalent positions corresponding to the N terminus, the β1-1 strand, the A', B', and F' helices are colored in green and to the αA helix in blue. Heme is in pink Van der Waals spheres; clotrimazole and isavuconazole are yellow in stick mode. Nitrogen atoms are in blue, oxygen in red, chlorine in green, and fluorine in cyan.

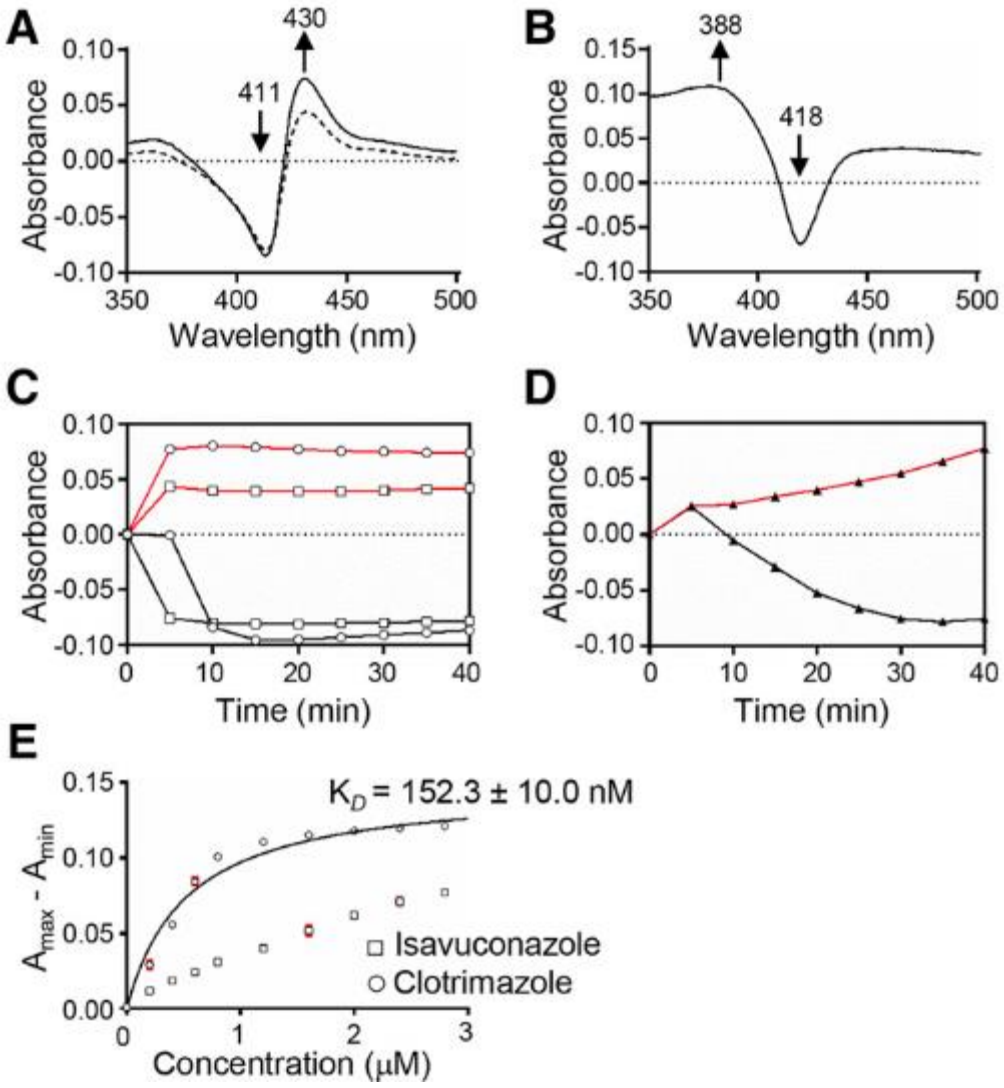

Figure 3.5 Ligand-Binding Properties of the AcCYP51 Dimer. (A) Type II difference binding spectra of 20 μM isavuconazole (dashed line) and 20 μM clotrimazole (solid line) to 5 μM AcCYP51. (B) Type I difference binding spectra of 20 μM 31-norlanosterol to 5 mM AcCYP51. (C) Binding kinetics of 20 μM isavuconazole (open squares) and clotrimazole (open circles) to 5 μM AcCYP51 at 430 (red curves) and 411 nm (black curves). (D) Binding kinetics of 20 μM 31-norlanosterol to 5 μM AcCYP51 at 388 (red curve) and 418 nm (black curve). Experiments in (C and D) were performed twice. A representative time course is shown for each ligand. Percentage of the ligand-bound fraction in Table 3.2 is calculated based on duplicates. (E) Binding isotherms of isavuconazole and clotrimazole; A_{max} is absorbance at 430, and A_{min} is absorbance at 410 nm. AcCYP51 concentration is 1 μM. S.D. are shown in red. For most data points, deviations are smaller than the size of the symbols.

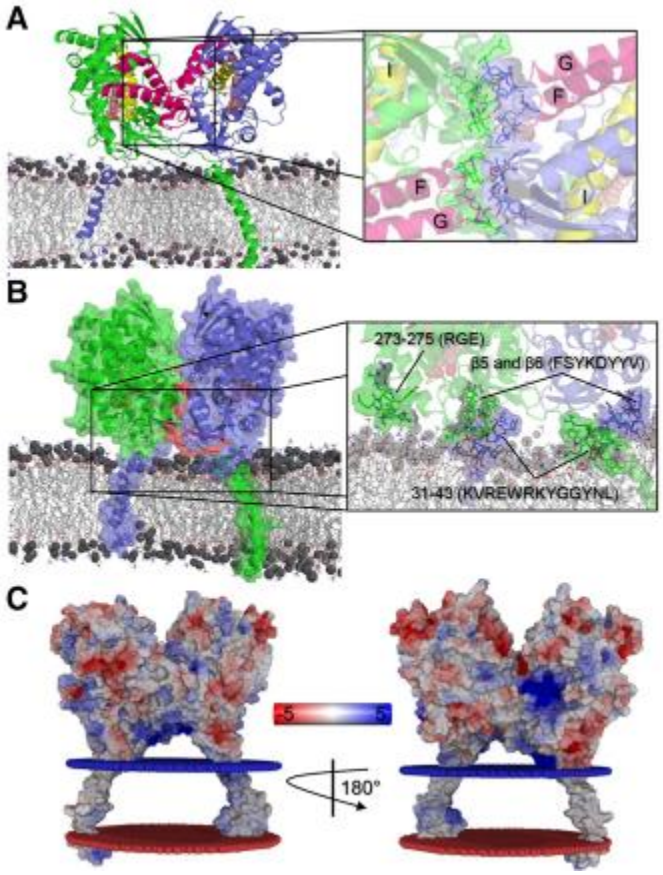

Figure 3.6 Molecular Model of the AcCYP51 Dimer in a Phospholipid Bilayer. (A) The full-length AcCYP51 dimer with the reconstituted TM helix is colored in blue and green. The F and G helices are highlighted in magenta, the I helix is in yellow, and heme is in pink Van der Waals spheres. Membrane lipids are in gray lines; phosphorous atoms of phospholipids are in black spheres. The dimer interface is displayed in the right panel, wherein the main interacting residues are depicted as sticks and surfaces. (B) Semitransparent surface representation of AcCYP51 dimer and a zoom in on protein-lipid interactions outside of the TM helices. The right panel zooms in on the protein-lipid interactions. The participating residues are labeled. (C) Electrostatic potential surface calculated for AcCYP51 dimer. The blue bead layer indicates the cytoplasmic side, and the red bead layer indicates the luminal side of the ER membrane.

Data S3.1 Recombinant AcCYP51.

Recombinant AcCYp51 amino acid sequence

MAKKTSSKGKLPPVVSSLIPFVGSGLSFAGGPLQYTTDAYKKYGDIFTMKVFGQRLTFL
VGPDAHVPFFSQGDAELSQDEPYQFSVPIFGPNVVYGADLAHRNQQLKFIAASLSTKA
LQSYVPLIVKEAEDFFAKWDKSGTVDIRDALAELIILTASRCLMGKEIRENLFTEVAKLYQ
TLDEGLLPISVFFPYLPIPAHKRRDEARLAMVRMFKKIIDERRANPEVKHNDCLQVFMD
ARYRGEEQALNDEEITGLMIALLFAGQHTSSVTGSWTGLLLFEANNKKKFLPGVLEEQ
EEIRKEFGDELTMEALNKMDKLHRCVKEALRMYPPLLFVMRKVIKPFSYKDYYVPEGD
TVFVSPALSMRVEEVFPNADQYNPERFVEEDKQAQKYRFVGFGAGRHGCMGENFAY
LQIKTIWSVLLRNFDIELVGELPKPDYTAMVVGPAHPCLLRYTRKHHHHHH

Codon-optimized DNA sequence

ATGGCCAAAAAGACGTCTTCAAAGGGTAAATTACCACCGGTTGTGAGCAGTTTGAT
TCCATTTGTGGGTAGCGGCCTGAGTTTCGCAGGTGGTCCGTTGCAATACACCACT
GATGCATACAAAAAGTACGGCGACATCTTTACGATGAAAGTTTTCGGCCAAAGATT
AACCTTTTTGGTCGGTCCAGATGCCCATGTACCGTTTTTCTCTCAGGGCGATGCGG
AACTGTCACAAGACGAACCTTATCAGTTTTCCGTTCCGATTTTCGGCCCTAATGTCG
TATACGGTGCTGATTTGGCACACCGCAACCAACAGCTGAAGTTTATTGCTGCATCT
CTGTCAACTAAAGCGTTACAATCGTACGTCCCACTGATCGTAAAAGAAGCCGAAGA
TTTCTTTGCGAAGTGGGACAAAAGCGGCACTGTGGATATTCGTGACGCCCTGGCG
GAATTAATTATCTTGACAGCCAGTCGTTGTTTGATGGGCAAGGAAATCAGAGAAAA
CCTGTTTACCGAAGTTGCGAAACTGTATCAGACATTAGATGAAGGTCTGTTGCCTA
TTTCTGTATTTTTCCCATACTTACCGATCCCTGCTCATAAACGTAGAGATGAAGCCC
GCCTGGCGATGGTTCGTATGTTCAAAAAGATTATCGATGAACGCCGTGCAAATCCG
GAAGTTAAACACAACGATTGCCTGCAAGTGTTCATGGACGCCCGTTATCGTGGTGA
AGAACAGGCGTTAAATGATGAAGAAATTACAGGCTTGATGATCGCTTTGCTGTTTG
CAGGTCAACATACATCCTCGGTTACGGGCAGTTGGACCGGTTTGTTGCTGTTCGAA
GCTAACAACAAAAAGAAATTCTTGCCAGGCGTGCTGGAAGAACAGGAAGAAATTCG
TAAAGAATTTGGCGATGAATTGACTATGGAAGCTCTGAACAAGATGGACAAACTGC
ATAGATGTGTCAAAGAAGCATTACGCATGTATCCTCCATTATTGTTCGTTATGAGAA
AAGTTATTAAACCATTCTCTTACAAAGATTATTACGTTCCGGAAGGTGACACAGTCT
TTGTATCCCCTGCCCTGTCGATGAGAGTTGAAGAAGTGTTTCCGAATGCGGATCAA
TATAACCCTGAACGCTTCGTTGAAGAAGACAAGCAAGCTCAGAAATACCGCTTTGT
GGGTTTCGGCGCAGGTCGTCATGGCTGTATGGGTGAAAATTTTGCTTATCTGCAGA
TTAAGACCATCTGGTCTGTCCTGTTACGCAACTTCGATATTGAATTAGTAGGCGAAT
TGCCAAAACCGGACTATACGGCTATGGTTGTGGGTCCTGCACACCCATGCTTGCT
GCGTTACACCAGAAAACATCACCATCACCATCACTAA

The codon-optimized cDNA sequence of AcCYP51 (NCBI Reference: XP_004334294.1) was generated synthetically (GenScript, Piscataway, New Jersey). The 42 N-terminal residues were replaced with the MAKKTSSKGK lead sequence and the 6xHis tag is added at the C-terminus. The synthetic DNA construct was cloned between the NdeI and HindIII restriction sites into the pCW-LIC expression vector obtained from the non-profit

plasmid repository (Addgene, Cambridge, MA). Engineered sequences are shaded in cyan and region involved in the domain swap interactions is underlined.

Data S3.2 - AcCYP51 expression and purification protocols.

Expression: Fresh transformants containing the pCW-AcCYP51 vector were obtained after transforming ~ 50 ng of vector DNA into HMS 174 *E.coli* cells pre-transformed with pGro7 plasmid (Takara) carrying GroEL/ES chaperones. After overnight incubation at 37 °C on an LB agar plate supplemented with 50 g/mL ampicillin and 20g/mL chloramphenicol, a selected single colony was used to set up a primary culture in LB media supplemented with 50 g/mL ampicillin and 20 g/mL chloramphenicol. Primary culture was incubated overnight at 37 °C, 250 rpm. 10 mL of the primary culture were used to set up secondary culture in 1 liter of Terrific Broth media supplemented with 1 mM Thiamine, 50 g/mL ampicillin, 20 g/mL chloramphenicol, 1X rare salt solution (**Table S3.1**). After inoculation, the culture was incubated for 5 h at 37 °C with constant stirring at 200 rpm. When OD 600 reached approximately 0.4-0.5 a.u., the incubation temperature was reduced to 25 °C and stirring was reduced to 145 rpm. Growth continued until OD 600 reached 0.6-0.8 a.u., then AcCYP51 expression was induced with 0.25 mM isopropyl-ß-D-thiogalactopyranoside (IPTG). Simultaneously, arabinose was added to 0.5 mg/mL to induce chaperone expression. Finally, the media was also supplemented with a heme precursor - 1 mM delta-aminolevulinic acid - and incubated for 45-48 h at 25 °C, 145 rpm. After incubation, the culture was harvested at 6000 g, 4 °C for 15 min and the cell pellet was suspended evenly in 10-15 mL of lysis buffer (**Table S3.2**) and 25 l of lysozyme (from 50 mg/mL stock) was added per liter of culture. Cell suspension was stored at -80 °C.

Purification: Cells were disrupted using a fluid processor Microfluidics M-110P (Microfluidics Inc.) and cell debris were removed by centrifuging at 4 °C, for 30 min. at 15000 rpm. The supernatant thus obtained was loaded onto a pre-equilibrated Ni-NTA column. Following loading, the column was washed with 10 column volumes (CV) of wash buffer I (refer **Table S3.3** for buffer compositions) followed by 10 CV of wash buffer II. Finally, column-bound His-tagged protein was eluted under a linear gradient of 0-100 mM L-histidine (Sigma).

Table S3.1 Composition of 4000X Rare Salt Solution

$FeCl_3.6H_2O$	2.7g
$ZnCl_2.4H_2O$	0.2g
$CoCl_2.6H_2O$	0.2g
$Na_2MoO_4.2H_2O$	0.2g
$CaCl_2.2H_2O$	0.1g
$CuSO_4.5H_2O$	0.186g
H_3BO_3	0.05g
Add HCl until salts dissolve	
Deionized water	Make up to 100 mL

Table S3.2 Composition of lysis buffer

Reagents	Working concentration
Glycerol	5%
K-Phosphate, pH-8.0	50 mM
EDTA	0.5 mM
NaCl	300 mM
PMSF	0.5 mM
DTT	1 mM

Table S3.3 Composition of Purification Buffers

Component	Reagent	Working concentration
Ni-NTA		
Equilibration buffer	K-phosphate, pH 8.0 NaCl Glycerol	50 mM 300 mM 10%
Wash buffer I	Same as equilibration buffer	
Wash buffer II	K-phosphate, pH 8.0 Glycerol	50 mM 10%
Elution buffer	K-phosphate, pH 8.0 Glycerol L-Histidine	50 mM 10% 0 – 100 mM
Q-Sepharose		
Equilibration and running buffer	K-phosphate, pH 8.0 Glycerol	50 mM 10%
HAP		
Equilibration buffer	K-Phosphate, pH 8.0 Glycerol	50 mM 10%
Elution buffer	K-Phosphate, pH 8.0 Glycerol EDTA	0.05 – 1 M 10% 0.5 mM
Superdex 200 XK 26		
Equilibration and running buffer	K-Phosphate, pH 8.0 Glycerol	50 mM 5%

Chapter 4: Evaluation of Amebicidal and Cysticidal Activities of Antifungal Drug Isavuconazonium Sulfate against *Acanthamoeba* T4 Strains

4.1 Introduction

Acanthamoeba castellanii is a causative agent of *Acanthamoeba* keratitis (AK). It is a serious infection of the eye that causes inflammation in the cornea and can result in permanent visual impairment or blindness. *Acanthamoeba* is common in nature and can be found in soil, air and water, including insufficiently chlorinated pools, hot tubs, tap and shower water. In unfavorable environments, the ameboid form of the organism called a 'trophozoite' transforms into a drug-resistant double-walled cyst. Cyst resistance to therapeutic agents, and recurrence of infection due to *Acanthamoeba* excystment, remain challenges for disease prevention and cures. Infection recurrence occurs in approximately 10% of cases (32) , due possibly to excystment. No single drug has yet been shown effective at therapeutic concentrations against both the trophozoite and cyst stages of *Acanthamoeba*. Current treatment of AK involves an aggressive disinfectant chlorhexidine, in combination with diamidines, polyhexamethylene biguanide (PHMB) and neomycin. Combination therapies have proven more successful than monotherapies (288–290). The most aggressive and severe cases of AK require corneal grafts or surgical removal of the eye (291). Despite advances in combination therapies and surgery, the resistance of cysts to therapeutic agents poses challenges that are yet to be addressed (292). Therefore, discovering and identifying therapeutics that are effective against both stages of the parasite would be critical to reducing AK recurrence and improving existing therapies.

Earlier, we identified isavuconazole as amebicidal and cysticidal (152), but clinically the prodrug isavuconazonium sulfate is administered orally or intravenously for the treatment of fungal infections. Isavuconazonium sulfate is metabolized by plasma esterase enzymes, specifically butyrylcholinesterase, into isavuconazole (293). However, it is unknown if isavuconazonium can be metabolized into isavuconazole in the human eye. As such, we evaluated the activity of isavuconazonium sulfate activity against the trophozoites and cysts of three separate T4 genotype strains of *Acanthamoeba*.

4.2 Results

Determination of Amebicidal Activity. The amebicidal activity of isavuconazonium sulfate was tested against three T4 genotype strains of *Acanthamoeba* (strains Ma, CDC:V240, and MEEI 0184). The trophozoites were exposed to serial dilutions of isavuconazonium sulfate with final concentrations ranging from 50 µM to 0.006 nM. All three strains of *Acanthamoeba* trophozoite appeared to be highly susceptible to isavuconazonium sulfate. Isavuconazonium displayed an EC_{50} of 0.001 µM against *Acanthamoeba* strain Ma (Fig. 4.1A), which was about 1700- to 5000-fold more potent than the current standards of care chlorhexidine and PHMB. The EC_{50} of isavuconazonium against *Acanthamoeba* strain CDC:V240 was 0.037 µM (Fig. 4.1B), which was about 30- to 300-fold more potent than chlorhexidine and PHMB, respectively. Isavuconazonium exhibited an EC_{50} of 0.024 µM against clinical strain MEEI 0184 (Fig. 4.1C). This EC_{50} was about 1.5-fold better than the EC_{50} demonstrated against the CDC:V240 strain (Table 4.1). Overall, these nanomolar potencies demonstrate that isavuconazonium retains its potency against trophozoites of *Acanthamoeba* T4 strains.

Determination of Cysticidal Activity. *Acanthamoeba* T4 cysts are also clinically relevant, as they are often more difficult to treat than trophozoites and require higher concentrations of antimicrobial compounds for efficacy. In order to determine the activity of isavuconazonium sulfate against cysts of *Acanthamoeba* T4 strains, cysts from all three strains were tested against higher concentrations of isavuconazonium sulfate than for evaluating trophozoites. Final concentrations of isavuconazonium ranged from 200 μM to 100 μM in increments of 10 μM, and a treatment was considered to be cysticidal if there was no evidence of trophozoite proliferation or excystation by day 7, which is a commonly used end point for cysticidal assays (35, 60, 103, 161, 162).

Acanthamoeba T4 cysts were treated with isavuconazonium and allowed to recover in PYG growth media for 7 days and evaluated for cysticidal activity. Isavuconazonium displayed cysticidal activity against all three tested strains, as no excystation was observed at day 7 (Fig. 4.2A, D, G). Isavuconazonium exhibited an average minimum cysticidal concentration (MCC) of 167.1 ± 23.6 μM against Acanthamoeba Ma strain. Acanthamoeba strain CDC:V240 had an average MCC of 136.0 ± 11.4 μM. Acanthamoeba strain MEEI 0184 displayed an average MCC of 187.5 ± 5.0 μM.

Effect of Combination of Isavuconazonium and PHMB on Cysts. While isavuconazonium has low nanomolar potency against trophozoites, it appears to display cysticidal activity only at high micromolar concentrations. Since cysts require higher isavuconazonium concentrations to prevent excystation, we wanted to evaluate if

isavuconazonium in combination with other currently used drugs can display synergy to reduce the isavuconazonium concentration required to treat cysts.

Isavuconazonium was combined with PHMB and qualitatively assessed for excystation after 7 days of incubation in growth media (Fig. 4.3). Isavuconazonium displayed an MCC of 167.1 μM. Combined with 40.41 μM PHMB, isavuconazonium was able to be lowered to 20.52 μM and still have minimal excystation (Fig. 4.4A). Monotherapy of 20.52 μM isavuconazonium was confluent with trophozoites by day 7 (Fig. 4.4B). Monotherapy of 40.41 μM PHMB had minimal to no excystation (Fig. 4.4C). Since the combination of 20.52 μM of isavuconazonium with 40.41 μM of PHMB elicited a similar effect to what was caused by 40.41 μM of PHMB alone, it is apparent that the combination of two compounds did not have a synergistic effect able to suppress excystation or kill cysts. It was clear that the combination of these two compounds at this concentration did not cause an antagonistic effect on the cysts of Ma strain of *Acanthamoeba*.

4.3 Discussion

Isavuconazole has previously been evaluated and demonstrated potent amebicidal and cysticidal activity (152). Since isavuconazole is typically administered as the prodrug isavuconazonium sulfate, there is a possibility that it may not be metabolized in the human eye and that *Acanthamoeba* T4 strains would not be susceptible to isavuconazole. Previously, isavuconazonium was identified as effective against *Acanthamoeba* T4 trophozoites (155), but its effect was not investigated against multiple strains and, more importantly, on the cysts of *Acanthamoeba* T4 strains. In this work, we

evaluated the amebicidal and cysticidal activity of isavuconazonium against multiple strains of *Acanthamoeba* T4, and also explored the possibility of combining isavuconazonium with PHMB against the cysts of *Acanthamoeba*.

Isavuconazonium had mean EC_{50} values against trophozoites ranging from 0.001 µM (strain Ma) to 0.037 µM (strain CDC:V240) (Table 4.1). Our reported values are lower than those reported by Rice et al. against *Acanthamoeba* strain Ma (EC_{50} of 0.09 ± 0.02 µM (155). This could be due to the differences in experimental conditions. We also previously evaluated the active drug isavuconazole against trophozoites and reported an EC_{50} of <0.001 µM (strain CDC:V240), 0.005 µM (strain Ma), and 0.026 µM (strain MEEI 0184) (152). The EC_{50} values of isavuconazonium for strains Ma and MEEI 0184 are comparable to those previously reported values for isavuconazole. Interestingly, the EC_{50} of isavuconazonium against CDC:V240 was approximately 40× higher than that of the previously reported isavuconazole EC_{50} value. Taken together, this suggests Acanthamoeba T4 trophozoites are still susceptible to the prodrug isavuconazonium.

To our knowledge, this is the first reported evaluation of the cysticidal activity of isavuconazonium sulfate against *Acanthamoeba* T4 strains. We previously reported that isavuconazole, the active form of isavuconazonium, displayed cysticidal activity against *Acanthamoeba* Ma at 70 µM (152). In this work, we determined the MCC of isavuconazonium against various *Acanthamoeba* T4 strains. The MCC of isavuconazonium varies from 1.9× (CDC:V240) to 2.6× (MEEI 0184) higher than previously reported about isavuconazole (152). Since isavuconazonium is a prodrug that must be metabolized to active isavuconazole, it is possible that higher concentrations of

the prodrug are required as not all of the isavuconazonium is metabolized into isavuconazole.

AK therapies frequently rely on chlorhexidine or PHMB as monotherapy, or in combination with propamidine isethionate and hexamidine(44, 45). Commonly used combinations include PHMB with propamidine, chlorhexidine with propamidine, chlorhexidine with PHMB, and PHMB with propamidine and neomycin (46). Since combination therapies were found to be more successful than monotherapies, we investigated the effect of the combination of isavuconazonium and PHMB on cysts of an *Acanthamoeba* T4 strain. In spite of the challenges associated with the excystation-based cysticidal assay that depends on a “cysticidal-or-not” readout rather than percentage inhibition (294), we identified that the combination of isavuconazonium and PHMB did not cause antagonistic or synergistic cysticidal effects on the cysts of the Ma strain of *Acanthamoeba*. Future studies will require confirmation of the effect of the combination of isavuconazonium and PHMB on trophozoites and cysts of different strains. Whether isavuconazonium can be combined with other commonly used drugs will require further investigation.

Isavuconazoium sulfate is FDA-approved for the treatment of invasive aspergillosis and mucormycosis (295) . In terms of fungal infections, isavuconazonium sulfate inhibits lanosterol 14α-demethylase (293), which prevents the biosynthesis of ergosterol and results in its eventual depletion. It is available in both oral and intravenous formulations and following administration, it is rapidly cleaved to the active isavuconazole. Tissue distribution of isavuconazole was evaluated in animals after oral and intravenous administrations of isavuconazonium sulfate, and a low concentration of isavuconazole

was detected in the eye lens (295, 296). This low concentration of isavuconazole may not be sufficient to kill *Acanthamoeba* T4 cysts if the drug is administered orally or intravenously. The preferable route of administration of drugs for the treatment of AK is topical, but distribution of isavuconazole in eye has not been evaluated when administered topically. Therefore, it was important to determine the effect of the prodrug isavuconazonium sulfate in case topical administration of prodrug isavuconazonium sulfate does not lead to the formation of active isavuconazole in human eyes. The potent amebicidal and cysticidal activities of the prodrug isavuconazonium sulfate against multiple T4 strains of *Acanthamoeba* provide confidence that the FDA-approved isavuconazonium sulfate is a promising lead for the treatment of AK.

4.4 Conclusion

In this work, we tested isavuconazonium sulfate against *Acanthamoeba* T4 trophozoites and cysts to evaluate its potential as an anti-*Acanthamoeba* treatment. We found multiple T4 strains of *Acanthamoeba* to be susceptible to isavuconazonium, with appreciable activity against trophozoites even at low nanomolar concentrations. Cysts required significantly higher micromolar concentrations to prevent excystation. These findings suggest isavuconazonium to be potentially useful for clinical treatment of *Acanthamoeba* keratitis. Future studies should focus on *in vivo* animal models to validate isavuconazonium as a treatment option.

Author Contributions

Conceptualization, A.D. and B.S.; methodology, B.S., A.D. and M.B.; formal analysis, B.S. and M.B.; investigation, B.S. and M.B.; writing—original draft preparation, B.S. and M.B..; writing—review and editing, A.D., B.S. and M.B.; visualization, B.S. and M.B..; supervision, A.D. and B.S.; project administration, A.D., and B.S. All authors have read and agreed to the published version of the manuscript.

Funding

A.D. was supported by the National Eye Institute of the National Institutes of Health under Award Number R21EY032601.

Institution Review Board Statement

Not applicable.

Data Availability Statement

Data is contained within the article.

Acknowledgments

We thank Dr. Ibne Karim M. Ali and Shantanu Roy of CDC for providing CDC:V240 strain of *Acanthamoeba*. We are grateful to Dr. Noorjahan Panjwani of Tufts University for providing MEEI 0184 strain of *Acanthamoeba*. M.B. acknowledges the support of Undergraduate Research Scholarship Ledell Family Research Award for Science and Engineering.

Chapter 4, in full, is a reprint of the material as it appears in Brian Shing, Mina Balen, Anjan Debnath “Evaluation of Amebicidal and Cysticidal Activities of Antifungal Drug Isavuconazonium Sulfate against *Acanthamoeba* T4 Strains” Pharmaceuticals, 2021. The dissertation author was the primary author and major contributor to this paper.

Conflicts of Interest

The authors declare no conflict of interest.

4.5 Materials and Methods

Cell Culture. *Acanthamoeba* strains Ma (American Type Culture Collection #50370, Manassas, VA, USA), CDC:V240 (CDC, Atlanta, GA, USA), and MEEI 0184 (Tufts University, Medford, MA, USA), belonging to T4 genotype, were cultured as described by Shing *et al*. (152). Trophozoites were cultured at 28°C and 5% CO_2 in peptone yeast glucose (PYG) medium supplemented with 100 U/mL penicillin and 100 µg/mL streptomycin.

Determination of Amebicidal Activity. Stock 10 mM isavuconazonium sulfate (Cayman Chemical, Ann Arbor, MI, USA) and 10 mM chlorhexidine were prepared in DMSO. Isavuconazonium sulfate was serially diluted two-fold to generate solutions ranging in concentration from 10 mM to 1.2 nM. Next, 0.5 µL of each of these isavuconazonium sulfate dilutions was added to 96-well white, flat bottom microplates (Greiner Bio-One, Kremsmünster, Austria). This was followed by the addition of 5×10^3 trophozoites in 99.5 µL of PYG media to each well, giving final isavuconazonium sulfate

concentrations ranging from 50 µM to 5.96 pM. Additionally, 0.5 µL of DMSO was added as a negative control (0.5% (v/v) DMSO), while 0.5 µL of chlorhexidine (50 µM) was added as a positive control. The plates were incubated for 48 h at 28 °C and 5% CO_2. At 48 h, viability measurements were taken using the CellTiter-Glo luminescent cell viability assay (Promega, Madison, WI, USA) (152). For the measurements, 25 µL of CellTiter-Glo was added to each well and shaken on an orbital shaker at 360 RPM for 10 min prior to luminescence readings on an EnVision 2104 Multilabel Reader (PerkinElmer, Waltham, MA, USA). Data from a minimum of three independent experiments (biological replicates) conducted in triplicate were analyzed on GraphPad Prism 6 to determine EC_{50} values.

Cyst Generation. Encystment of *Acanthamoeba* T4 strains was induced by culturing trophozoites in an encystation media (95 mM NaCl; 5 mM KCl; 8 mM MgSO4; 0.4 mM CaCl2; 1 mM NaHCO3; 20 mM Tris-HCl, pH 9.0) (227). The trophozoite harvesting and encystation protocol were conducted as previously described by Shing *et al.* (152). Briefly, trophozoites of Acanthamoeba T4 strains were centrifuged at 200x g for 5 minutes and washed in phosphate-buffered saline (PBS) three times prior to resuspension in encystation media. Then, 5×10^3 cells in 99.5 µL were added to each well of a 96 well clear-bottom plate (Corning, Corning, NY, USA). The cells were incubated in encystation media to facilitate the encystation of trophozoites into cysts for 48 h prior to any cysticidal or combination experiments.

Determination of Cysticidal Activity. Cyst plate generation was conducted as previously described in section “Cyst Generation” (152). After 48 h, 0.5 µL of

isavuconazonium sulfate solution was added to a final concentration of 200, 190, 180, 170, 160, 150, 140, 130, 120, 110, or 100 μM. To serve as negative and positive controls, 0.5% (v/v) DMSO and 461.85 μM PHMB were used, respectively. The cysts were incubated for 48 h. Afterwards, the wells were washed four times with 100 μL of PBS before the addition of 100 μL of PYG medium. The cysts were then incubated for one week and imaged by an ImageXpress Micro XLS (Molecular Devices, San Jose, CA, USA) at 200× magnification. The PYG growth media were exchanged for fresh media on day 3 and day 5. The images were manually reviewed for excysted trophozoites, and cysticidal activity was defined as having no trophozoites by day 7. Image brightness and contrast were adjusted by ImageJ. All experiments were conducted in triplicate and images were analyzed from a minimum of four independent experiments.

Effect of Combination of Isavuconazonium and PHMB on Cysts. Isavuconazonium was evaluated in combination with PHMB to assess potential synergy. After generating a plate of cysts using the methods described in section “Cyst Generation”, the cysts were treated with a checkerboard dilution scheme.

Isavuconazonium sulfate was serially diluted two-fold to generate solutions ranging in concentration from 65.7 mM to 512 μM. PHMB was serially diluted two-fold to generate solutions ranging in concentration from 64.7 mM to 504 μM. Then, 0.25 μL of each of the isavuconazonium sulfate and PHMB dilutions were added to each well of the plate to generate various concentration combinations. Isavuconazonium’s dilution gradient varied horizontally across the plate to give final concentrations ranging from 164.14 to 1.28 μM. PHMB’s dilution gradient varied vertically across the plate to give final

concentrations ranging from 161.15 to 1.26 µM. As a negative control, 0.5% (v/v) DMSO was used, while 461.85 µM PHMB served as a positive control. Additionally, isavuconazonium sulfate and PHMB were also tested in monotherapy using the same final concentrations (164.14 to 1.28 µM and 161.15 to 1.26 µM, respectively) in separate columns.

After treatment for 48 h, the plate was washed with PBS and imaged for one week on the ImageXpress Micro XLS as described in section “Determination of Cysticidal Activity”. Images from three independent experiments were manually reviewed for excystation.

4.6 Figures and Tables

TABLE 4.1 EC_{50} Values of Isavuconazonium Sulfate against Trophozoites of *Acanthamoeba* T4 Strains. [a]CL, confidence limit

Inhibitor	Strain	Mean (μM)	95% lower CL (μM)[a]	95% upper CL (μM)[a]
Isavuconazonium sulfate	Ma	0.001	0.001	0.002
	CDC:V240	0.037	0.027	0.049
	MEEI 0184	0.024	0.021	0.027
Standards of care				
Chlorhexidine (152)	Ma	1.7	1.4	1.9
	CDC:V240	1.1	1.0	1.2
	MEEI 0184	1	0.9	1.1
PHMB (152)	Ma	7.2	6.6	8.0
	CDC:V240	11.8	10.5	13.4
	MEEI 0184	4.6	3.0	7.1

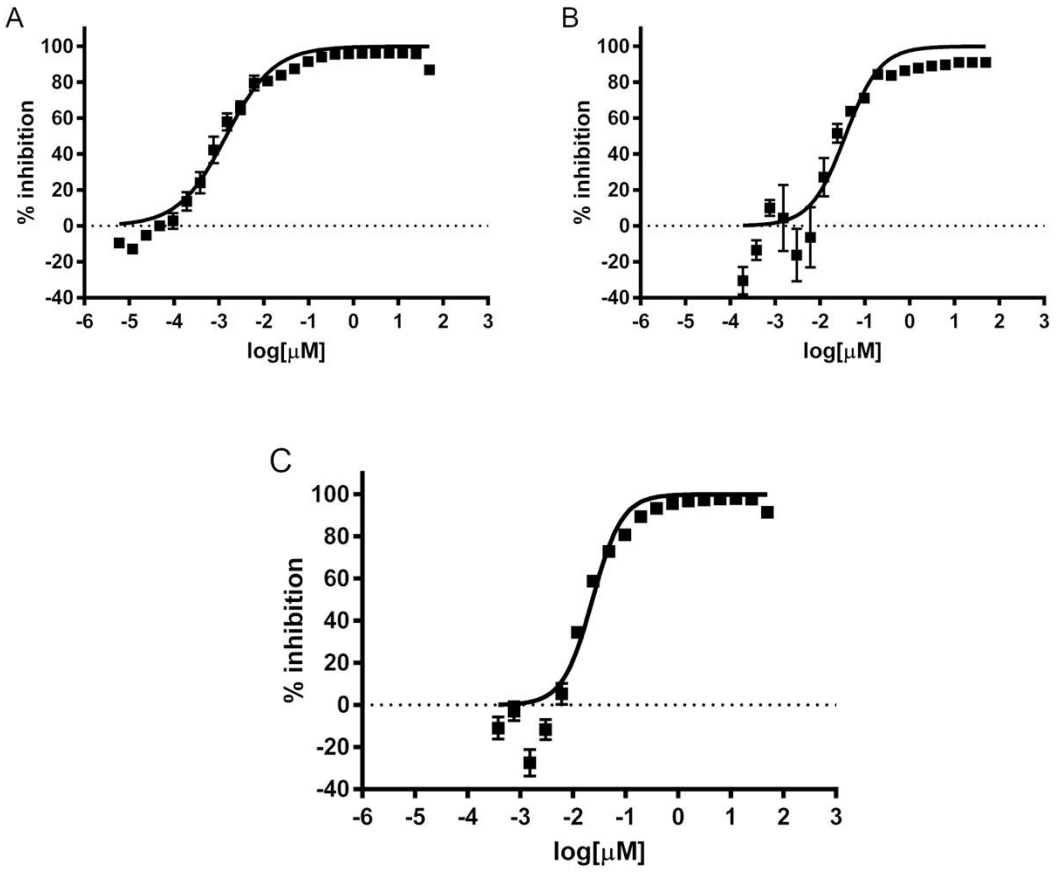

Figure 4.1 Concentration—Dependent Inhibition of Growth of *Acanthamoeba* Trophozoites by Isavuconazonium Sulfate. Different concentrations of isavuconazonium were tested in triplicate for activity against trophozoites of *Acanthamoeba* T4 strains. The data points represent mean percentage growth inhibition of (A) Ma strain, (B) CDC:V240, and (C) MEEI 0184 of different concentrations of isavuconazonium. EC_{50} curves were generated from mean values of percentage growth inhibition of isavuconazonium against *Acanthamoeba*.

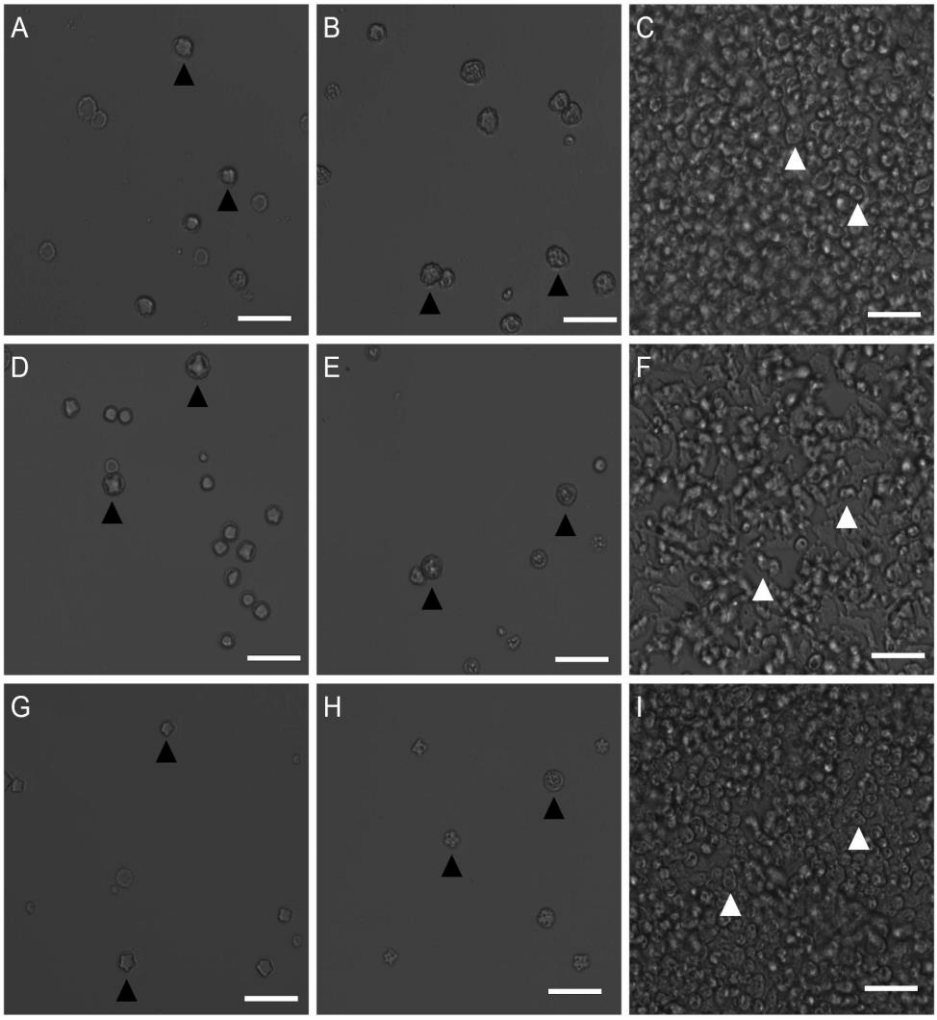

Figure 4.2 Effect of Isavuconazonium Sulfate on the Morphology of *Acanthamoeba* Ma, CDC:V240, and MEEI 0184 Cysts. Ma cysts were treated with (A) 170 µM isavuconazonium, (B) 461.85 µM PHMB, (C) 0.5% (v/v) DMSO. CDC:V240 strain cysts were treated with (D) 140 µM isavuconazonium, (E) 461.85 µM PHMB, (F) 0.5% (v/v) DMSO. MEEI 0184 strain cysts were treated with (G) 190 µM isavuconazonium, (H) 461.85 µM PHMB, (I) 0.5% (v/v) DMSO. Morphology and excystation of *Acanthamoeba* T4 cysts after 7 days of incubation in PYG growth media are displayed. Black arrowheads: cysts. White arrowheads: trophozoites. Magnification: 200x. Scale bar: 50 µm.

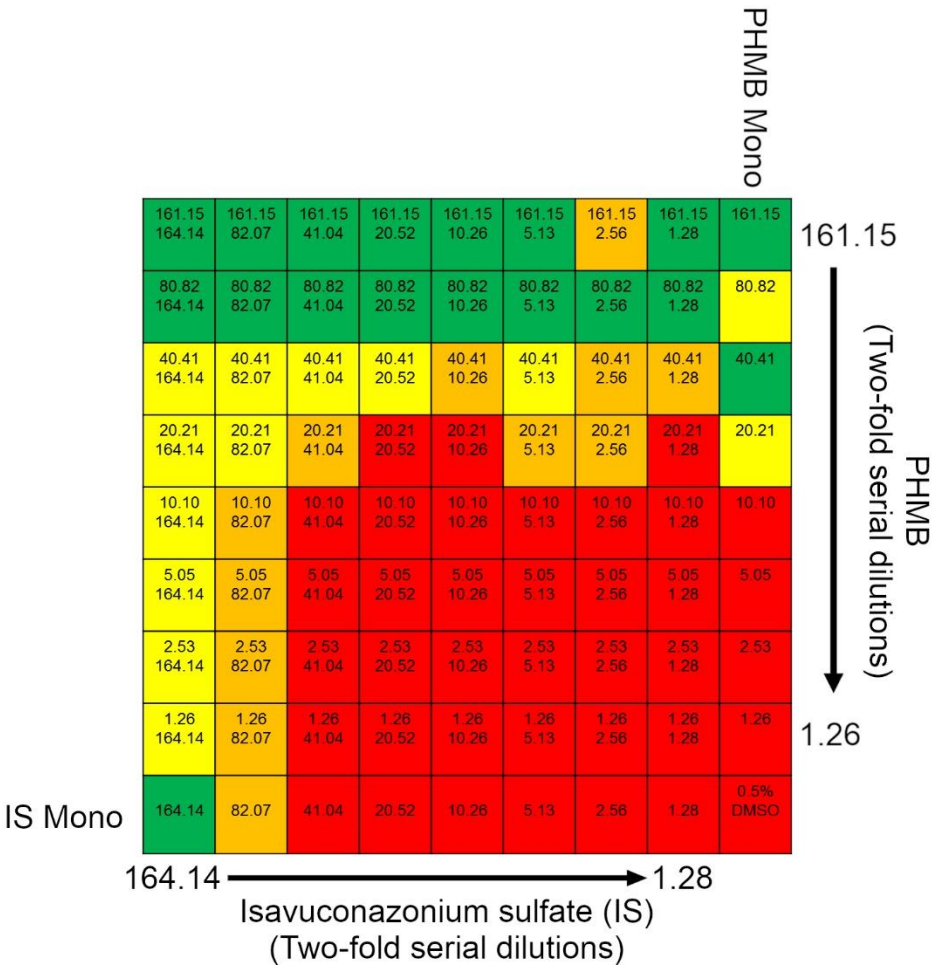

Figure 4.3 Isavuconazonium-PHMB Combination Excystation Heatmap. Heatmap displaying qualitative scoring of excystation for different isavuconazonium sulfate (IS)–PHMB combination treatments. Top number in grids represents PHMB concentration in μM, bottom number in grids represents isavuconazonium sulfate concentration in μM. Green: 0% trophozoite plate coverage; yellow: 0 - 1% trophozoite plate coverage; orange: 50 - 80% trophozoite plate coverage; red: 100% trophozoite plate coverage.

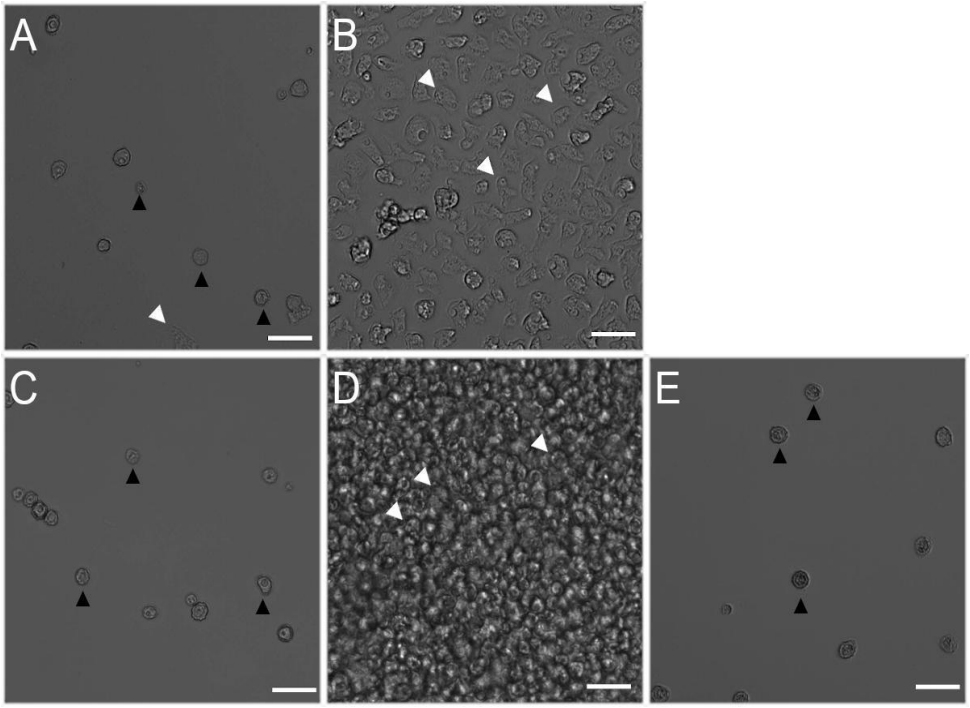

Figure 4.4 Effect of Combination of Isavuconazonium Sulfate and PHMB on the Morphology of *Acanthamoeba* Ma Cysts. Ma cysts were treated with (A) 20.52 μM isavuconazonium and 40.41 μM PHMB, (B) 20.52 μM isavuconazonium monotherapy, (C) 40.41 μM PHMB monotherapy, (D) 0.5% (v/v) DMSO, (E) 461.85 μM PHMB. Morphology and excystation of *Acanthamoeba* cysts were evaluated after 7 days of incubation in PYG growth media. Black arrowheads: cysts. White arrowheads: trophozoites. Magnification: 200x. Scale bar: 50 μm.

Chapter 5: Development of a Machine Learning-based Cysticidal Assay and Identification of an Amebicidal and Cysticidal Marine Microbial Metabolite against *Acanthamoeba*

5.1 Introduction

Acanthamoeba spp. are free-living amoebae that can be opportunistic and non-opportunistic pathogens commonly associated with *Acanthamoeba* keratitis, a severe corneal infection (1). Current *Acanthamoeba* keratitis treatment relies upon a combination of antimicrobials, but despite aggressive treatment, 10% of patients suffer recurrent *Acanthamoeba* keratitis (32). This recurrence has been suggested to be due to the resilience of cysts to antimicrobials, which allows viable cysts to persist through treatment to excyst at a later date (15, 297).

Currently, there is a lack of interest by the pharmaceutical industry to identify compounds with activity against *Acanthamoeba*. As such, there is a lack of innovation in cysticidal compound discovery. The current standard for screening compounds for cysticidal activity is to treat *Acanthamoeba* cysts with a compound of interest and manually observe for evidence of excystation, such as proliferating trophozoites or distinctive trails left in agar media by trophozoites (70, 161). These cysticidal screening techniques are labor-intensive and low-throughput, which limits their utility and efficiency.

Improving automation for cysticidal assays could significantly enhance current screening capabilities for *Acanthamoeba* and accelerate the rate of discovering cysticidal compounds. Recent advances in machine learning and object-detection algorithms present a unique asset to be leveraged for automating cysticidal assays. Convolution

neural network object-detection algorithms, such as R-CNN, SSD, and YOLOv3, allow computers to locate and classify objects within an image (298). Coupling automated high-content imaging systems with these machine learning object-detection algorithms could allow for novel automated cysticidal assays. Microscopy images could be analyzed through these object-detection algorithms to determine the change in trophozoite number over a period of time and identify if a compound is cysticidal. To demonstrate the utility of our cysticidal assay, we performed screening of a marine microbial natural products library to identify marine metabolites that are both trophocidal and cysticidal.

5.2 Results

Trophozoite Counting Algorithm Machine Learning Training. A google colaboratory environment was created to train a YOLOv3 object detection algorithm. The algorithm was trained for 1000 epochs on manually labeled images of cysts and trophozoites. Over the course of the training, the algorithm gradually improved identification of cysts and trophozoites within microscopy images. The precision, recall, F1, and mAP@0.5 increased monotonically and plateaued around 800 training epochs (Fig. 5.1G - J), indicating additional training past epoch 800 would not significantly improve the model's performance. The final model (1000 epochs) used for inference mode to count the cysts and trophozoites had a precision of 0.563, recall of 0.821, F1 score of 0.665, and mAP@0.5 of 0.721 (Fig. 5.1G - J). Sample bounding boxes labeling trophozoites and cysts qualitatively demonstrate the object detection algorithm was able to identify cysts and trophozoites (Fig. 5.2A).

The counts of trophozoites as determined by the YOLOv3 algorithm were compared to manual counting techniques to determine if these techniques provided comparable cell counts. *A. castellanii* trophozoites were seeded at serially diluted concentrations ranging from 4.0 x 10^4 to 625 trophozoites/100 µL. These trophozoites were imaged one hour after seeding to minimize the effect of proliferation on cell numbers and accurately reflect the starting number of cells. Equivalence between the YOLOv3 algorithm and manual counting techniques was confirmed by linear correlation between trophozoites manually counted by light microscopy and YOLOv3 algorithm-derived counts (Fig. 5.2B).

Cysticidal Assay Validation. A cysticidal compound would result in non-viable cysts, which should not result in an increase in trophozoites even with incubation in growth media. A non-cysticidal compound should have excystation and trophozoite proliferation after incubation in growth media. The trained YOLOv3 algorithm was utilized to count the number of trophozoites on days 0 and 3 following removal of compounds and exchange with PYG growth media. These counts were analyzed to determine if a well of the plate displayed evidence of excystation and trophozoite proliferation.

This novel phenotypic screen was first validated on reference compounds. *A. castellanii* cysts were treated with literature-relevant dilutions of reference compounds chlorhexidine, alexidine, caspofungin, amphotericin B, corifungin, and fluconazole and imaged. The change in number of trophozoites from day 0 to day 3 was determined for each well, and a logistic regression for each plate was calibrated using wells treated with 461.85 µM polyhexamethylene biguanide (PHMB) as positive controls (cysticidal hits) and

0.5% (v/v) DMSO as negative controls (non-cysticidal). Wells with a probability of being cysticidal > 0.9 as determined by the logistic regression were considered to be cysticidal.

Each reference compound was serially diluted two-fold at concentrations relevant to previously reported literature values to assess their minimum cysticidal concentrations (Table 5.1).

Alexidine has been classically reported to be cysticidal at 100 µg/mL (equivalent 171.91 µM) (58). Manual observation determined all dilutions of alexidine were cysticidal, which suggests a minimum cysticidal concentration <10.74 µM. The YOLOv3 algorithm successfully predicted the same minimum cysticidal concentration as the manual observation. While the minimum cysticidal concentration as determined by manual observation and YOLOv3 are lower than literature reported values, this could be due to these results being taken at day 3 as opposed to a later time point.

Chlorhexidine has been previously reported to have mean minimum cysticidal concentration of 7.02 µg/mL (equivalent 13.89 µM) with a minimum cysticidal concentration ranging from 13.52 – 3.12 µg/mL (equivalent 26.75 – 6.17 µM) (60). In this validation, chlorhexidine was manually verified to have a minimum cysticidal concentration between 13.89 and 6.94 µM. In contrast, the YOLOv3 predictions suggested a minimum cysticidal concentration between 6.94 and 3.47 µM.

Amphotericin B, caspofungin, fluconazole, and corifungin were not detected as cysticidal at any of the tested concentrations by both the YOLOv3 and manual observation. These findings are consistent with previous reports of amphotericin B, caspofungin, and fluconazole being non-cysticidal (161).

Interestingly, corifungin was not cysticidal at any of the concentrations tested. The YOLOv3 predictions were consistent with manual observations that none of the tested concentrations proved to be cysticidal. These findings seem to contrast previously reported observations of subcellular damage in *A. castellanii* cysts treated with high concentrations of corifungin (299). It is not clear whether this is due to the degradation of the stock compound or due to the use of a different strain.

While there were some variations in the minimum cysticidal concentration predicted by the YOLOv3 algorithm and manual observation for Chlorhexidine, a closer analysis of the YOLOv3 predictions against the manual observations reveal this assay has a high accuracy and specificity in predicting cysticidal and non-cysticidal compounds at day 3.

The predictions from the YOLOv3 algorithm were compared against manual observations for excystation in each well on day 3. The YOLOv3 algorithm had an overall accuracy of 0.97. The algorithm also displayed a recall of 1, specificity of 0.96, and precision of 0.90 (Table 5.2). The high specificity of this assay suggests it can accurately identify non-cysticidal compounds.

Screening of Marine Natural Products Library.

Amebicidal Assay. A library of 9,286 unique marine natural products fractions were screened for activity against *A. castellanii* trophozoites at 60 µg/mL. 29 fractions displayed >90% inhibition and were selected for further secondary screening on cysts (Fig. 5.3).

Cysticidal Assay. The 29 fractions identified in the primary screen were then evaluated against cysts at 120 µg/mL. Images from the fractions were processed through the YOLOv3 machine learning algorithm to determine the counts of trophozoites on days 0 and 3. After analyzing the change in trophozoites, fraction 12FP47A9 was identified as potentially cysticidial (Fig. 5.4A). This potentially cysticidal well was manually evaluated. At day 3, fraction 12FP47A9 displayed minimal amount of excystation (Fig. 5.4B) while all other fractions and the negative control (Fig. 5.4D) were confluent by day 3.

EC_{50} Determination. The top 10 fractions displaying the highest inhibition against trophozoites were assessed to determine their EC_{50} values. The fractions had EC_{50} values ranging from 0.4 to >60 µg/mL (Table 5.3). Interestingly, these EC_{50} values had little to no correlation with the probability of the compound being cysticidal, suggesting amebicidal activity is not a good predictor of cysticidal activity. Fraction 12FP47A9, which was the strongest candidate for being cysticidal, did not appear to have the strongest amebicidal activity of these fractions. Fractions with significantly lower EC_{50} values against trophozoites, such as 12FP15E5, were completely non-cysticidal.

Determination of Minimum Cysticidal Concentration of 12FP47A9. Since fraction 12FP47A9 demonstrated cysticidal activity, it was evaluated manually to determine its minimum cysticidal concentration. Cysts were treated with final concentrations of 12FP47A9 ranging from 480 to 3.75 µg/mL and evaluated for excystation and trophozoite growth up to 7 days. Fraction 12FP47A9 demonstrated minimal to no excystation at 480 µg/mL (Fig. 5.5A). Lower concentration of 12FP47A9 (240 µg/mL) resulted in moderate

excystation and trophozoite proliferation (Fig. 5.5B), suggesting a minimum cysticidal concentration between 480 and 240 µg/mL. These findings suggest fraction 12FP47A9 may provide promising anti-*Acanthamoeba* drug-like molecule candidates for further study.

5.3 Discussion

Current screening techniques for identifying cysticidal compounds against *Acanthamoeba* largely rely upon manual observation. Unfortunately, the manual nature of these assays can be a bottleneck that hampers the rate of cysticidal drug discovery. Machine learning, object-detection algorithms are relatively new, albeit promising, technologies since these algorithms could be adapted to recognize specific cell types and take over the role of manual observation to significantly improve the rate of cysticidal drug discovery.

This novel cysticidal assay screens for cysticidal compounds under axenic cell culture conditions. For the purposes of screening, potential cysticidal compounds were defined as having minimal to no excystation by day 3. Day 3 was considered to be the end point since cysts in wells treated with DMSO (negative control) excysted out and became confluent with trophozoites by day 3. These wells became over confluent and individual trophozoites were difficult to distinguish past day 3.

This assay was validated against known cysticidal and non-cysticidal compounds. These compounds were diluted serially and were screened by this assay. Predictions of the minimum cysticidal concentration of each compound by machine learning algorithm were compared to manual observations. Notably, the assay's prediction of minimum

cysticidal concentration of chlorhexidine was lower than what was manually observed by a factor of 2, suggesting the rare possibility for false positives (i.e. predicting a treatment to be cysticidal when it is not). However, this assay displayed very high specificity and correctly identified all non-cysticidal wells, suggesting it can accurately screen out non-cysticidal compounds. This still provides major utility as this assay is amenable to high-throughput screening and could be used to screen out non-cysticidal compounds in large compound libraries, leaving only a small amount of potentially cysticidal compounds for further manual evaluation.

Although natural products have been used for the treatment of parasitic diseases, none of them came from marine sources (300, 301). Drug discovery research for *Acanthamoeba* keratitis with marine natural products was only limited to a marine alga *Laurencia* sp. (302, 303). In order to identify novel marine metabolites with anti-*Acanthamoeba* activity, a marine natural products fraction library was evaluated to demonstrate the utility of this novel cysticidal assay. Since compounds useful for *Acanthamoeba* keratitis treatment should have dual activity against the trophozoite and cyst stages, these fractions were first screened against trophozoites of *Acanthamoeba*. Any compound that is not amebicidal would not be worth further consideration for investigation as trophozoites play an active role in *Acanthamoeba* keratitis.

The primary screen identified 29 fractions with high inhibition (>90%) against trophozoites. These fractions were then screened through this novel cysticidal assay, which identified fraction 12FP47A9 as potentially cysticidal (Fig. 5.6). At 120 µg/mL, fraction 12FP47A9 displayed minimal to no excystation by day 3, suggesting its potential as a cysticidal compound. This was followed with further manual evaluation, and 480

μg/mL displayed minimal to no excystation by day 7. This new cysticidal assay helped identify a new potentially cysticidal fraction, which was subsequently verified by manual observation, demonstrating its utility as a cysticidal screen. Furthermore, this assay is also useful since it can weed out non-cysticidal treatments and is amenable to high-throughput screening. The lack of correlation between EC_{50} (amebicidal) and cysticidal data further demonstrates the need for cysticidal assays as amebicidal compounds are not necessarily cysticidal. While this particular assay utilized YOLOv3 for classifying, identifying, and counting trophozoites and cysts, machine learning, object-detection algorithms are highly flexible and adaptable platforms that could be used to automate cell counting and identification for other phenotypically distinct cells to improve any morphological cell studies.

Taken together, our machine learning-based cysticidal assay and screening of marine microbial metabolites identified an amebicidal and cysticidal fraction 12FP47A9. This fraction may harbor anti-*Acanthamoeba* molecules that would serve as attractive drug development lead molecules. Future studies will involve isolation of pure compounds, testing of compounds to identify the actives and comprehensive assignment of structure.

Acknowledgments

The authors would like to thank and acknowledge Jeng Hau-Lin and Aryan Misra for helpful discussions and introduction to YOLOv3 object detection algorithms. The authors would also like to thank Dr. James H. McKerrow for his support throughout the study.

Chapter 5, is a print of the manuscript in preparation: Brian Shing, Mina Balen, William Fenical, Anjan Debnath “Development of a Machine Learning-based Cysticidal Assay and Identification of an Amebicidal and Cysticidal Marine Microbial Metabolite against *Acanthamoeba*”. The dissertation author was the primary author and major contributor to this paper.

5.4 Methods and Materials

A. castellanii Cell Culture. *A. castellanii* strain Ma trophozoites from the American Type Culture Collection (#50370) were cultured and maintained at 28°C and 5% CO_2 in Peptone Yeast Glucose (PYG) medium supplemented with 100 U/mL penicillin and 100 µg/mL streptomycin (225).

Cyst Microplate Preparation. Cysts were prepared by culturing trophozoites in an encystation media (95 mM NaCl, 5 mM KCl, 8 mM $MgSO_4$, 0.4 mM $CaCl_2$, 1 mM $NaHCO_3$, 20 mM Tris-HCl, pH 9.0) (227). Trophozoites were collected by centrifugation at 200 g for five minutes and washed in PBS three times before resuspension in encystation media. 5×10^3 trophozoites in 99.5 µL of encystation media were seeded into each well of a 96-well microplate for 48 hours to promote encystation. After 48 hours, the cysts were treated with 0.5 µL of compounds of interest dissolved in DMSO in triplicate wells. 0.5% (v/v) DMSO served as negative controls while 468.15 µM PHMB served as positive controls. The cysts were incubated for 48 hours with compounds of interest. Afterwards, the encystation medium was removed and the wells were washed four times with PBS before

addition of 100 µL of PYG medium. *A. castellanii* cysts were incubated in PYG media to promote excystation.

Trophozoite Counting Algorithm Machine-Learning Training. A google colaboratory notebook environment was created for the ultralytics YOLOv3 object-detection algorithm implementation downloaded from https://github.com/ultralytics/yolov3.

A. castellanii trophozoites were encysted as previously described and allowed to excyst for 24 hours in PYG growth media. These cells were imaged, and the .tiff microscopy images were converted in batches to .jpg file format using a custom python script. The trophozoites and cysts in these images were hand-labeled and annotated using labelImg. The training set consisted of 58 images with 3598 trophozoites and 3937 cysts labeled. The test set consisted of 20 images with 2127 trophozoites and 2099 cysts labeled. The validation set consisted of 10 images with 814 trophozoites and 785 cysts labeled. These datasets were utilized to train a custom model. Setup was as per ultralytics YOLOv3 instructions for training on custom data within a google colaboratory environment (304). The training was conducted in a Python 3 runtime environment with GPU acceleration and utilizing the provided yolov3-tiny.cfg configuration file. The model was trained for 1,000 epochs, and the last epoch model was utilized for object detection.

To determine equivalence between manual and the machine learning derived counts, trophozoites were serially diluted two-fold from 4.0×10^4 to 625 trophozoites and seeded into microplate wells in 100 µL of PYG growth media and allowed to attach for an hour. The wells were then imaged by an ImageXpress Micro XLS (Molecular Devices).

The images were inputted into the trained YOLOv3 model to count the number of trophozoites in each image. These counts were compared to the number of trophozoites in each image as determined by manual counting to assess equivalency.

Cysticidal Assay Validation. A microplate of cysts was generated following the microplate preparation method previously described. *A. castellanii* cysts were treated with serial two-fold dilutions of compounds reported to be cysticidal or non-cysticidal at concentrations relevant to previously reported literature.

Chlorhexidine gluconate (Acros Organics) was tested from 111.11 to 0.86 μM. Alexidine dihydrochloride (Sigma Aldrich) was tested from 1,375.26 to 10.74 μM. Corifungin (Dalton Chemicals) was tested from 1,600 to 12.5 μM. Amphotericin B (Gold Bio) was tested from 138.52 to 1.08 μM. Caspofungin diacetate (Sigma Aldrich) was tested from 105.49 to 0.82 μM. Fluconazole (Fluka Analytical) was tested from to 6,686.91 to 52.24 μM.

Each well of the microplate was imaged on the ImageXpress Micro XLS on day 0 and day 3 following removal of encystation media with compounds and addition of PYG media. The images were run through the YOLOv3 algorithm to count the number of trophozoites and determine the change in trophozoite number from day 0 to day 3. The Realstatistics Excel plugin was used to run logistic regressions with the change in trophozoites for 0.5% (v/v) DMSO serving as negative controls while change in trophozoite count for 461.85 μM PHMB served as positive controls. Wells with a probability of being cysticidal > 0.9 were defined as hits. Images were also viewed manually for evidence of excystation at day 3 manually and compared to the YOLOv3

predictions to generate a confusion matrix for assessing the accuracy, precision, recall, and specificity of the assay.

Screening of Marine Natural Products Library.

Marine Natural Products Library Composition. The test samples in this study were derived from the collection, cultivation and extraction of marine bacteria cultures. These bacteria, which are mainly members of the Actinomycetales, were collected from numerous locations world-wide. The samples are test fractions derived from the chromatographic purification of 5 L culture whole ethyl acetate extracts. The test samples vary containing 5-8 polar to nonpolar materials in each.

Amebicidal Assay. A marine natural products library of 9,286 unique fractions was assayed for anti-*Acanthamoeba* activity on trophozoites. A BioSero ATS (EDC Biosystems) was used to transfer 0.25 µL of each marine natural product fraction (12 mg/mL stock) or control into each well of Greiner Bio-One Cellstar white, flat bottom microplates. 0.5% (v/v) DMSO and 461.85 µM PHMB served as negative and positive controls, respectively. The fractions were tested in duplicate. Afterwards, a Multidrop Combi liquid handler (Thermo Fisher) was used to transfer 50 µL of cell solution containing 5×10^3 trophozoites into each well.

The plates were incubated at 28°C and 5% CO_2 for 48 hours prior to luminescence readings. 25 µL of CellTiter-Glo luminescence cell viability assay (Promega) was added to each well using the Multidrop Combi liquid handler. The plates were shaken on an orbital microplate shaker (VWR) at 360 rpm for 10 minutes, and then they were left for an additional 10 minutes prior to luminescence measurements on an EnVision 2104

Multilabel Reader (Perkin Elmer). The luminescence reading data was processed through excel to determine growth inhibition percentages.

Cysticidal Assay. 29 fractions displaying >90% inhibition were selected for screening against cysts. 5 x 10^3 trophozoites were seeded in 99 µL of encystation media into a 96 well black, clear bottom microplate (Corning 3603) and incubated for 48 hours to encyst the cells.

Afterwards, 1 µL of each fraction or control was added to the cysts in duplicate. 1% (v/v) DMSO and 923.71 µM PHMB served as negative and positive controls, respectively. After 48 hours of incubation at 28°C and 5% CO_2, the media was removed and washed four times with 100 µL PBS. Each well was then replaced with 100 µL of PYG growth media and incubated for imaging.

After 3 days of incubation, each well of the plate was imaged on the ImageXpress Micro XLS. The images were converted from .tiff to .jpg images with a custom python script and run through the YOLOv3 algorithm to determine the counts of trophozoites on images taken 0 days and 3 days after switching to PYG growth media. The trophozoite counts from the positive and negative control wells were used to generate a logistic regression, which was used to determine the cysticidal likelihood of each fraction. Duplicate wells displaying an average probability >0.9 of being cysticidal were considered hits. Additionally, the day 3 images were also manually verified to determine if the predictions were accurate. Since this was used as a filtering method to identify if a treatment was cysticidal or not, it was only performed once with technical replicates.

EC_{50} Determination. The top 10 trophocidal compounds identified previously in the primary amebicidal screen were evaluated for their EC_{50} values. These fractions were serially diluted two-fold (60 µg/mL - 468.75 ng/mL) using the BioSero ATS and 0.5 µL of each fraction was added to a Greiner Bio-One Cellstar white, flat bottom microplate. Afterwards, 100 µL of PYG growth media containing 5 x 10^3 trophozoites was added via the Multidrop Combi liquid handler.

These plates were allowed to incubate for 48 hours prior to CellTiter-Glo luminescence readings on the EnVision 2104 Multilabel Reader. Data from a minimum of three independent experiments (biological replicates) conducted in triplicate were analyzed on GraphPad Prism 6 to determine EC_{50} values.

Determination of Minimum Cysticial Concentration of 12FP47A9. Fraction 12FP47A9 was evaluated for a minimum cysticidal concentration. A plate of *A. castellanii* cysts was prepared following methods described in previous sections with minor alterations. To evaluate higher concentrations of 12FP47A9, 5 x 10^3 trophozoites were encysted in 96, 98, and 99 µL of media to achieve final concentrations ranging from 480 to 120 µg/mL. Additionally, 5 x 10^3 trophozoites were also encysted in 99.5 µL of media to achieve final concentrations ranging from 60 to 3.75 µg/mL. 4% (v/v) DMSO and 3,694.8 µM PHMB served as negative and positive controls, respectively. The experiment was repeated three times with biological and technical replicates on different days. Mature cysts were incubated with fraction 12FP47A9 for 48 hours prior to exchange with PYG growth media. Once in PYG media, the cysts were imaged by on the ImageXpress Micro XLS and images were manually evaluated for excystation at 7 days.

5.5 Figures and Tables

TABLE 5.1 Comparison of YOLOv3 and Manual Determination of Minimum Cysticidal Concentrations. MCC—Minimum cysticidal concentration; concentrations are in μM.

	YOLOv3 MCC	Manual MCC
Chlorhexidine	6.94 – 3.47	13.89 – 6.94
Alexidine	< 10.74	< 10.74
Corifungin	>1,600	>1,600
Amphotericin B	>138.52	>138.52
Caspofungin	>105.49	>105.49
Fluconazole	>6,686.91	>6,686.91

Table 5.2 Confusion Matrix and Statistics on Evaluation of Validation Screen.

$$\text{Recall} = \frac{True\ Positive}{True\ Positive + False\ Negative} \quad \text{Precison} = \frac{True\ Positive}{True\ Positive + False\ Positive}$$

$$\text{Specificity} = \frac{True\ Negative}{True\ Negative + False\ Positive}$$

$$\text{Accuracy} = \frac{True\ Positive + True\ Negative}{True\ Positive + False\ Positive + True\ Negative + False\ Negative}$$

	Predict cysticidal	Predict non-cysticidal	Total
Observed cysticidal	109	0	109
Observed non-cysticidal	12	311	323
Total	121	311	432

Accuracy	0.97
Recall	1
Specificity	0.96
Precision	0.90

Table 5.3 Sources and EC_{50} Concentrations of Top 10 Trophocidal Fractions. Sources and EC_{50} concentrations (µg/mL) of the top 10 fractions displaying most inhibition against trophozoites. P(cysticidal)—probability a fraction is cysticidal as determined by cysticidal assay; CL—confidence limit.

Fraction	Source/Strain No.	Location/date	EC_{50}	95% Lower CL	95% Upper CL	P (cysticidal)
12FP15E5	TAA522	Coarse sand, Channel Islands, 2012	0.4	0.1	2.2	0.00
12FP15E6	TAA522	Coarse sand, Channel Islands, 2012	1.9	0.8	4.4	0.00
12FP15E4	TAA522	Coarse sand, Channel Islands, 2012	3.0	1.3	6.6	0.00
12FP15E7	TAA522	Coarse sand, Channel Islands, 2012	4.9	2.5	9.4	0.00
SIOFP89H4	CNT714	Sand, San Diego Bay, 2008	6.4	6.0	6.7	0.00
12FP25A7	TAA584	Coarse Sand, Channel Islands, 2012	6.8	3.6	12.8	0.00
12FP47A9	TAA844	Sand, Marianas Islands, 2012	20.3	19.7	21.0	1.00
12FP42B3	TAA734	Sand, Marianas Islands, 2012	21.2	15.3	29.3	0.00
SIOFP68D6	CNT284	Sponge, Bahamas, 2007	55.9	32.4	96.2	0.00
SIOFP70C6	CNT292	Sponge, Bahamas, 2007	>60			0.00

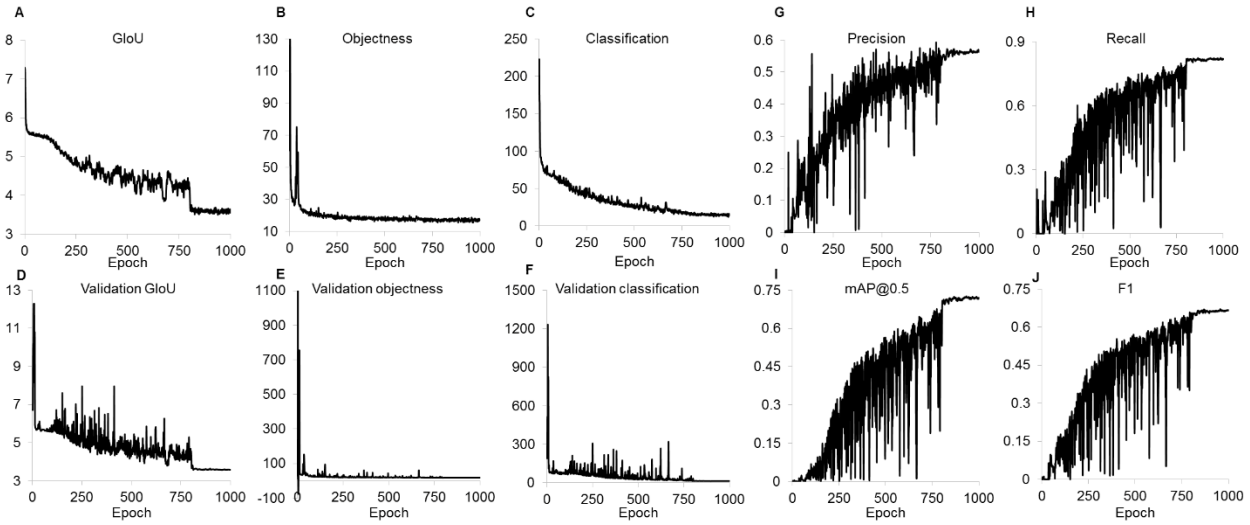

Figure 5.1 Training and Validation Metrics. Training and validation metrics provided by YOLOv3 as a function of training epoch. (A) Generalized intersection over union (GIoU) is a measure of the smallest box that encompasses both the predicted bounding boxes and actual ground truth boxes. (B) Objectness is the confidence a bounding box contains an object. (C) Classification is measure of the accuracy of classifying objects in an image. (D) Validation GIoU is the GIoU for the validation set of images. (E) Validation objectness is the objectness score for the validation set (F) Validation classification is the classification score for the validation set. (G) $\text{Precison} = \frac{True\ Positive}{True\ Positive + False\ Positive}$. (H)$\text{Recall} = \frac{True\ Positive}{True\ Positive + False\ Negative}$. (I) Mean average precision (mAP) for predictions with intersection of union (IoU) > 0.5 is the average of average precision for all classes (area under precision-recall curves for each class averaged). (J) $\text{F1} = \frac{2*(Precision*Recall)}{(Precision+Recall)}$.

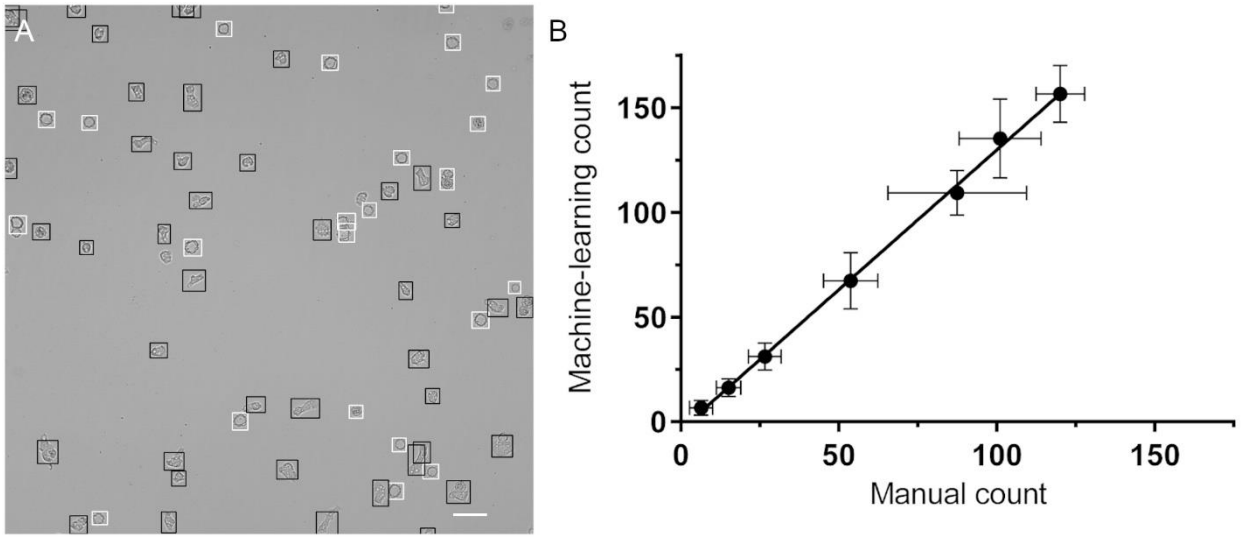

Figure 5.2 Evaluation of Trophozoite and Cyst Cell Count Predictions. (A) Sample predictions of trophozoites and cysts one day after switching to PYG growth media from encystation media. Black boxes—detected trophozoites; white boxes—detected cysts. Magnification: 200x; Scale bar: 50 μm. (B) Linear correlation between manual (x-axis) and machine learning (y-axis) counts of seeded trophozoites; R^2: 0.9984; n = 4.

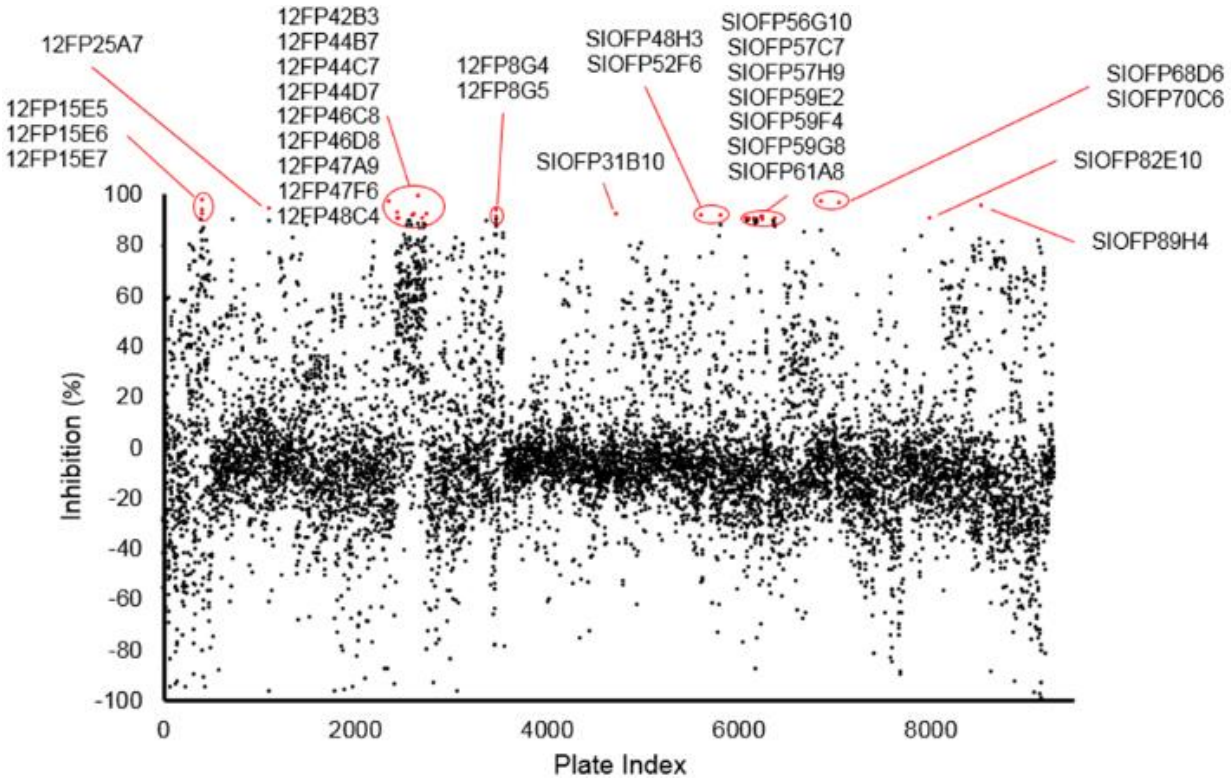

Figure 5.3 Normalized Growth Inhibition of Marine Fractions. 9,286 unique marine microbial natural products test fractions were screened against *A. castellanii* trophozoites at 60 µg/mL. Black—fractions displaying <90% inhibition against *A. castellanii* trophozoites. Red—fractions displaying >90% inhbition against trophozoites.

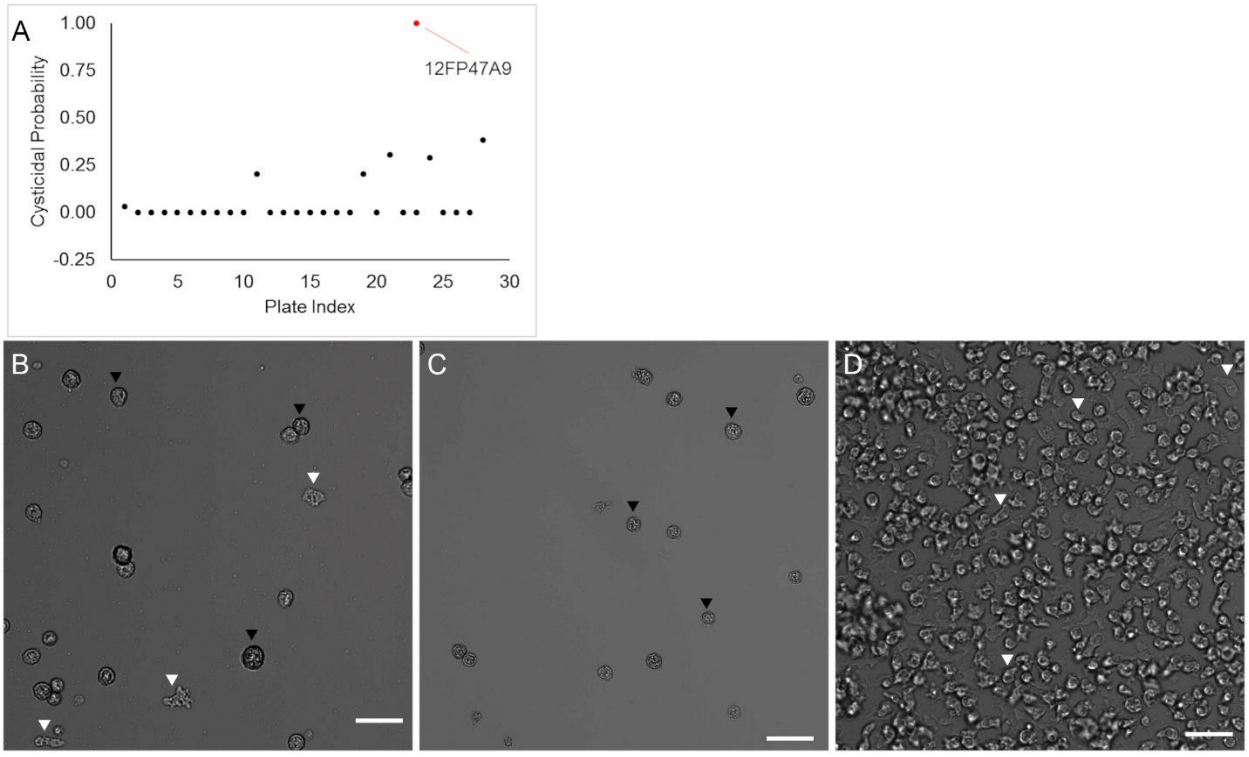

Figure 5.4 Cysticidal Screen. 29 fractions identified as having trophocidal activity were screened against *A. castellanii* cysts. (A) The probability of a treatment being cysticidal (y-axis) is plotted as a function of the fraction's location on a plate (x-axis). Red—trophocidal hit 12FP47A9 flagged as cysticidal fraction; black—trophocidal hits that were not cysticidal. Microscopy images taken on day 3 of incubation in PYG growth media. Wells were treated with: (B) 120 µg/mL fraction 12FP47A9; (C) 923.71 µM (0.04% (w/v)) polyhexamethylene biguanide (positive control); (D) 1% (v/v) DMSO (negative control). Black arrowhead—cyst; white arrowhead—trophozoite; 200x magnification; scale bar: 50 µm.

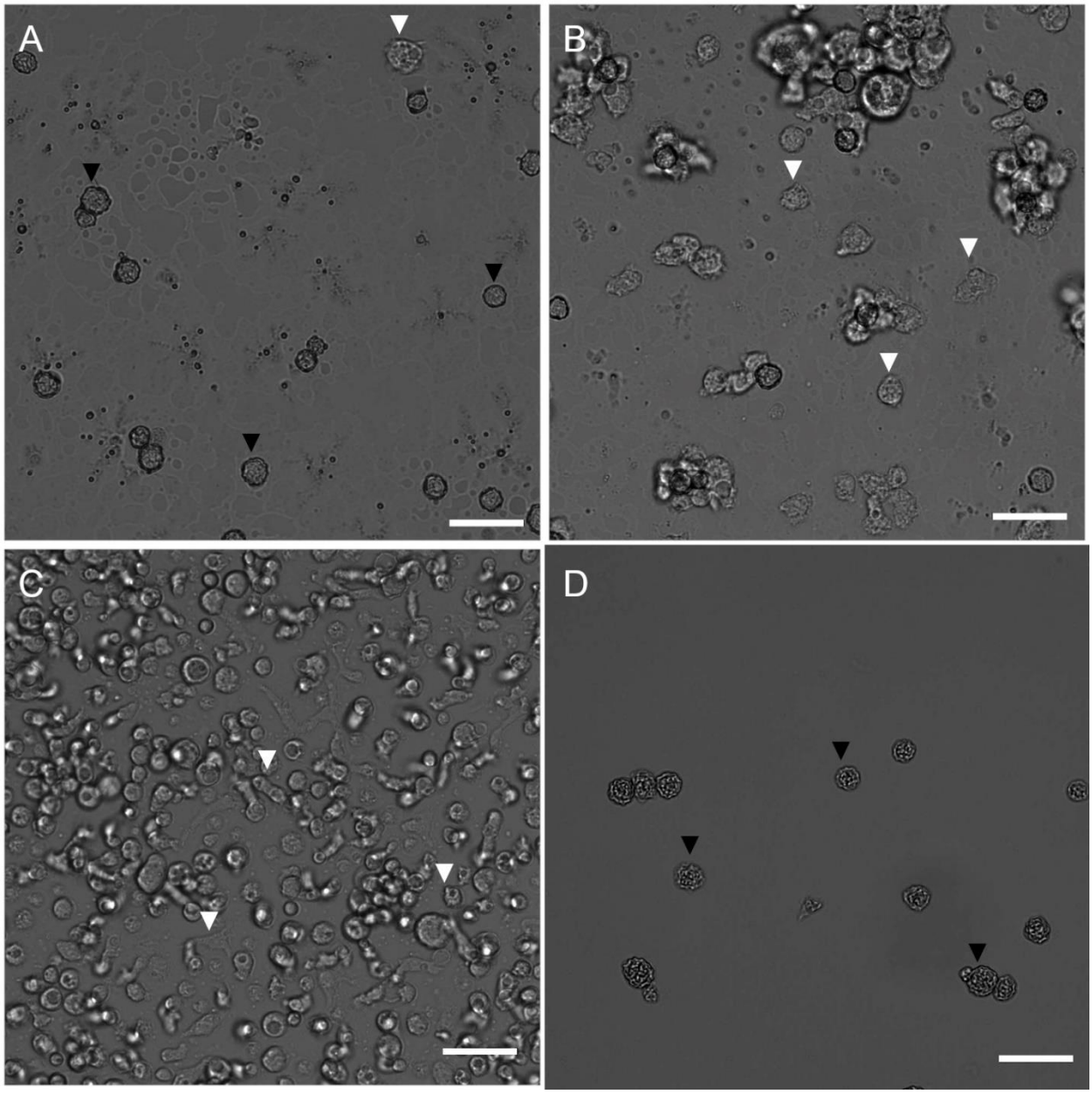

Figure 5.5 12FP47A9 Minimum Cysticidal Concentration Determination. Microscopy taken on day 7 of incubation in PYG growth media. Wells are treated with: (A) 480 µg/mL 12FP47A9; (B) 240 µg/mL 12FP47A9; (C) 4% (v/v) DMSO (negative control); (D) 0.16% (w/v) PHMB (positive control). Black arrowhead—cyst; white arrowhead—trophozoite; 200x magnification; scale bar: 50 µm.

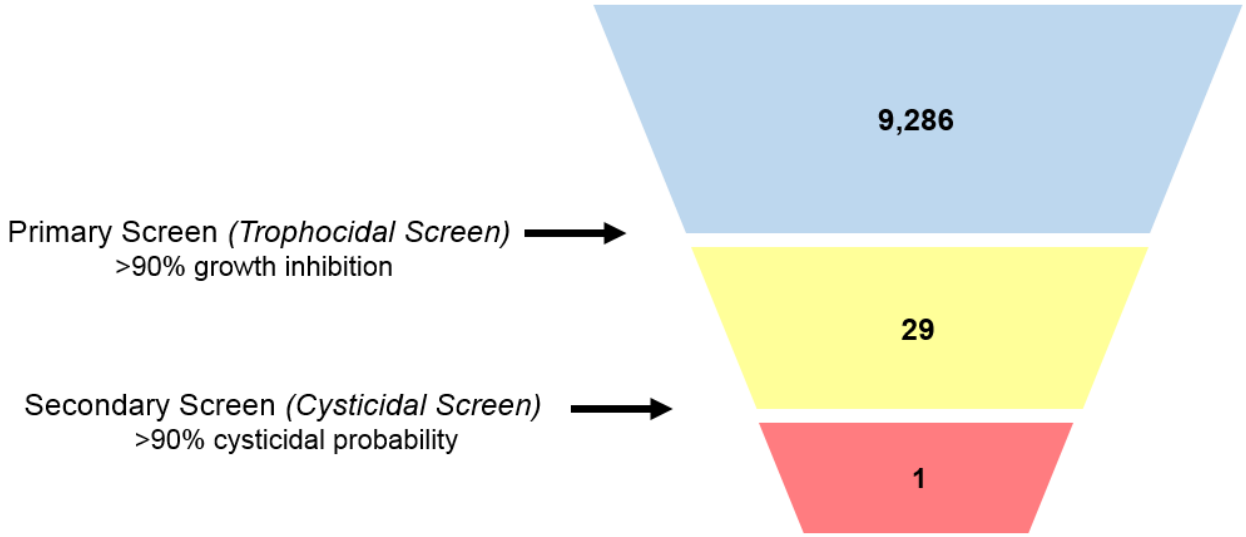

Figure 5.6 Screening Summary. Overview of marine natural product library screen. 9,286 unique test fractions were screened against trophozoites. 29 fractions displaying >90% inhibition against trophozoites were screened against cysts, and fraction(s) with >90% probability of being cysticidal were considered potentially cysticidal compounds.

Chapter 6: Conclusions and Future Directions

6.1: Preface

Acanthamoeba consists of several species of free-living amoeba that can be the causative agents of keratitis. While topical drugs, such as biguanide and diamidine agents, are commonly used for treating *Acanthamoeba* keratitis, these medications are not panaceas. *Acanthamoeba* is a relatively neglected disease, so screening and repurposing existing drugs presents an attractive avenue for improving *Acanthamoeba* keratitis treatments.

This dissertation presents four research projects into characterizing anti-fungal conazoles as anti-*Acanthamoeba* agents and developing research techniques for identifying new potential drugs for *Acanthamoeba* keratitis treatment.

6.2: Isavuconazole is Amebicidal and Cysticidal against *A. castellanii*

In chapter 2, a systematic screen of anti-fungal conazoles identified isavuconazole as having potent activity against *A. castellanii*. Isavuconazole displayed EC_{50} values ranging from 0.9 to 4.6 nM against several strains of *A. castellanii* (152). 70 μM isavuconazole also prevented excystation, suggesting it has activity against cysts (152). Considering the amebicidal activity of isavuconazole at such low concentrations and its demonstration of cysticidal activity, isavuconazole appears to be an attractive drug candidate for repurposing.

6.3: Structural Insights into *A. castellanii* CYP51 (AcCYP51) and Isavuconazole Mechanism of Inhibition

In chapter 3, *A. castellanii* CYP51, the putative target of anti-fungal conazoles, was expressed, purified, and structurally characterized. Crystal structures and spectroscopy revealed AcCYP51 homodimerizes through N-terminal domain-swap (305). The conazoles clotrimazole and isavuconazole both were able to bind AcCYP51 and prevent the enzyme from dimerizing. While clotrimazole-bound AcCYP51 displayed a canonical CYP structure, isavuconazole-bound AcCYP51 failed to properly refold 74 residues at the N-terminus (305). This unique mechanism has never been previously reported with the CYP family of enzymes and suggests a potential mechanism to explain isavuconazole's potency against *A. castellanii*.

6.4: Evaluation of Amebicidal and Cysticidal Activities of Antifungal Drug Isavuconazonium Sulfate against *Acanthamoeba* T4 Strains

Isavuconazole is clinically administered as the prodrug isavuconazonium sulfate. While we previously demonstrated significant amebicidal and cysticidal activity of isavuconazole against *A. castellanii* (152), it was unclear if isavuconazonium retained such activity. As such, chapter 4 evaluates isavuconazonium's efficacy against multiple T4 genotype *Acanthamoeba* strains.

Isavuconazonium had potent activity against *Acanthamoeba* trophozoites at nanomolar concentrations, displaying EC_{50} values ranging from 1.4 to 37 nM (306). These EC_{50} values are comparable to previously reported values for isavuconazole, suggesting *Acanthamoeba* trophozoites are also susceptible to isavuconazonium. Isavuconazonium

was also evaluated against cysts, and concentrations ranging from 136 to 187.5 μM prevented excystation up to seven days (306). While higher concentrations of isavuconazonium were required to prevent excystation, it appears the prodrug still has strong potential for killing *Acanthamoeba* trophozoites and cysts.

6.5: Development of a Machine Learning-based Cysticidal Assay and Identification of an Amebicidal and Cysticidal Marine Microbial Metabolite against *Acanthamoeba*

A systematic screen of conazoles identified isavuconazole as having potent activity against *A. castellanii*. While several cell viability assays can be used for high-throughput screening of amebicidal compounds, cysticidal screening techniques largely rely upon manual microscopy observation.

Chapter 5 discusses the development and validation of a novel cysticidal assay amenable to high-throughput compound screening. Briefly, a YOLOv3 machine-learning object-detection algorithm is trained on *A. castellanii* trophozoites and cysts to develop an automated cell counter for screening cysticidal compounds. This novel cysticidal assay was validated on a small set of literature-reported cysticidal and non-cysticidal compounds and compared to manual observations. When compared to manual observations, this automated assay displayed a high specificity of 0.96, suggesting its effectiveness at accurately identifying non-cysticidal compounds (Manuscript in preparation).

Additionally, the utility of this high-throughput cysticidal assay was demonstrated to identify the cysticidal activity of a set of marine natural product fractions that displayed

>90% inhibition of trophozoites. The assay identified one fraction as both trophocidal and cysticidal, which upon further examination, was found to prevent excystation at 480 µg/mL, suggesting a minimum cysticidal concentration between 480 µg/mL and 240 µg/mL (Manuscript in preparation). Since this novel assay is amenable to medium- and high-throughput screening, it can help significantly improve cysticidal screening studies and be utilized to screen out non-cysticidal compounds.

6.6: Future Directions

This dissertation explores several projects into evaluating anti-fungal conazoles as potential treatments for *Acanthamoeba* keratitis. While isavuconazonium is already clinically used for treating fungal infections, our *in vitro* studies, for the first time, demonstrate potent activities of both the prodrug isavuconazonium and the active moiety isavuconazole against T4 strains of *Acanthamoeba*. Further *in vivo* validation of isavuconazonoium sulfate in animal models of *Acanthamoeba* keratitis would be prudent.

Currently, mouse keratitis models adapted from fungal keratitis can be used to evaluate the efficacy of isavuconazole (307). A mouse keratitis model would allow for critical studies. In particular, an animal model would evaluate if administration of isavuconazole or isavuconazonium would successfully resolve an active infection and prevent recurrent *Acanthamoeba* keratitis. Additionally, an animal model would also be crucial for determining other data, such as the penetration and bioavailability of isavuconazole in the cornea, which would inform dosing decisions and provide further support for the use of isavuconazole as a treatment for *Acanthamoeba* keratitis.

This dissertation also discussed the development and validation of a novel machine-learning, object-detection algorithm for a cysticidal assay. Since current cysticidal screening techniques are largely manual and not amenable to high-throughput screening, cysticidal compounds are relatively unexplored. This newly developed cysticidal assay should be combined with the already available high-throughput trophocidal assay to screen large compound libraries to identify new classes of compounds possessing dual activity against trophozoites and cysts. Overall, this has the potential to improve the treatment of *Acanthamoeba* keratitis.

References

1. Marciano-Cabral F, Cabral G. 2003. Acanthamoeba spp. as agents of disease in humans. Clin Microbiol Rev 16:273–307.

2. Acanthamoeba castellanii - an overview | ScienceDirect Topics.

3. Coulon C, Collignon A, McDonnell G, Thomas V. 2010. Resistance of Acanthamoeba cysts to disinfection treatments used in health care settings. J Clin Microbiol 48:2689–2697.

4. Elder MJ, Kilvington S, Dart JK. 1994. A clinicopathologic study of in vitro sensitivity testing and Acanthamoeba keratitis. Investigative ophthalmology & ….

5. Sheng W-H, Hung C-C, Huang H-H, Liang S-Y, Cheng Y-J, Ji D-D, Chang S-C. 2009. First case of granulomatous amebic encephalitis caused by Acanthamoeba castellanii in Taiwan. Am J Trop Med Hyg 81:277–279.

6. CDC. 2019. Pathogen & Environment | Acanthamoeba | Parasites | CDC.

7. Baig AM, Iqbal J, Khan NA. 2013. In vitro efficacies of clinically available drugs against growth and viability of an Acanthamoeba castellanii keratitis isolate belonging to the T4 genotype. Antimicrob Agents Chemother 57:3561–3567.

8. CDC. 2010. Illness & Symptoms | Acanthamoeba | Parasites | CDC.

9. Szentmáry N, Daas L, Shi L, Laurik KL, Lepper S, Milioti G, Seitz B. 2019. Acanthamoeba keratitis - Clinical signs, differential diagnosis and treatment. Journal of Current Ophthalmology 31:16–23.

10. Clarke DW, Alizadeh H, Mayhew E, Mellon J, Neelam S, Niederkorn JY. 2005. Why Does Acanthamoeba castellanii Not Progress Beyond the Cornea to Produce Intraocular Infections? Invest Ophthalmol Vis Sci.

11. Neelam S, Niederkorn JY. 2017. Pathobiology and Immunobiology of Acanthamoeba Keratitis: Insights from Animal Models . Yale J Biol Med 90:261–268.

12. McClellan K, Howard K, Mayhew E, Niederkorn J, Alizadeh H. 2002. Adaptive immune responses to Acanthamoeba cysts. Exp Eye Res 75:285–293.

13. Kelley PS, Dossey AP, Patel D, Whitson JT, Hogan RN, Cavanagh HD. 2006. Secondary glaucoma associated with advanced acanthamoeba keratitis. Eye Contact Lens 32:178–182.

14. Herz NL, Matoba AY, Wilhelmus KR. 2008. Rapidly progressive cataract and iris atrophy during treatment of Acanthamoeba keratitis. Ophthalmology 115:866–869.

15. Lorenzo-Morales J, Khan NA, Walochnik J. 2015. An update on Acanthamoeba keratitis: diagnosis, pathogenesis and treatment. Parasite 22:10.

16. Szentmáry N, Shi L, Daas L, Seitz B. 2020. Diagnostics and management approaches for *Acanthamoeba* keratitis. Expert Opin Orphan Drugs 8:227–236.

17. Hahn TW, O'Brien TP, Sah WJ, Kim JH. 1998. Acridine orange staining for rapid diagnosis of Acanthamoeba keratitis. Jpn J Ophthalmol 42:108–114.

18. Chew SJ, Beuerman RW, Assouline M, Kaufman HE, Barron BA, Hill JM. 1992. Early diagnosis of infectious keratitis with in vivo real time confocal microscopy. CLAO J 18:197–201.

19. Villani E, Baudouin C, Efron N, Hamrah P, Kojima T, Patel SV, Pflugfelder SC, Zhivov A, Dogru M. 2014. In vivo confocal microscopy of the ocular surface: from bench to bedside. Curr Eye Res 39:213–231.

20. Kanavi MR, Javadi M, Yazdani S, Mirdehghanm S. 2007. Sensitivity and specificity of confocal scan in the diagnosis of infectious keratitis. Cornea 26:782–786.

21. Tu EY, Joslin CE, Sugar J, Booton GC, Shoff ME, Fuerst PA. 2008. The relative value of confocal microscopy and superficial corneal scrapings in the diagnosis of Acanthamoeba keratitis. Cornea 27:764–772.

22. Yera H, Ok V, Lee Koy Kuet F, Dahane N, Ariey F, Hasseine L, Delaunay P, Martiano D, Marty P, Bourges JL. 2020. PCR and culture for diagnosis of Acanthamoeba keratitis. Br J Ophthalmol.

23. Mathers WD, Nelson SE, Lane JL, Wilson ME, Allen RC, Folberg R. 2000. Confirmation of confocal microscopy diagnosis of Acanthamoeba keratitis using polymerase chain reaction analysis. Arch Ophthalmol 118:178–183.

24. Maubon D, Dubosson M, Chiquet C, Yera H, Brenier-Pinchart M-P, Cornet M, Savy O, Renard E, Pelloux H. 2012. A one-step multiplex PCR for acanthamoeba keratitis diagnosis and quality samples control. Invest Ophthalmol Vis Sci 53:2866–2872.

25. Schroeder JM, Booton GC, Hay J, Niszl IA, Seal DV, Markus MB, Fuerst PA, Byers TJ. 2001. Use of subgenic 18S ribosomal DNA PCR and sequencing for genus and genotype identification of acanthamoebae from humans with keratitis and from sewage sludge. J Clin Microbiol 39:1903–1911.

26. Pasricha G, Sharma S, Garg P, Aggarwal RK. 2003. Use of 18S rRNA gene-based PCR assay for diagnosis of acanthamoeba keratitis in non-contact lens wearers in India. J Clin Microbiol 41:3206–3211.

27. Rivière D, Szczebara FM, Berjeaud J-M, Frère J, Héchard Y. 2006. Development of a real-time PCR assay for quantification of Acanthamoeba trophozoites and cysts. J Microbiol Methods 64:78–83.

28. Lehmann OJ, Green SM, Morlet N, Kilvington S, Keys MF, Matheson MM, Dart JK, McGill JI, Watt PJ. 1998. Polymerase chain reaction analysis of corneal epithelial and tear samples in the diagnosis of Acanthamoeba keratitis. Invest Ophthalmol Vis Sci 39:1261–1265.

29. Fittipaldi M, Pino Rodriguez NJ, Adrados B, Agustí G, Peñuela G, Morató J, Codony F. 2011. Discrimination of viable Acanthamoeba castellani trophozoites and cysts by propidium monoazide real-time polymerase chain reaction. J Eukaryot Microbiol 58:359–364.

30. Panjwani N. 2010. Pathogenesis of acanthamoeba keratitis. Ocul Surf 8:70–79.

31. Clarke DW, Niederkorn JY. 2006. The pathophysiology of Acanthamoeba keratitis. Trends Parasitol 22:175–180.

32. Siddiqui R, Aqeel Y, Khan NA. 2016. The Development of Drugs against Acanthamoeba Infections. Antimicrob Agents Chemother 60:6441–6450.

33. Ting DSJ, Henein C, Said DG, Dua HS. 2019. Photoactivated chromophore for infectious keratitis - Corneal cross-linking (PACK-CXL): A systematic review and meta-analysis. Ocul Surf 17:624–634.

34. Gatti S, Cevini C, Bruno A, Penso G, Rama P, Scaglia M. 1998. In vitro effectiveness of povidone-iodine on Acanthamoeba isolates from human cornea. Antimicrob Agents Chemother 42:2232–2234.

35. Heaselgrave W, Hamad A, Coles S, Hau S. 2019. In vitro evaluation of the inhibitory effect of topical ophthalmic agents on acanthamoeba viability. Transl Vis Sci Technol 8:17.

36. Hirabayashi KE, Lin CC, Ta CN. 2019. Oral miltefosine for refractory Acanthamoeba keratitis. Am J Ophthalmol Case Rep 16:100555.

37. Thulasi P, Saeed HN, Rapuano CJ, Hou JH, Appenheimer AB, Chodosh J, Kang JJ, Morrill AM, Vyas N, Zegans ME, Zuckerman R, Tu EY. 2020. Oral miltefosine as salvage therapy for refractory acanthamoeba keratitis. Am J Ophthalmol 223:75–82.

38. Avdagic E, Chew HF, Veldman P, Tu EY, Jafri M, Doshi R, Boggild AK, Reidy JJ, Farooq AV. 2019. Resolution of Acanthamoeba Keratitis with Adjunctive Use of Oral Miltefosine. Ocul Immunol Inflamm 1–4.

39. Dewan N, Ming W, Holland SP, Yeung SN, Iovieno A. 2019. Oral miltefosine as adjunctive treatment for recalcitrant acanthamoeba keratitis. Cornea 38:914–917.

40. Tavassoli S, Buckle M, Tole D, Chiodini P, Darcy K. 2018. The use of miltefosine in the management of refractory Acanthamoeba keratitis. Cont Lens Anterior Eye 41:400–402.

41. Naranjo A, Martinez JD, Miller D, Tonk R, Amescua G. 2020. Systemic miltefosine as an adjunct treatment of progressive acanthamoeba keratitis. Ocul Immunol Inflamm 1–9.

42. Jori G, Fabris C, Soncin M, Ferro S, Coppellotti O, Dei D, Fantetti L, Chiti G, Roncucci G. 2006. Photodynamic therapy in the treatment of microbial infections: basic principles and perspective applications. Lasers Surg Med 38:468–481.

43. Sharma S, Srinivasan M, George C. 1990. Acanthamoeba keratitis in non-contact lens wearers. Arch Ophthalmol 108:676–678.

44. Haburchak DR. 2017. Acanthamoeba Infection Treatment & Management: Medical Care, Surgical Care, Consultations. Medscape.

45. CDC. 2017. Acanthamoeba Keratitis Fact Sheet for Healthcare Professionals | Acanthamoeba | Parasites | CDC.

46. Oldenburg CE, Acharya NR, Tu EY, Zegans ME, Mannis MJ, Gaynor BD, Whitcher JP, Lietman TM, Keenan JD. 2011. Practice patterns and opinions in the treatment of acanthamoeba keratitis. Cornea 30:1363–1368.

47. Maycock NJR, Jayaswal R. 2016. Update on acanthamoeba keratitis: diagnosis, treatment, and outcomes. Cornea 35:713–720.

48. Stepp MA, Zieske JD, Trinkaus-Randall V, Kyne BM, Pal-Ghosh S, Tadvalkar G, Pajoohesh-Ganji A. 2014. Wounding the cornea to learn how it heals. Exp Eye Res 121:178–193.

49. Dart JKG, Saw VPJ, Kilvington S. 2009. Acanthamoeba keratitis: diagnosis and treatment update 2009. Am J Ophthalmol 148:487–499.e2.

50. Saidel MA. 2006. Acanthamoeba Keratitis Treatment. American Academy of Opthalmology.

51. Kitzmann AS, Goins KM, Sutphin JE, Wagoner MD. 2009. Keratoplasty for treatment of Acanthamoeba keratitis. Ophthalmology 116:864–869.

52. Amoils SP, Heney C. 1999. Acanthamoeba keratitis with live isolates treated with cryosurgery and fluconazole. Am J Ophthalmol 127:718–720.

53. Meisler DM, Ludwig IH, Rutherford I, Bican FE, Langston RH, Visvesvara GS. 1986. Susceptibility of Acanthamoeba to cryotherapeutic method. Arch Ophthalmol 104:130–131.

54. Binder PS. 1989. Cryotherapy for medically unresponsive acanthamoeba keratitis. Cornea 8:106–114.

55. Kuyyakanond T, Quesnel LB. 1992. The mechanism of action of chlorhexidine. FEMS Microbiol Lett 100:211–215.

56. McDonnell G, Russell AD. 1999. Antiseptics and disinfectants: activity, action, and resistance. Clin Microbiol Rev 12:147–179.

57. Turner NA, Russell AD, Furr JR, Lloyd D. 2000. Emergence of resistance to biocides during differentiation of Acanthamoeba castellanii. J Antimicrob Chemother 46:27–34.

58. Alizadeh H, Neelam S, Cavanagh HD. 2009. Amoebicidal activities of alexidine against 3 pathogenic strains of acanthamoeba. Eye Contact Lens 35:1–5.

59. Narasimhan S, Madhavan HN, K LT. 2002. Development and application of an in vitro susceptibility test for Acanthamoeba species isolated from keratitis to polyhexamethylene biguanide and chlorhexidine. Cornea 21:203–205.

60. Lee J-E, Oum BS, Choi HY, Yu HS, Lee JS. 2007. Cysticidal effect on acanthamoeba and toxicity on human keratocytes by polyhexamethylene biguanide and chlorhexidine. Cornea 26:736–741.

61. Kosrirukvongs P, Wanachiwanawin D, Visvesvara GS. 1999. Treatment of acanthamoeba keratitis with chlorhexidine. Ophthalmology 106:798–802.

62. Lim N, Goh D, Bunce C, Xing W, Fraenkel G, Poole TRG, Ficker L. 2008. Comparison of polyhexamethylene biguanide and chlorhexidine as monotherapy agents in the treatment of Acanthamoeba keratitis. Am J Ophthalmol 145:130–135.

63. Romanowski EG, Yates KA, O'Connor KE, Mah FS, Shanks RMQ, Kowalski RP. 2013. Evaluation of polyhexamethylene biguanide (PHMB) as a disinfectant for adenovirus. JAMA Ophthalmol 131:495–498.

64. Schnuch A, Geier J, Uter W, Basketter DA, Jowsey IR. 2007. The biocide polyhexamethylene biguanide remains an uncommon contact allergen. Contact Derm 56:235–239.

65. Sood A, Granick MS, Tomaselli NL. 2014. Wound dressings and comparative effectiveness data. Adv Wound Care (New Rochelle) 3:511–529.

66. Khunkitti W, Lloyd D, Furr JR, Russell AD. 1997. Aspects of the mechanisms of action of biguanides on trophozoites and cysts of Acanthamoeba castellanii. J Appl Microbiol 82:107–114.

67. Pérez-Santonja JJ, Kilvington S, Hughes R, Tufail A, Matheson M, Dart JKG. 2003. Persistently culture positive acanthamoeba keratitis: in vivo resistance and in vitro sensitivity. Ophthalmology 110:1593–1600.

68. Ferrari G, Matuska S, Rama P. 2011. Double-biguanide therapy for resistant acanthamoeba keratitis. Case Rep Ophthalmol 2:338–342.

69. Huang F-C, Shih M-H, Chang K-F, Huang J-M, Shin J-W, Lin W-C. 2017. Characterizing clinical isolates of Acanthamoeba castellanii with high resistance to polyhexamethylene biguanide in Taiwan. J Microbiol Immunol Infect 50:570–577.

70. Mafra CSP, Carrijo-Carvalho LC, Chudzinski-Tavassi AM, Taguchi FM de C, Foronda AS, Carvalho FR de S, de Freitas D. 2013. Antimicrobial action of biguanides on the viability of Acanthamoeba cysts and assessment of cell toxicity. Invest Ophthalmol Vis Sci 54:6363–6372.

71. Soeiro MNC, De Souza EM, Stephens CE, Boykin DW. 2005. Aromatic diamidines as antiparasitic agents. Expert Opin Investig Drugs 14:957–972.

72. Perrine D, Chenu JP, Georges P, Lancelot JC, Saturnino C, Robba M. 1995. Amoebicidal efficiencies of various diamidines against two strains of Acanthamoeba polyphaga. Antimicrob Agents Chemother 39:339–342.

73. Wright P, Warhurst D, Jones BR. 1985. Acanthamoeba keratitis successfully treated medically. Br J Ophthalmol 69:778–782.

74. Duguid IG, Dart JK, Morlet N, Allan BD, Matheson M, Ficker L, Tuft S. 1997. Outcome of acanthamoeba keratitis treated with polyhexamethyl biguanide and propamidine. Ophthalmology 104:1587–1592.

75. Varga JH, Wolf TC, Jensen HG, Parmley VC, Rowsey JJ. 1993. Combined treatment of Acanthamoeba keratitis with propamidine, neomycin, and polyhexamethylene biguanide. Am J Ophthalmol 115:466–470.

76. Hargrave SL, McCulley JP, Husseini Z. 1999. Results of a trial of combined propamidine isethionate and neomycin therapy for Acanthamoeba keratitis. Brolene Study Group. Ophthalmology 106:952–957.

77. Seal D, Hay J, Kirkness C, Morrell A, Booth A, Tullo A, Ridgway A, Armstrong M. 1996. Successful medical therapy of Acanthamoeba keratitis with topical chlorhexidine and propamidine. Eye (Lond) 10 (Pt 4):413–421.

78. Alizadeh H, Silvany RE, Meyer DR, Dougherty JM, McCulley JP. 1997. In vitro amoebicidal activity of propamidine and pentamidine isethionate against Acanthamoeba species and toxicity to corneal tissues. Cornea 16:94–100.

79. James EA, James BH, Nicholson AJ. 1942. Process for the preparation of diamidine derivatives. US Patent ….

80. 2007. Final report on the safety assessment of Hexamidine and Hexamidine Diisethionate. Int J Toxicol 26 Suppl 3:79–88.

81. Brasseur G, Favennec L, Perrine D, Chenu JP, Brasseur P. 1994. Successful treatment of Acanthamoeba keratitis by hexamidine. Cornea 13:459–462.

82. Lepelletier D, Maillard JY, Pozzetto B, Simon A. 2020. Povidone Iodine: Properties, Mechanisms of Action, and Role in Infection Control and Staphylococcus aureus Decolonization. Antimicrob Agents Chemother 64.

83. Bigliardi PL, Alsagoff SAL, El-Kafrawi HY, Pyon J-K, Wa CTC, Villa MA. 2017. Povidone iodine in wound healing: A review of current concepts and practices. Int J Surg 44:260–268.

84. Cho P, Reyes S, Boost MV. 2018. Microbiocidal characterization of a novel povidone-iodine based rigid contact lens disinfecting solution. Cont Lens Anterior Eye 41:542–546.

85. Martín-Navarro CM, Lorenzo-Morales J, López-Arencibia A, Valladares B, Piñero JE. 2010. Acanthamoeba spp.: efficacy of Bioclen FR One Step, a povidone-iodine based system for the disinfection of contact lenses. Exp Parasitol 126:109–112.

86. Kobayashi T, Gibbon L, Mito T, Shiraishi A, Uno T, Ohashi Y. 2011. Efficacy of commercial soft contact lens disinfectant solutions against Acanthamoeba. Jpn J Ophthalmol 55:547–557.

87. Padzik M, Baltaza W, Conn DB, Szaflik JP, Chomicz L. 2018. Effect of povidone iodine, chlorhexidine digluconate and toyocamycin on amphizoic amoebic strains, infectious agents of *Acanthamoeba* keratitis - a growing threat to human health worldwide. Ann Agric Environ Med 25:725–731.

88. Roongruangchai J, Sookkua T, Kummalue T, Roongruangchai K. 2009. Pouzolzia indica methanolic extract fraction 2 and povidone-iodine induced changes in the cyst of Acanthamoeba spp.: light and electron microscopic studies. J Med Assoc Thai 92:1492–1499.

89. Sunada A, Kimura K, Nishi I, Toyokawa M, Ueda A, Sakata T, Suzuki T, Inoue Y, Ohashi Y, Asari S, Iwatani Y. 2014. In vitro evaluations of topical agents to treat Acanthamoeba keratitis. Ophthalmology 121:2059–2065.

90. Shi L, Muthukumar V, Stachon T, Latta L, Elhawy MI, Gunaratnam G, Orosz E, Seitz B, Kiderlen AF, Bischoff M, Szentmáry N. 2020. The Effect of Anti-Amoebic Agents and Ce6-PDT on Acanthamoeba castellanii Trophozoites and Cysts, In Vitro. Transl Vis Sci Technol 9:29.

91. Pelletier JS, Miller D, Liang B, Capriotti JA. 2011. In vitro efficacy of a povidone-iodine 0.4% and dexamethasone 0.1% suspension against ocular pathogens. J Cataract Refract Surg 37:763–766.

92. Lim L, Coster DJ, Badenoch PR. 2000. Antimicrobial susceptibility of 19 Australian corneal isolates of Acanthamoeba. Clin Experiment Ophthalmol 28:119–124.

93. Dorlo TPC, Balasegaram M, Beijnen JH, de Vries PJ. 2012. Miltefosine: a review of its pharmacology and therapeutic efficacy in the treatment of leishmaniasis. J Antimicrob Chemother 67:2576–2597.

94. Chao M, Thongseesuksai T, Boonmars T, Laummaunwai P. 2020. Investigation of the in vitro cysticidal activity of miltefosine against Acanthamoeba spp. J Parasit Dis 44:491–495.

95. Walochnik J, Duchêne M, Seifert K, Obwaller A, Hottkowitz T, Wiedermann G, Eibl H, Aspöck H. 2002. Cytotoxic activities of alkylphosphocholines against clinical isolates of Acanthamoeba spp. Antimicrob Agents Chemother 46:695–701.

96. Mrva M, Garajová M, Lukáč M, Ondriska F. 2011. Weak cytotoxic activity of miltefosine against clinical isolates of Acanthamoeba spp. J Parasitol 97:538–540.

97. Kwiatkowski S, Knap B, Przystupski D, Saczko J, Kędzierska E, Knap-Czop K, Kotlińska J, Michel O, Kotowski K, Kulbacka J. 2018. Photodynamic therapy - mechanisms, photosensitizers and combinations. Biomed Pharmacother 106:1098–1107.

98. Kassab K, Dei D, Roncucci G, Jori G, Coppellotti O. 2003. Phthalocyanine-photosensitized inactivation of a pathogenic protozoan, Acanthamoeba palestinensis. Photochem Photobiol Sci 2:668–672.

99. Chen Z, Xuguang S, Zhiqun W, Ran L. 2008. In vitro amoebacidal activity of photodynamic therapy on Acanthamoeba. Br J Ophthalmol 92:1283–1286.

100. Siddiqui R, Khan NA. 2012. Photochemotherapeutic strategies against Acanthamoeba keratitis. AMB Express 2:47.

101. Mito T, Suzuki T, Kobayashi T, Zheng X, Hayashi Y, Shiraishi A, Ohashi Y. 2012. Effect of photodynamic therapy with methylene blue on Acanthamoeba in vitro. Invest Ophthalmol Vis Sci 53:6305–6313.

102. Del Buey MA, Cristóbal JA, Casas P, Goñi P, Clavel A, Mínguez E, Lanchares E, García A, Calvo B. 2012. Evaluation of in vitro efficacy of combined riboflavin and ultraviolet a for Acanthamoeba isolates. Am J Ophthalmol 153:399–404.

103. Lamy R, Chan E, Good SD, Cevallos V, Porco TC, Stewart JM. 2016. Riboflavin and ultraviolet A as adjuvant treatment against Acanthamoeba cysts. Clin Experiment Ophthalmol 44:181–187.

104. Gomart G, Denis J, Bourcier T, Dory A, Abou-Bacar A, Candolfi E, Sauer A. 2018. In Vitro Amoebicidal Activity of Titanium Dioxide/UV-A Combination Against Acanthamoeba. Invest Ophthalmol Vis Sci 59:4567–4571.

105. Dwia Pertiwi Y, Chikama T, Sueoka K, Ko J-A, Kiuchi Y, Onodera M, Sakaguchi T. 2020. Efficacy of Photodynamic Anti-Microbial Chemotherapy for Acanthamoeba Keratitis In Vivo. Lasers Surg Med.

106. Pertiwi YD, Chikama T, Sueoka K, Ko J-A, Kiuchi Y, Onodera M, Sakaguchi T. 2019. Antimicrobial Photodynamic Therapy with the photosensitizer TONS504 eradicates Acanthamoeba. Photodiagnosis Photodyn Ther 28:166–171.

107. Atalay HT, Uysal BS, Sarzhanov F, Usluca S, Yeşilırmak N, Özmen MC, Erganiş S, Tefon AB, Dogruman-Al F, Bilgihan K. 2020. Rose Bengal-Mediated Photodynamic Antimicrobial Treatment of Acanthamoeba Keratitis. Curr Eye Res 45:1205–1210.

108. Morén H, Malmsjö M, Mortensen J, Ohrström A. 2010. Riboflavin and ultraviolet a collagen crosslinking of the cornea for the treatment of keratitis. Cornea 29:102–104.

109. Khan YA, Kashiwabuchi RT, Martins SA, Castro-Combs JM, Kalyani S, Stanley P, Flikier D, Behrens A. 2011. Riboflavin and ultraviolet light a therapy as an adjuvant treatment for medically refractive Acanthamoeba keratitis: report of 3 cases. Ophthalmology 118:324–331.

110. Price MO, Tenkman LR, Schrier A, Fairchild KM, Trokel SL, Price FW. 2012. Photoactivated riboflavin treatment of infectious keratitis using collagen cross-linking technology. J Refract Surg 28:706–713.

111. Naranjo A, Arboleda A, Martinez JD, Durkee H, Aguilar MC, Relhan N, Nikpoor N, Galor A, Dubovy SR, Leblanc R, Flynn HW, Miller D, Parel J-M, Amescua G. 2019. Rose bengal photodynamic antimicrobial therapy for patients with progressive infectious keratitis: A pilot clinical study. Am J Ophthalmol 208:387–396.

112. Sharma R, Jhanji V, Satpathy G, Sharma N, Khokhar S, Agarwal T. 2013. Coinfection with Acanthamoeba and Pseudomonas in contact lens-associated keratitis. Optom Vis Sci 90:e53–5.

113. Beattie AM, Slomovic AR, Rootman DS, Hunter WS. 1990. Acanthamoeba keratitis with two species of Acanthamoeba. Can J Ophthalmol 25:260–262.

114. Skarin A, Florén I, Kiss K, Miörner H, Stenevi U. 1996. Acanthamoeba keratitis in the south of Sweden. Acta Ophthalmol Scand 74:593–597.

115. Moore MB, McCulley JP. 1989. Acanthamoeba keratitis associated with contact lenses: six consecutive cases of successful management. Br J Ophthalmol 73:271–275.

116. Berger ST, Mondino BJ, Hoft RH, Donzis PB, Holland GN, Farley MK, Levenson JE. 1990. Successful medical management of Acanthamoeba keratitis. Am J Ophthalmol 110:395–403.

117. Natamycin | C33H47O13N - PubChem.

118. Kitagawa K, Nakamura T, Takahashi N, Oikawa Y, Ikeda T. 2003. A novel combination treatment of chlorhexidine gluconate, natamycin (pimaricin) and debridement for a Acanthamoeba keratitis. Jpn J Ophthalmol 47:616–617.

119. Noor A, Preuss CV. Amphotericin BStatPearls. StatPearls Publishing, Treasure Island (FL).

120. Taravaud A, Loiseau PM, Pomel S. 2017. In vitro evaluation of antimicrobial agents on Acanthamoeba sp. and evidence of a natural resilience to amphotericin B. Int J Parasitol Drugs Drug Resist 7:328–336.

121. Biser SA, Perry HD, Donnenfeld ED, Doshi SJ, Chaturvedi V. 2004. Arthrographis keratitis mimicking acanthamoeba keratitis. Cornea 23:314–317.

122. Austin A, Lietman T, Rose-Nussbaumer J. 2017. Update on the management of infectious keratitis. Ophthalmology 124:1678–1689.

123. Behrens-Baumann W, Klinge B, Uter W. 1990. Clotrimazole and bifonazole in the topical treatment of Candida keratitis in rabbits. Mycoses 33:567–573.

124. Sheehan DJ, Hitchcock CA, Sibley CM. 1999. Current and emerging azole antifungal agents. Clin Microbiol Rev 12:40–79.

125. Lamb DC, Warrilow AGS, Rolley NJ, Parker JE, Nes WD, Smith SN, Kelly DE, Kelly SL. 2015. Azole Antifungal Agents To Treat the Human Pathogens Acanthamoeba castellanii and Acanthamoeba polyphaga through Inhibition of Sterol 14α-Demethylase (CYP51). Antimicrob Agents Chemother 59:4707–4713.

126. Elsheikha HM, Siddiqui R, Khan NA. 2020. Drug Discovery against Acanthamoeba Infections: Present Knowledge and Unmet Needs. Pathogens 9.

127. Miller D, Alfonso EC. 2014. Management of fungal keratitis: Topical or Systemic therapy? Vision Pan-America.

128. Gokhale NS. 2008. Medical management approach to infectious keratitis. Indian J Ophthalmol 56:215–220.

129. Moiseev RV, Morrison PWJ, Steele F, Khutoryanskiy VV. 2019. Penetration enhancers in ocular drug delivery. Pharmaceutics 11.

130. Yang W, Wiederhold NP, Williams RO. 2008. Drug delivery strategies for improved azole antifungal action. Expert Opin Drug Deliv 5:1199–1216.

131. Lakhani P, Patil A, Majumdar S. 2019. Challenges in the Polyene- and Azole-Based Pharmacotherapy of Ocular Fungal Infections. J Ocul Pharmacol Ther 35:6–22.

132. Driebe WT, Stern GA, Epstein RJ, Visvesvara GS, Adi M, Komadina T. 1988. Acanthamoeba keratitis. Potential role for topical clotrimazole in combination chemotherapy. Arch Ophthalmol 106:1196–1201.

133. Lin H-C, Hsiao C-H, Ma DH-K, Yeh L-K, Tan H-Y, Lin M-Y, Huang SC-M. 2009. Medical treatment for combined Fusarium and Acanthamoeba keratitis. Acta Ophthalmol 87:199–203.

134. Duma RJ, Finley R. 1976. In vitro susceptibility of pathogenic naegleria and acanthamoeba species to a variety of therapeutic agents. Antimicrob Agents Chemother 10:370–376.

135. Ishibashi Y, Matsumoto Y, Kabata T, Watanabe R, Hommura S, Yasuraoka K, Ishii K. 1990. Oral itraconazole and topical miconazole with débridement for Acanthamoeba keratitis. Am J Ophthalmol 109:121–126.

136. Nagington J, Richards JE. 1976. Chemotherapeutic compounds and Acanthamoebae from eye infections. J Clin Pathol 29:648–651.

137. Saunders PP, Proctor EM, Rollins DF, Richards JS. 1992. Enhanced killing of Acanthamoeba cysts in vitro using dimethylsulfoxide. Ophthalmology 99:1197–1200.

138. Foster CS, Stefanyszyn M. 1979. Intraocular penetration of miconazole in rabbits. Arch Ophthalmol 97:1703–1706.

139. Demirci G, Ay GM, Karabas LV, Altintas O, Tamer GS, Cağlar Y. 2006. Acanthamoeba keratitis in a 5-year-old boy without a history of contact lens usage. Cornea 25:356–358.

140. Wynter-Allison Z, Lorenzo Morales J, Calder D, Radlein K, Ortega-Rivas A, Lindo JF. 2005. Acanthamoeba infection as a cause of severe keratitis in a soft contact lens wearer in Jamaica. Am J Trop Med Hyg 73:92–94.

141. Hemady RK, Chu W, Foster CS. 1992. Intraocular penetration of ketoconazole in rabbits. Cornea 11:329–333.

142. Hirst LW, Green WR, Merz W, Kaufmann C, Visvesvara GS, Jensen A, Howard M. 1984. Management of acanthamoeba keratitis. Ophthalmology 91:1105–1111.

143. Poirier JM, Cheymol G. 1998. Optimisation of itraconazole therapy using target drug concentrations. Clin Pharmacokinet 35:461–473.

144. Hernández-Martínez D, Reyes-Batlle M, Castelan-Ramírez I, Hernández-Olmos P, Vanzzini-Zago V, Ramírez-Flores E, Sifaoui I, Piñero JE, Lorenzo-Morales J, Omaña-Molina M. 2019. Evaluation of the sensitivity to chlorhexidine, voriconazole and itraconazole of T4 genotype Acanthamoeba isolated from Mexico. Exp Parasitol 197:29–35.

145. Kaur IP, Rana C, Singh H. 2008. Development of effective ocular preparations of antifungal agents. J Ocul Pharmacol Ther 24:481–493.

146. Sobel JD, Wiesenfeld HC, Martens M, Danna P, Hooton TM, Rompalo A, Sperling M, Livengood C, Horowitz B, Von Thron J, Edwards L, Panzer H, Chu T-C. 2004. Maintenance fluconazole therapy for recurrent vulvovaginal candidiasis. N Engl J Med 351:876–883.

147. Anwar A, Siddiqui R, Hussain MA, Ahmed D, Shah MR, Khan NA. 2018. Silver nanoparticle conjugation affects antiacanthamoebic activities of amphotericin B, nystatin, and fluconazole. Parasitol Res 117:265–271.

148. Anwar A, Siddiqui R, Raza Shah M, Ahmed Khan N. 2019. Gold nanoparticles conjugation enhances antiacanthamoebic properties of nystatin, fluconazole and amphotericin B. J Microbiol Biotechnol 29:171–177.

149. O'Day DM, Foulds G, Williams TE, Robinson RD, Allen RH, Head WS. 1990. Ocular uptake of fluconazole following oral administration. Arch Ophthalmol 108:1006–1008.

150. Abbasoğlu OE, Hoşal BM, Sener B, Erdemoğlu N, Gürsel E. 2001. Penetration of topical fluconazole into human aqueous humor. Exp Eye Res 72:147–151.

151. Jenks JD, Salzer HJ, Prattes J, Krause R, Buchheidt D, Hoenigl M. 2018. Spotlight on isavuconazole in the treatment of invasive aspergillosis and mucormycosis: design, development, and place in therapy. Drug Des Devel Ther 12:1033–1044.

152. Shing B, Singh S, Podust LM, McKerrow JH, Debnath A. 2020. The Antifungal Drug Isavuconazole Is both Amebicidal and Cysticidal against Acanthamoeba castellanii. Antimicrob Agents Chemother 64.

153. Mada PK, Castano G, Gutierrez-Roberts MG. 2018. A Case of Rhizopus Keratitis. Clin Med Rev Case ….

154. Falci DR, Pasqualotto AC. 2013. Profile of isavuconazole and its potential in the treatment of severe invasive fungal infections. Infect Drug Resist 6:163–174.

155. Rice CA, Troth EV, Russell AC, Kyle DE. 2020. Discovery of Anti-Amoebic Inhibitors from Screening the MMV Pandemic Response Box on Balamuthia mandrillaris, Naegleria fowleri, and Acanthamoeba castellanii. Pathogens 9.

156. Brunet K, Eestermans R, Rodier MH, Cateau E. 2020. In vitro activity of isavuconazole against three species of Acanthamoeba. J Fr Ophtalmol 43:330–333.

157. Jeu L, Piacenti FJ, Lyakhovetskiy AG, Fung HB. 2003. Voriconazole. Clin Ther 25:1321–1381.

158. Hou T-Y, Chen Y-C, Hsu C-C. 2017. Rapid resolution of stromal keratitis with the assistance of oral voriconazole in resistant acanthamoeba keratitis. Taiwan J Ophthalmol 7:224–226.

159. Tu EY, Joslin CE, Shoff ME. 2010. Successful treatment of chronic stromal acanthamoeba keratitis with oral voriconazole monotherapy. Cornea 29:1066–1068.

160. Masselam KL, Pineda R. 2008. Topical Voriconazole as an Effective Co-Agent Against Acanthamoeba Keratitis. Investigative Ophthalmology & ….

161. Iovieno A, Miller D, Ledee DR, Alfonso EC. 2014. Cysticidal activity of antifungals against different genotypes of Acanthamoeba. Antimicrob Agents Chemother 58:5626–5628.

162. Talbott M, Cevallos V, Chen MC, Chin SA, Lalitha P, Seitzman GD, Lietman TM, Keenan JD. 2019. Synergy testing of antiamoebic agents for acanthamoeba: antagonistic effect of voriconazole. Cornea 38:1309–1313.

163. Gueudry J, Le Goff L, Compagnon P, Lefevre S, Colasse E, Aknine C, Duval F, François A, Razakandrainibe R, Ballet JJ, Muraine M, Favennec L. 2018. Evaluation of voriconazole anti-Acanthamoeba polyphaga in vitro activity, rat cornea penetration and efficacy against experimental rat Acanthamoeba keratitis. J Antimicrob Chemother 73:1895–1898.

164. Sponsel W, Chen N, Dang D, Paris G, Graybill J, Najvar LK, Zhou L, Lam K-W, Glickman R, Scribbick F. 2006. Topical voriconazole as a novel treatment for fungal keratitis. Antimicrob Agents Chemother 50:262–268.

165. Lau D, Fedinands M, Leung L, Fullinfaw R, Kong D, Davies G, Daniell M. 2008. Penetration of voriconazole, 1%, eyedrops into human aqueous humor: a prospective open-label study. Arch Ophthalmol 126:343–346.

166. Lebeaux D, Lanternier F, Elie C, Suarez F, Buzyn A, Viard J-P, Bougnoux M-E, Lecuit M, Jullien V, Lortholary O. 2009. Therapeutic drug monitoring of posaconazole: a monocentric study with 54 adults. Antimicrob Agents Chemother 53:5224–5229.

167. Altun A, Kurna SA, Sengor T, Altun G, Olcaysu OO, Aki SF, Simsek MH. 2014. Effectiveness of posaconazole in recalcitrant fungal keratitis resistant to conventional antifungal drugs. Case Rep Ophthalmol Med 2014:701653.

168. Sifaoui I, Martín-Navarro C, López-Arencibia A, Reyes-Batlle M, Valladares B, Piñero J, Maciver S, Lorenzo-Morales J. 2019. Optimized combinations of statins and azoles against Acanthamoeba trophozoites and cysts in vitro. Asian Pac J Trop Med 12:283.

169. Tu EY, McCartney DL, Beatty RF, Springer KL, Levy J, Edward D. 2007. Successful treatment of resistant ocular fusariosis with posaconazole (SCH-56592). Am J Ophthalmol 143:222–227.

170. Tu EY, Park AJ. 2007. Recalcitrant Beauveria bassiana keratitis: confocal microscopy findings and treatment with posaconazole (Noxafil). Cornea 26:1008–1010.

171. Rampersad SN. 2012. Multiple applications of Alamar Blue as an indicator of metabolic function and cellular health in cell viability bioassays. Sensors (Basel) 12:12347–12360.

172. McBride J, Ingram PR, Henriquez FL, Roberts CW. 2005. Development of colorimetric microtiter plate assay for assessment of antimicrobials against Acanthamoeba. J Clin Microbiol 43:629–634.

173. Martín-Navarro CM, López-Arencibia A, Lorenzo-Morales J, Oramas-Royo S, Hernández-Molina R, Estévez-Braun A, Ravelo AG, Valladares B, Piñero JE. 2010. Acanthamoeba castellanii Neff: In vitro activity against the trophozoite stage of a natural sesquiterpene and a synthetic cobalt(II)-lapachol complex. Exp Parasitol 126:106–108.

174. Fears AC, Metzinger RC, Killeen SZ, Reimers RS, Roy CJ. 2018. Comparative in vitro effectiveness of a novel contact lens multipurpose solution on Acanthamoeba castellanii. J Ophthalmic Inflamm Infect 8:19.

175. Jha BK, Seo I, Kong H-H, Suh S-I, Suh M-H, Baek W-K. 2015. Tigecycline inhibits proliferation of Acanthamoeba castellanii. Parasitol Res 114:1189–1195.

176. Sifaoui I, Reyes-Batlle M, López-Arencibia A, Wagner C, Chiboub O, De Agustino Rodríguez J, Rocha-Cabrera P, Valladares B, Piñero JE, Lorenzo-Morales J. 2017. Evaluation of the anti-Acanthamoeba activity of two commercial eye drops commonly used to lower eye pressure. Exp Parasitol 183:117–123.

177. Sifaoui I, Reyes-Batlle M, López-Arencibia A, Chiboub O, Bethencourt-Estrella CJ, San Nicolás-Hernández D, Rodríguez Expósito RL, Rizo-Liendo A, Piñero JE, Lorenzo-Morales J. 2019. Screening of the pathogen box for the identification of anti-Acanthamoeba agents. Exp Parasitol 201:90–92.

178. Thermo Fisher Scientific. alamarBlue™ Cell Viability Reagent.

179. Hannah R, Beck M, Moravec R, Riss T. 2001. CellTiter-Glo™ Luminescent cell viability assay: a sensitive and rapid method for determining cell viability. Promega Cell Notes.

180. Hahn HJ, Escrig JI, Shing B, Debnath A. 2020. In Vitro Effect of Pitavastatin and Its Synergistic Activity with Isavuconazole against Acanthamoeba castellanii. Pathogens 9.

181. Abjani F, Khan NA, Yousuf FA, Siddiqui R. 2016. Targeting cyst wall is an effective strategy in improving the efficacy of marketed contact lens disinfecting solutions against Acanthamoeba castellanii cysts. Cont Lens Anterior Eye 39:239–243.

182. Jha BK, Jung H-J, Seo I, Kim HA, Suh S-I, Suh M-H, Baek W-K. 2014. Chloroquine has a cytotoxic effect on Acanthamoeba encystation through modulation of autophagy. Antimicrob Agents Chemother 58:6235–6241.

183. Scruggs BA, Quist TS, Salinas JL, Greiner MA. 2019. Notes from the Field: Acanthamoeba Keratitis Cases - Iowa, 2002-2017. MMWR Morb Mortal Wkly Rep 68:448–449.

184. Mergeryan H. 1991. The prevalence of Acanthamoeba in the human environment. Rev Infect Dis 13 Suppl 5:S390–1.

185. Rivera F, Lares F, Ramirez E, Bonilla P, Rodriguez S, Labastida A, Ortiz R, Hernandez D. 1991. Pathogenic acanthamoeba isolated during an atmospheric survey in mexico city. Clin Infect Dis 13:S388–S389.

186. Horne DD, Frizell ME, Ingham L, Jans RG, Gubash SM, Anand CM, Athar MA. 1994. Acanthamoeba keratitis: an emerging clinical problem. Can Med Assoc J 150:923–925.

187. Marciano-Cabral F, Puffenbarger R, Cabral GA. 2000. The increasing importance of acanthamoeba infections. J Eukaryot Microbiol 47:29–36.

188. Murdoch D, Gray TB, Cursons R, Parr D. 1998. Acanthamoeba keratitis in New Zealand, including two cases with in vivo resistance to polyhexamethylene biguanide. Aust N Z J Ophthalmol 26:231–236.

189. Siddiqui R, Khan NA. 2012. Biology and pathogenesis of Acanthamoeba. Parasit Vectors 5:6.

190. Garner A. 1993. Pathogenesis of acanthamoebic keratitis: hypothesis based on a histological analysis of 30 cases. Br J Ophthalmol 77:366–370.

191. Mathers W, Stevens G, Rodrigues M, Chan CC, Gold J, Visvesvara GS, Lemp MA, Zimmerman LE. 1987. Immunopathology and electron microscopy of Acanthamoeba keratitis. Am J Ophthalmol 103:626–635.

192. Johns KJ, O'Day DM, Feman SS. 1988. Chorioretinitis in the contralateral eye of a patient with Acanthamoeba keratitis. Ophthalmology 95:635–639.

193. Moshari A, McLean IW, Dodds MT, Damiano RE, McEvoy PL. 2001. Chorioretinitis after keratitis caused by Acanthamoeba: case report and review of the literature. Ophthalmology 108:2232–2236.

194. Naginton J, Watson PG, Playfair TJ, McGill J, Jones BR, Steele AD. 1974. Amoebic infection of the eye. Lancet 2:1537–1540.

195. Niederkorn JY, Alizadeh H, Leher HF, McCulley JP. 1999. The immunobiology ofAcanthamoeba keratitis. Springer Semin Immunopathol 21:147–160.

196. Kumar R, Lloyd D. 2002. Recent advances in the treatment of Acanthamoeba keratitis. Clin Infect Dis 35:434–441.

197. Shahbandeh M. 2018. Contact lenses in the U.S. - Statistics & Facts. Statista.

198. Cope JR, Collier SA, Nethercut H, Jones JM, Yates K, Yoder JS. 2017. Risk Behaviors for Contact Lens-Related Eye Infections Among Adults and Adolescents - United States, 2016. MMWR Morb Mortal Wkly Rep 66:841–845.

199. Choi JY, Podust LM, Roush WR. 2014. Drug strategies targeting CYP51 in neglected tropical diseases. Chem Rev 114:11242–11271.

200. Thomson S, Rice CA, Zhang T, Edrada-Ebel R, Henriquez FL, Roberts CW. 2017. Characterisation of sterol biosynthesis and validation of 14α-demethylase as a drug target in Acanthamoeba. Sci Rep 7:8247.

201. Debnath A, Calvet CM, Jennings G, Zhou W, Aksenov A, Luth MR, Abagyan R, Nes WD, McKerrow JH, Podust LM. 2017. CYP51 is an essential drug target for the treatment of primary amoebic meningoencephalitis (PAM). PLoS Negl Trop Dis 11:e0006104.

202. Zhou W, Warrilow AGS, Thomas CD, Ramos E, Parker JE, Price CL, Vanderloop BH, Fisher PM, Loftis MD, Kelly DE, Kelly SL, Nes WD. 2018. Functional importance for developmental regulation of sterol biosynthesis in Acanthamoeba castellanii. Biochim Biophys Acta Mol Cell Biol Lipids 1863:1164–1178.

203. Ashley ED, Perfect JR. 2019. Pharmacology of azoles. UpToDate.

204. Warrilow AGS, Price CL, Parker JE, Rolley NJ, Smyrniotis CJ, Hughes DD, Thoss V, Nes WD, Kelly DE, Holman TR, Kelly SL. 2016. Azole Antifungal Sensitivity of Sterol 14α-Demethylase (CYP51) and CYP5218 from Malassezia globosa. Sci Rep 6:27690.

205. Ghannoum MA, Rice LB. 1999. Antifungal agents: mode of action, mechanisms of resistance, and correlation of these mechanisms with bacterial resistance. Clin Microbiol Rev 12:501–517.

206. Buck SL, Rosenthal RA. 1996. A quantitative method to evaluate neutralizer toxicity against Acanthamoeba castellanii. Appl Environ Microbiol 62:3521–3526.

207. Ondarza RN, Iturbe A, Hernández E. 2006. In vitro antiproliferative effects of neuroleptics, antimycotics and antibiotics on the human pathogens Acanthamoeba polyphaga and Naegleria fowleri. Arch Med Res 37:723–729.

208. Ortega-Rivas A, Padrón JM, Valladares B, Elsheikha HM. 2016. Acanthamoeba castellanii: A new high-throughput method for drug screening in vitro. Acta Trop 164:95–99.

209. Martín-Navarro CM, López-Arencibia A, Sifaoui I, Reyes-Batlle M, Valladares B, Martínez-Carretero E, Piñero JE, Maciver SK, Lorenzo-Morales J. 2015. Statins and voriconazole induce programmed cell death in Acanthamoeba castellanii. Antimicrob Agents Chemother 59:2817–2824.

210. Booton GC, Visvesvara GS, Byers TJ, Kelly DJ, Fuerst PA. 2005. Identification and distribution of Acanthamoeba species genotypes associated with nonkeratitis infections. J Clin Microbiol 43:1689–1693.

211. Debnath A, Parsonage D, Andrade RM, He C, Cobo ER, Hirata K, Chen S, García-Rivera G, Orozco E, Martínez MB, Gunatilleke SS, Barrios AM, Arkin MR, Poole LB, McKerrow JH, Reed SL. 2012. A high-throughput drug screen for Entamoeba histolytica identifies a new lead and target. Nat Med 18:956–960.

212. Debnath A, Tunac JB, Galindo-Gómez S, Silva-Olivares A, Shibayama M, McKerrow JH. 2012. Corifungin, a new drug lead against Naegleria, identified from a high-throughput screen. Antimicrob Agents Chemother 56:5450–5457.

213. Cooksey RC, Crawford JT, Jacobs WR, Shinnick TM. 1993. A rapid method for screening antimicrobial agents for activities against a strain of Mycobacterium tuberculosis expressing firefly luciferase. Antimicrob Agents Chemother 37:1348–1352.

214. Debnath A, Shahinas D, Bryant C, Hirata K, Miyamoto Y, Hwang G, Gut J, Renslo AR, Pillai DR, Eckmann L, Reed SL, McKerrow JH. 2014. Hsp90 inhibitors as new leads to target parasitic diarrheal diseases. Antimicrob Agents Chemother 58:4138–4144.

215. Mackey ZB, Baca AM, Mallari JP, Apsel B, Shelat A, Hansell EJ, Chiang PK, Wolff B, Guy KR, Williams J, McKerrow JH. 2006. Discovery of trypanocidal compounds by whole cell HTS of Trypanosoma brucei. Chem Biol Drug Des 67:355–363.

216. Sykes ML, Avery VM. 2009. A luciferase based viability assay for ATP detection in 384-well format for high throughput whole cell screening of Trypanosoma brucei brucei bloodstream form strain 427. Parasit Vectors 2:54.

217. Xia M, Huang R, Witt KL, Southall N, Fostel J, Cho M-H, Jadhav A, Smith CS, Inglese J, Portier CJ, Tice RR, Austin CP. 2008. Compound cytotoxicity profiling using quantitative high-throughput screening. Environ Health Perspect 116:284–291.

218. Van Daele R, Spriet I, Wauters J, Maertens J, Mercier T, Van Hecke S, Brüggemann R. 2019. Antifungal drugs: What brings the future? Med Mycol 57:S328–S343.

219. Schmitt-Hoffmann A, Desai A, Kowalski D, Pearlman H, Yamazaki T, Townsend R. 2016. Isavuconazole absorption following oral administration in healthy subjects is comparable to intravenous dosing, and is not affected by food, or drugs that alter stomach pH. Int J Clin Pharmacol Ther 54:572–580.

220. Desai A, Kovanda L, Kowalski D, Lu Q, Townsend R, Bonate PL. 2016. Population Pharmacokinetics of Isavuconazole from Phase 1 and Phase 3 (SECURE) Trials in Adults and Target Attainment in Patients with Invasive Infections Due to Aspergillus and Other Filamentous Fungi. Antimicrob Agents Chemother 60:5483–5491.

221. Maertens JA, Raad II, Marr KA, Patterson TF, Kontoyiannis DP, Cornely OA, Bow EJ, Rahav G, Neofytos D, Aoun M, Baddley JW, Giladi M, Heinz WJ, Herbrecht R, Hope W, Karthaus M, Lee D-G, Lortholary O, Morrison VA, Oren I, Selleslag D, Shoham S, Thompson GR, Lee M, Maher RM, Schmitt-Hoffmann A-H, Zeiher B, Ullmann AJ. 2016. Isavuconazole versus voriconazole for primary treatment of invasive mould disease caused by Aspergillus and other filamentous fungi (SECURE): a phase 3, randomised-controlled, non-inferiority trial. Lancet 387:760–769.

222. Díaz-Tomé V, Luaces-Rodríguez A, Silva-Rodríguez J, Blanco-Dorado S, García-Quintanilla L, Llovo-Taboada J, Blanco-Méndez J, García-Otero X, Varela-Fernández R, Herranz M, Gil-Martínez M, Lamas MJ, González-Barcia M, Otero-Espinar FJ, Fernández-Ferreiro A. 2018. Ophthalmic econazole hydrogels for the treatment of fungal keratitis. J Pharm Sci 107:1342–1351.

223. Harrington R, Lee E, Yang H, Wei J, Messali A, Azie N, Wu EQ, Spalding J. 2017. Cost-Effectiveness Analysis of Isavuconazole vs. Voriconazole as First-Line Treatment for Invasive Aspergillosis. Adv Ther 34:207–220.

224. Otri AM, Mohammed I, Abedin A, Cao Z, Hopkinson A, Panjwani N, Dua HS. 2010. Antimicrobial peptides expression by ocular surface cells in response to Acanthamoeba castellanii: an in vitro study. Br J Ophthalmol 94:1523–1527.

225. DSMZ GmbH. 2009. Acanthamoeba Medium.

226. Schuster FL. 2002. Cultivation of pathogenic and opportunistic free-living amebas. Clin Microbiol Rev 15:342–354.

227. Sohn H-J, Kang H, Seo G-E, Kim J-H, Jung S-Y, Shin H-J. 2017. Efficient Liquid Media for Encystation of Pathogenic Free-Living Amoebae. Korean J Parasitol 55:233–238.

228. Choi JY, Calvet CM, Gunatilleke SS, Ruiz C, Cameron MD, McKerrow JH, Podust LM, Roush WR. 2013. Rational development of 4-aminopyridyl-based inhibitors targeting Trypanosoma cruzi CYP51 as anti-chagas agents. J Med Chem 56:7651–7668.

229. Choi JY, Calvet CM, Vieira DF, Gunatilleke SS, Cameron MD, McKerrow JH, Podust LM, Roush WR. 2014. R-Configuration of 4-Aminopyridyl-Based Inhibitors of CYP51 Confers Superior Efficacy Against Trypanosoma cruzi. ACS Med Chem Lett 5:434–439.

230. Calvet CM, Vieira DF, Choi JY, Kellar D, Cameron MD, Siqueira-Neto JL, Gut J, Johnston JB, Lin L, Khan S, McKerrow JH, Roush WR, Podust LM. 2014. 4-Aminopyridyl-based CYP51 inhibitors as anti-Trypanosoma cruzi drug leads with improved pharmacokinetic profile and in vivo potency. J Med Chem 57:6989–7005.

231. Vieira DF, Choi JY, Calvet CM, Siqueira-Neto JL, Johnston JB, Kellar D, Gut J, Cameron MD, McKerrow JH, Roush WR, Podust LM. 2014. Binding mode and potency of N-indolyloxopyridinyl-4-aminopropanyl-based inhibitors targeting Trypanosoma cruzi CYP51. J Med Chem 57:10162–10175.

232. Vieira DF, Choi JY, Roush WR. 2014. Expanding the binding envelope of CYP51 inhibitors targeting Trypanosoma cruzi with 4-aminopyridyl-based sulfonamide derivatives. … : a European journal of ….

233. Zhou W, Debnath A, Jennings G, Hahn HJ, Vanderloop BH, Chaudhuri M, Nes WD, Podust LM. 2018. Enzymatic chokepoints and synergistic drug targets in the sterol biosynthesis pathway of Naegleria fowleri. PLoS Pathog 14:e1007245.

234. Zhou W, Ramos E, Zhu X, Fisher PM, Kidane ME, Vanderloop BH, Thomas CD, Yan J, Singha U, Chaudhuri M, Nagel MT, Nes WD. 2019. Steroidal antibiotics are antimetabolites of Acanthamoeba steroidogenesis with phylogenetic implications. J Lipid Res 60:981–994.

235. Reed JR, Connick JP, Cheng D, Cawley GF, Backes WL. 2012. Effect of homomeric P450-P450 complexes on P450 function. Biochem J 446:489–497.

236. Szczesna-Skorupa E, Mallah B, Kemper B. 2003. Fluorescence resonance energy transfer analysis of cytochromes P450 2C2 and 2E1 molecular interactions in living cells. J Biol Chem 278:31269–31276.

237. Ozalp C, Szczesna-Skorupa E, Kemper B. 2005. Bimolecular fluorescence complementation analysis of cytochrome p450 2c2, 2e1, and NADPH-cytochrome p450 reductase molecular interactions in living cells. Drug Metab Dispos 33:1382–1390.

238. Praporski S, Ng SM, Nguyen AD, Corbin CJ, Mechler A, Zheng J, Conley AJ, Martin LL. 2009. Organization of cytochrome P450 enzymes involved in sex steroid synthesis: PROTEIN-PROTEIN INTERACTIONS IN LIPID MEMBRANES. J Biol Chem 284:33224–33232.

239. Hu G, Johnson EF, Kemper B. 2010. CYP2C8 exists as a dimer in natural membranes. Drug Metab Dispos 38:1976–1983.

240. Davydov DR, Davydova NY, Sineva EV, Halpert JR. 2015. Interactions among cytochromes P450 in microsomal membranes: oligomerization of cytochromes P450 3A4, 3A5, and 2E1 and its functional consequences. J Biol Chem 290:3850–3864.

241. Scott EE, He YA, Wester MR, White MA, Chin CC, Halpert JR, Johnson EF, Stout CD. 2003. An open conformation of mammalian cytochrome P450 2B4 at 1.6-A resolution. Proc Natl Acad Sci USA 100:13196–13201.

242. Schoch GA, Yano JK, Wester MR, Griffin KJ, Stout CD, Johnson EF. 2004. Structure of human microsomal cytochrome P450 2C8. Evidence for a peripheral fatty acid binding site. J Biol Chem 279:9497–9503.

243. Ouellet H, Podust LM, de Montellano PRO. 2008. Mycobacterium tuberculosis CYP130: crystal structure, biophysical characterization, and interactions with antifungal azole drugs. J Biol Chem 283:5069–5080.

244. Reed JR, Backes WL. 2017. Physical Studies of P450-P450 Interactions: Predicting Quaternary Structures of P450 Complexes in Membranes from Their X-ray Crystal Structures. Front Pharmacol 8:28.

245. Krissinel E, Henrick K. 2007. Inference of macromolecular assemblies from crystalline state. J Mol Biol 372:774–797.

246. Lewis DFV, Ito Y, Goldfarb PS. 2006. Structural modelling of the human drug-metabolizing cytochromes P450. Curr Med Chem 13:2645–2652.

247. Morrison JF. 1969. Kinetics of the reversible inhibition of enzyme-catalysed reactions by tight-binding inhibitors. Biochimica et Biophysica Acta (BBA) - Enzymology 185:269–286.

248. Mustafa G, Nandekar PP, Camp TJ, Bruce NJ, Gregory MC, Sligar SG, Wade RC. 2019. Influence of Transmembrane Helix Mutations on Cytochrome P450-Membrane Interactions and Function. Biophys J 116:419–432.

249. Gotoh O. 2012. Evolution of cytochrome p450 genes from the viewpoint of genome informatics. Biol Pharm Bull 35:812–817.

250. Otyepka M, Skopalík J, Anzenbacherová E, Anzenbacher P. 2007. What common structural features and variations of mammalian P450s are known to date? Biochim Biophys Acta 1770:376–389.

251. Perera R, Sono M, Sigman JA, Pfister TD, Lu Y, Dawson JH. 2003. Neutral thiol as a proximal ligand to ferrous heme iron: implications for heme proteins that lose cysteine thiolate ligation on reduction. Proc Natl Acad Sci USA 100:3641–3646.

252. Dunford AJ, McLean KJ, Sabri M, Seward HE, Heyes DJ, Scrutton NS, Munro AW. 2007. Rapid P450 heme iron reduction by laser photoexcitation of Mycobacterium tuberculosis CYP121 and CYP51B1. Analysis of CO complexation reactions and reversibility of the P450/P420 equilibrium. J Biol Chem 282:24816–24824.

253. Sabat J, Stuehr DJ, Yeh S-R, Rousseau DL. 2009. Characterization of the proximal ligand in the P420 form of inducible nitric oxide synthase. J Am Chem Soc 131:12186–12192.

254. Driscoll MD, McLean KJ, Cheesman MR, Jowitt TA, Howard M, Carroll P, Parish T, Munro AW. 2011. Expression and characterization of Mycobacterium tuberculosis CYP144: common themes and lessons learned in the M. tuberculosis P450 enzyme family. Biochim Biophys Acta 1814:76–87.

255. Martinis SA, Blanke SR, Hager LP, Sligar SG, Hoa GH, Rux JJ, Dawson JH. 1996. Probing the heme iron coordination structure of pressure-induced cytochrome P420cam. Biochemistry 35:14530–14536.

256. Sun Y, Zeng W, Benabbas A, Ye X, Denisov I, Sligar SG, Du J, Dawson JH, Champion PM. 2013. Investigations of heme ligation and ligand switching in cytochromes p450 and p420. Biochemistry 52:5941–5951.

257. Jung C, Friedrich J, Ristau O. 1979. Quantum chemical interpretation of the spectral properties of the CO and O2 complexes of hemoglobin and cytochrome P-450. Acta Biol Med Ger 38:363–377.

258. Sun L, Wang Z, Jiang H, Tan X, Huang Z. 2010. Novel Conformational Transitions of Human Cytochrome P450 2C8 during Thermal and Acid-induced Unfolding. Chin J Chem 28:1491–1502.

259. Arendse LB, Blackburn JM. 2018. Effects of polymorphic variation on the thermostability of heterogenous populations of CYP3A4 and CYP2C9 enzymes in solution. Sci Rep 8:11876.

260. Chen Y-J, Zhang J, Zhu P-P, Tan X-W, Lin Q-H, Wang W-X, Yin S-S, Gao L-Z, Su M-M, Liu C-X, Xu L, Jia W, Sevrioukova IF, Lan K. 2019. Stereoselective Oxidation Kinetics of Deoxycholate in Recombinant and Microsomal CYP3A Enzymes:

Deoxycholate 19-Hydroxylation Is an In Vitro Marker of CYP3A7 Activity. Drug Metab Dispos 47:574–581.

261. Ogura H, Nishida CR, Hoch UR, Perera R, Dawson JH, Ortiz de Montellano PR. 2004. EpoK, a cytochrome P450 involved in biosynthesis of the anticancer agents epothilones A and B. Substrate-mediated rescue of a P450 enzyme. Biochemistry 43:14712–14721.

262. Greinert R, Finch SA, Stier A. 1982. Cytochrome P-450 rotamers control mixed-function oxygenation in reconstituted membranes. Rotational diffusion studied by delayed fluorescence depolarization. Xenobiotica 12:717–726.

263. Kawato S, Gut J, Cherry RJ, Winterhalter KH, Richter C. 1982. Rotation of cytochrome P-450. I. Investigations of protein-protein interactions of cytochrome P-450 in phospholipid vesicles and liver microsomes. J Biol Chem 257:7023–7029.

264. Myasoedova KN, Berndt P. 1990. Cytochrome P-450LM2 oligomers in proteoliposomes. FEBS Lett 275:235–238.

265. Schwarz D, Pirrwitz J, Meyer HW, Coon MJ, Ruckpaul K. 1990. Membrane topology of microsomal cytochrome P-450: saturation transfer EPR and freeze-fracture electron microscopy studies. Biochem Biophys Res Commun 171:175–181.

266. Myasoedova KN, Magretova NN. 2001. Cross-Linking study of cytochrome P450 1A2 in proteoliposomes. Biosci Rep 21:63–72.

267. Von Wachenfeldt C, Johnson EF. 1995. Structures of eukaryotic cytochrome P450 enzymes, p. 183–223. *In* de Montellano, PRO (ed.), Cytochrome P450. Springer US, Boston, MA.

268. von Wachenfeldt C, Richardson TH, Cosme J, Johnson EF. 1997. Microsomal P450 2C3 Is Expressed as a Soluble Dimer inEscherichia coliFollowing Modifications of Its N-terminus. Arch Biochem Biophys 339:107–114.

269. Davydov DR, Fernando H, Baas BJ, Sligar SG, Halpert JR. 2005. Kinetics of dithionite-dependent reduction of cytochrome P450 3A4: heterogeneity of the enzyme caused by its oligomerization. Biochemistry 44:13902–13913.

270. Davydov DR, Sineva EV, Sistla S, Davydova NY, Frank DJ, Sligar SG, Halpert JR. 2010. Electron transfer in the complex of membrane-bound human cytochrome P450 3A4 with the flavin domain of P450BM-3: the effect of oligomerization of the heme protein and intermittent modulation of the spin equilibrium. Biochim Biophys Acta 1797:378–390.

271. Davydov DR, Davydova NY, Sineva EV, Kufareva I, Halpert JR. 2013. Pivotal role of P450-P450 interactions in CYP3A4 allostery: the case of α-naphthoflavone. Biochem J 453:219–230.

272. Šrejber M, Navrátilová V, Paloncýová M, Bazgier V, Berka K, Anzenbacher P, Otyepka M. 2018. Membrane-attached mammalian cytochromes P450: An overview of the membrane's effects on structure, drug binding, and interactions with redox partners. J Inorg Biochem 183:117–136.

273. Monk BC, Tomasiak TM, Keniya MV, Huschmann FU, Tyndall JDA, O'Connell JD, Cannon RD, McDonald JG, Rodriguez A, Finer-Moore JS, Stroud RM. 2014. Architecture of a single membrane spanning cytochrome P450 suggests constraints that orient the catalytic domain relative to a bilayer. Proc Natl Acad Sci USA 111:3865–3870.

274. Björkhem I, Lütjohann D, Breuer O, Sakinis A. 1997. Importance of a Novel Oxidative Mechanism for Elimination of Brain Cholesterol: TURNOVER OF CHOLESTEROL AND 24 (S)-HYDROXYCHOLESTEROL IN RAT …. Journal of Biological ….

275. Omura T, Sato R. 1964. The carbon monoxide-binding pigment of liver microsomes. i. evidence for its hemoprotein nature. J Biol Chem 239:2370–2378.

276. Luthra A, Denisov IG, Sligar SG. 2011. Spectroscopic features of cytochrome P450 reaction intermediates. Arch Biochem Biophys 507:26–35.

277. Wang A, Savas U, Hsu M-H, Stout CD, Johnson EF. 2012. Crystal structure of human cytochrome P450 2D6 with prinomastat bound. J Biol Chem 287:10834–10843.

278. Kabsch W. 2012. *XDS*, p. 304–310. *In* Arnold, E, Himmel, DM, Rossmann, MG (eds.), International Tables for Crystallography: Crystallography of biological macromolecules. International Union of Crystallography, Chester, England.

279. Emsley P, Cowtan K. 2004. Coot: model-building tools for molecular graphics. Acta Crystallogr Sect D, Biol Crystallogr 60:2126–2132.

280. Koehler Leman J, Mueller BK, Gray JJ. 2017. Expanding the toolkit for membrane protein modeling in Rosetta. Bioinformatics 33:754–756.

281. Koehler Leman J, Bonneau R. 2018. A Novel Domain Assembly Routine for Creating Full-Length Models of Membrane Proteins from Known Domain Structures. Biochemistry 57:1939–1944.

282. Jo S, Kim T, Iyer VG, Im W. 2008. CHARMM-GUI: a web-based graphical user interface for CHARMM. J Comput Chem 29:1859–1865.

283. Maier JA, Martinez C, Kasavajhala K, Wickstrom L, Hauser KE, Simmerling C. 2015. ff14SB: Improving the Accuracy of Protein Side Chain and Backbone Parameters from ff99SB. J Chem Theory Comput 11:3696–3713.

284. DA Case, Ben-Shalom IY, Brozell SR, Cerutti DS, TE Cheatham III, Cruzeiro VW, Darden TA, Duke RE, Ghoreishi D, Gilson MK, Gohlke H. 2018. AMBER 2018; 2018. University of California, San Francisco.

285. Rydberg P, Olsen L, Norrby P-O, Ryde U. 2007. General Transition-State Force Field for Cytochrome P450 Hydroxylation. J Chem Theory Comput 3:1765–1773.

286. Dolinsky TJ, Nielsen JE, McCammon JA, Baker NA. 2004. PDB2PQR: an automated pipeline for the setup of Poisson-Boltzmann electrostatics calculations. Nucleic Acids Res 32:W665–7.

287. Phillips JC, Braun R, Wang W, Gumbart J, Tajkhorshid E, Villa E, Chipot C, Skeel RD, Kalé L, Schulten K. 2005. Scalable molecular dynamics with NAMD. J Comput Chem 26:1781–1802.

288. Gupta D, Panda GS, Bakhshi S. 2008. Successful treatment of acanthamoeba meningoencephalitis during induction therapy of childhood acute lymphoblastic leukemia. Pediatr Blood Cancer 50:1292–1293.

289. Singhal T, Bajpai A, Kalra V, Kabra SK, Samantaray JC, Satpathy G, Gupta AK. 2001. Successful treatment of Acanthamoeba meningitis with combination oral antimicrobials. Pediatr Infect Dis J 20:623–627.

290. Visvesvara GS. 2010. Amebic meningoencephalitides and keratitis: challenges in diagnosis and treatment. Curr Opin Infect Dis 23:590–594.

291. Schuster FL, Visvesvara GS. 2004. Free-living amoebae as opportunistic and non-opportunistic pathogens of humans and animals. Int J Parasitol 34:1001–1027.

292. Ledee DR, Iovieno A, Miller D, Mandal N, Diaz M, Fell J, Fini ME, Alfonso EC. 2009. Molecular identification of t4 and t5 genotypes in isolates from acanthamoeba keratitis patients. J Clin Microbiol 47:1458–1462.

293. Murrell D, Bossaer JB, Carico R, Harirforoosh S, Cluck D. 2017. Isavuconazonium sulfate: a triazole prodrug for invasive fungal infections. Int J Pharm Pract 25:18–30.

294. Shing B, Balen M, McKerrow JH, Debnath A. 2021. Acanthamoeba Keratitis: an update on amebicidal and cysticidal drug screening methodologies and potential treatment with azole drugs. Expert Rev Anti Infect Ther 1–15.

295. Schmitt-Hoffmann A-H, Kato K, Townsend R, Potchoiba MJ, Hope WW, Andes D, Spickermann J, Schneidkraut MJ. 2017. Tissue Distribution and Elimination of Isavuconazole following Single and Repeat Oral-Dose Administration of Isavuconazonium Sulfate to Rats. Antimicrob Agents Chemother 61.

296. Natesan SK, Chandrasekar PH. 2016. Isavuconazole for the treatment of invasive aspergillosis and mucormycosis: current evidence, safety, efficacy, and clinical recommendations. Infect Drug Resist 9:291–300.

297. Patel DV, McGhee CN. 2013. Presumed late recurrence of Acanthamoeba keratitis exacerbated by exposure to topical corticosteroids. Oman J Ophthalmol 6:S40–2.

298. Zhao Z-Q, Zheng P, Xu S-T, Wu X. 2019. Object detection with deep learning: A review. IEEE Trans Neural Netw Learn Syst 30:3212–3232.

299. Debnath A, Tunac JB, Silva-Olivares A, Galindo-Gómez S, Shibayama M, McKerrow JH. 2014. In vitro efficacy of corifungin against Acanthamoeba castellanii trophozoites and cysts. Antimicrob Agents Chemother 58:1523–1528.

300. Kayser O, Kiderlen AF, Croft SL. 2003. Natural products as antiparasitic drugs. Parasitol Res 90 Suppl 2:S55–62.

301. Newman DJ, Cragg GM. 2016. Natural Products as Sources of New Drugs from 1981 to 2014. J Nat Prod 79:629–661.

302. García-Davis S, Sifaoui I, Reyes-Batlle M, Viveros-Valdez E, Piñero JE, Lorenzo-Morales J, Fernández JJ, Díaz-Marrero AR. 2018. Anti-Acanthamoeba Activity of Brominated Sesquiterpenes from Laurencia johnstonii. Mar Drugs 16.

303. Lorenzo-Morales J, Díaz-Marrero AR, Cen-Pacheco F, Sifaoui I, Reyes-Batlle M, Souto ML, Hernández Daranas A, Piñero JE, Fernández JJ. 2019. Evaluation of Oxasqualenoids from the Red Alga Laurencia viridis against Acanthamoeba. Mar Drugs 17.

304. Ultralytics, LLC. 2020. Train Custom Data. Github.

305. Sharma V, Shing B, Hernandez-Alvarez L, Debnath A, Podust LM. 2020. Domain-Swap Dimerization of Acanthamoeba castellanii CYP51 and a Unique Mechanism of Inactivation by Isavuconazole. Mol Pharmacol 98:770–780.

306. Shing B, Balen M, Debnath A. 2021. Evaluation of Amebicidal and Cysticidal Activities of Antifungal Drug Isavuconazonium Sulfate against Acanthamoeba T4 Strains. Pharmaceuticals 14:1294.

307. Suryawanshi A, Cao Z, Sampson JF, Panjwani N. 2015. IL-17A-mediated protection against Acanthamoeba keratitis. J Immunol 194:650–663.